# Six Degree of Freedom Joystick

Simon Yi Y CHAU BE (Hons)

A thesis submitted in partial fulfilment
of the requirements for the degree of
Master of Engineering
in
Mechanical Engineering
at the
University of Canterbury,
Christchurch, New Zealand.

6th October 2003

# ABSTRACT

Industrial robotics concentrates on developing automated alternatives to human function. Most of the equipment is controlled by means of joystick. Through a joystick input, a robotic arm can be guided through the trajectories to accomplish complex manipulation tasks for its user. Nevertheless, conventional joysticks are mainly two dimensional input devices such as mouse or joystick with additional buttons. Hence it is necessary to design and build a more intuitive and user-friendly joystick model. This thesis aims at designing and building a six degree of freedom (DOF) joystick. Different designs are reviewed in the beginning of the thesis, the final prototype is proposed by refining the different designs. Structural analysis of the model is performed and verified using finite element software ANSYS and PATRAN. The prototype is tested to model the movement of the wire strips when various forces are applied. Preliminary test results are obtained and explained.

# ACKNOWLEDGEMENTS

I would like to thank my supervisor Professor Reg Dunlop for his insightful comments and ever useful help. He is always there when I needed his advice especially when one runs out of time to complete his thesis.

Thank you, Dr. Ilanko for his knowledge of structural analysis. He is like a mentor to me, he always gives me helpful guidelines when the progress of the project is almost idle.

Thank you to Rodney Elliott for preparing the testing equipment and the electronic devices for me to run the testing. His practical experience has greatly helped me to overcome many setup issues.

Thank you, Wing Tham for all the support that he gave me throughout the period of my study.

Most of all, I would like to thank my parents for their love and support.

# CONTENTS

# LIST OF FIGURES

# LIST OF TABLES

# CHAPTER 1

# INTRODUCTION

## 1.1 Background

Over the years, techniques in controlling machines in three dimensions have been thoroughly analyzed and well-developed. However, most of the techniques revolve around using only two-dimensional input device, such as a standard mouse, a joystick with additional buttons etc. for 3-D manipulation. Methods, which lacked full six degree of freedom (DOF) only manipulate the two DOF at a time. While there are also methods providing full six DOF control, these are at the cost of complex user operations and complex implementations. These devices require formal trainings so that the users understand and operate the device or user interface correctly.

Simultaneous control of multiple degrees of freedom (DOFs) is required in many control interfaces. Examples include teleoperation, cursor control in computer-aided design and manufacturing software, and virtual environments.Understanding the limitations of the human operator in manual control tasks with multiple DOFs is necessary for an adequate design of systems that require the simultaneous control of multiple DOFs.

In view of this factor, it is desirable to have an input device - joystick, which can fully provide 6 DOF manipulations. The joystick has to be user friendly, so that user could use the joystick to perform tasks with minimal training and familiarization. This is considered to be an essential factor in most of the human operated control system applications, particularly in industrial robotics – e.g. large scale manufacturing plants.

Hence this research investigates different conceptual designs for a user-friendly 6-DOF joystick.

## 1.2 Usefulness of Joysticks

The generic term 'joystick' refers to any input device of a specified number of degrees of freedom that transduces motion and/or force to electrical signals. Nowadays, joysticks are the most common way of controlling robotic arms in the automobile manufacturing industry. There are two common joystick types [1]: the displacement and force joysticks. The output of the displacement joystick (also known as isotonic joystick) is proportional to the joystick displacement, whereas the output of the force joystick (also known as isometric or stiff joystick) is proportional to the force applied by the human operator. The advantage of the force joystick is that it requires only minute joystick displacements (a few micrometers) in contrast with the displacement joystick (a few centimeters).

Industrial robotics concentrates on developing fully automated alternatives to human function; telemanipulation research endeavours to produce a perfect mechanical extension of man for the handling of materials in inhospitable or dangerous environments. In between these 2 fields lies Interactive Robotics. The goal of this field is to combine direct human control of a mechanical arm with automation, by an on-board computer, of low-level operations such as obstacle avoidance, object centering and grasping, peg-in-hole insertions, and line or plane-following. The concept of distributed decision-making involves human switching of operation modes through a symbolic information channel (keyboard or voice), and human analogue control of real-time processes through a joystick configuration.

Through a joystick input, a robotic arm can be guided through the trajectories to accomplish complex manipulation tasks for its user. A typical joystick can be simply

represented by a rod. The rod is operable in 2 dimensions, i.e. the x and y-axes. When the rod is shifted in a direction, the associated control mechanism will ensure that the controlled machine will move in the same direction. Additional buttons are used to operate the object in the third dimension. When the button is pressed, the controlled object will move in the positive direction of the third axis. Vice versa, the object will move in the negative direction of the third axis when the other button is pressed.

## 1.3 Six DOFs Joystick

The concept of a 3D joystick is similar to the conventional joystick as described before. Nevertheless, the joystick is operated in 3 dimensions, i.e. the x, y and z-axes. The actual movement of the rod is matched and translated such that the controlled object is moved in the appropriate direction. The displacement or the movement speed of the controlled object is scaled by the control interface.

The joystick design for this thesis takes a form similar to a parallel manipulator where the structural topologies are made up of closed-loop chains. It consists of a moving platform that is connected to a fixed base by several limbs or legs. Typically the number of limbs is equal to the number of degrees of freedom. This concept is sourced from the general Gough-Stewart platform.

## 1.4 Research Undertaken

All developments of the 6DOF model are documented to reflect the changes and modifications carried out along the way.

### 1.4.1 Designing and Building the Controller

Conceptual design of the six DOF joystick is based on the Gough-Stewart platform. Drawings of the design and prototypes of each design have been built. The designs

are modelled using Solidworks CAD software. Refinements are performed on each design in order to determine and correct any weakness or problems.

### 1.4.2 Structural Analysis

Structural analysis was performed for each case and finite element analysis was performed using the Ansys application software. A prototype of the conceptual design was built once the finite element analysis provided positive results.

### 1.4.3 Experiments / Testing

The prototype was tested using DSPACE to determine the accuracy of readings and for calibration purposes. Mathematical calculations were performed in order to test the validity of the hypothesised relationship.

## 1.5 Background Research

### 1.5.1 Gough-Steward Platform

Steward platform has six degrees and is often used as a motion platform [2] that is capable of moving in three linear directions and three angular directions singly or in any combination. The platform is often a truncated triangular plane, on which each of the three corners is connected to one of three pairs legs. The 6 legs are connected to the base at 3 pairs of closely spaced points. Often the platform has 3 pairs of closely spaced points connecting to the actuators rather then only 3 corners connected to 3 pairs of actuators.

### 1.5.2 Mechanical Linkages Joystick

With mechanical linkages for commanding hydraulic valves via dual-axis joysticks, the main disadvantage is the complexity of the linkage arrangement, which makes it

difficult to install and adjust [1]. The simplest linkages are levers and rods, but these become cumbersome if a straight path from the joystick to the hydraulic component does not exist. When the mechanical linkage must be routed over, under, around, or through obstacles, mechanical push-pull cables have found favour.
All mechanical linkages may require operators to generate objectionably high actuating forces if the mechanical advantage of the assembly is not well designed. Otherwise, operator fatigue results, and as with all mechanical arrangements, regular lubrication and adjustment for wear is necessary.

A neater arrangement uses hydraulical pilot valves and joysticks. With this setup, low-pressure fluid is routed to the joystick, which, in turn, routes fluid to the appropriate pilot-operated hydraulic devices based on joystick position. The advantages of this system over a mechanical linkage arrangement are simplified installation, lower actuating force required by the operator, and less maintenance.

Among the disadvantages of piloted joysticks are the potential for leakage, noise, and heat from hydraulic fluid in close proximity to the operator. In winter weather, cold oil adversely affects response and increases operator effort. Hydraulic pilot installation still involves the routing of multiple hoses or soft-metal tubing.

### 1.5.3 Electric Joystick

Electronic joysticks are furnished as independent control devices. They include contact-less, proportional controls with either inductive or hall effect operation, as well as models utilizing switches and/or potentiometers. They can be furnished as separate signal devices or can include built-in valve drivers

### 1.5.4 Inductive Joystick

There are two major categories of electric joysticks - displacement and non-displacement - as well as a hybrid non-displacement sensor with a displacement lever. The displacement type uses the motion of a lever, transducing that motion eventually into an electrical output. The non-displacement type has a lever similar to the displacement type. However, the motion of the joystick is not transduced directly to an electrical output. Instead, the force applied to the lever is transduced via a strain gauge or similar medium to electrical output. An advantage of the non-displacement joystick is the absence of moving parts. A disadvantage is the loss of tactile feedback to the operator normally associated with the motion of a joystick. The hybrid non-displacement sensor with a displacement lever uses a heavy spring to connect the sensor to a lever and create the desired joystick feel, so that movement and force are related.

**Figure 1.1 Example of an inductive joystick**

An electric joystick uses a power supply and sends electric signals to command an electro-hydraulic valve. Because thin wires are so much easier to route through a machine than mechanical cables, hoses, or tubing, electric joysticks greatly simplify installation and provide the freedom of remote mounting. Serial communications make this process even easier. Electronic control also provides the advantage of being able to create unique response curves for lever position versus flow and/or pressure and the incorporation of integral safety interlocks. The valves can be located very far from the joystick. The principal disadvantage of the electric joystick until recently has been the higher cost of electro-hydraulic valves over their manually

driven or pilot-operated counterparts. The cost trade-off between hydraulic and electric joysticks is about even.

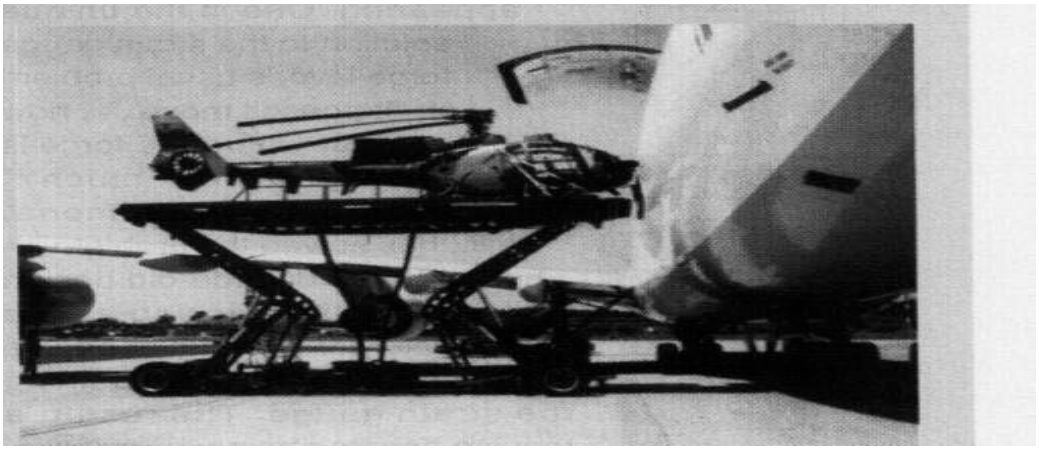

**Figure 1.2 Joystick controller helps moving mountains of cargo**

Aircraft Maintenance Support Services, Bridgend, Wales, a manufacturer of ground support equipment for military and civilian customers worldwide, has specified the Penny & Giles JC150 joystick controller for its latest Atlas 2000 air-portable cargo transporter/loader.

The four-wheel-drive vehicle, which is sold to air forces and international peacekeeping and relief agencies, weighs less than 12 tonnes and will load and transport up to 18 tonnes of cargo. It is used to load military and civilian aircraft, from a C130 Hercules to the 8747 Main Deck, which requires a 4.5-m vertical lift.

The Penny & Giles JC150 provides full control of the Atlas 2000's platform through its processor control system. The functions include lowering and raising from 1 to 5.5m plus pitching and rolling fore and aft, as well as left and right.

AMSS fitted the Penny & Giles JC600 joystick to the Atlas 2000 and its predecessor, the Atlas MK2, found that both gave excellent service throughout the world.

There are three popular designs of displacement-type joysticks, the potentiometric movement, the inductive coupling, and the Hall Effect types.

### 1.5.5 Potentiometric Joystick

The potentiometric joystick, as shown in Figure 1.3, uses a rotary or linear potentiometer to convert mechanical displacement to electrical output. The conversion from curvilinear motion of the joystick lever to potentiometer movement usually involves shafts, gimbals, gears, and torsion springs. These mechanisms contain many parts, which can make these joysticks vulnerable to damage and give a shortened lifespan - especially if they are exposed to machine vibration.

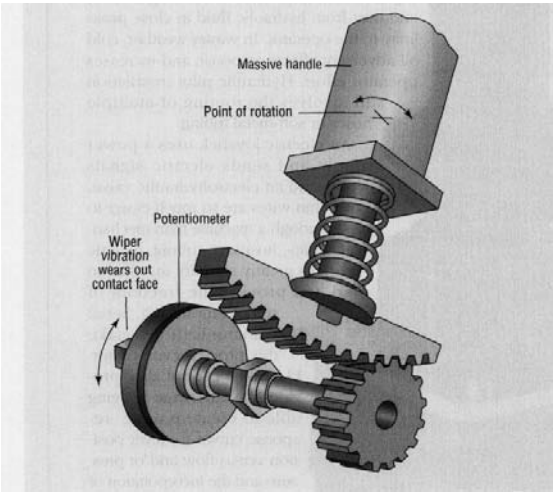


**Figure 1.3 Potentiometric movement joystick**

Potentiometric joysticks are available in high-cycle-life construction with published life in excess of 106 full cycles. Most joysticks spend the greater part of their working lives in a neutral position, with the wipers of their pots being dithered continuously due to the vibration of the machinery on which they are mounted. This low amplitude cycling (dithering) of the pot wiper proves more destructive to the pot than full-cycle movements. The constant dithering and high accumulation of cycles over a narrow area may cause the conductive element to wear-in locally, causing a "dead" or "noisy" spot.

One big advantage to potentiometric joysticks is high noise immunity. When choosing either an inductively coupled or Hall-effect sensor based joystick, care must be taken to ensure that the potential EMI/RFI interference is not sufficient to self-activate the joystick output. Various designs by various manufacturers have different response levels and frequencies e.g. sensor in one unit is a strain gauge based hybrid non-displacement sensor with a displacement lever that has been placed so as to be insensitive to EMI/RFI in excess of 100 volts per meter.

### 1.5.6 Inductively Coupled Movement

An inductively coupled joystick uses a variable-transformer-type relationship. A primary coil sets up a field that is induced into a set of secondary coils. Through movement of either the drive coil or a ferrous shaft, which commutates the field, the induced field will vary proportionally. The closer the drive coil is to a secondary coil, the stronger the pickup field. The secondary coil that is further away from the primary coil will have a proportionally smaller pickup. The relationship of primary and secondary coils is shown in Figure 1.4.

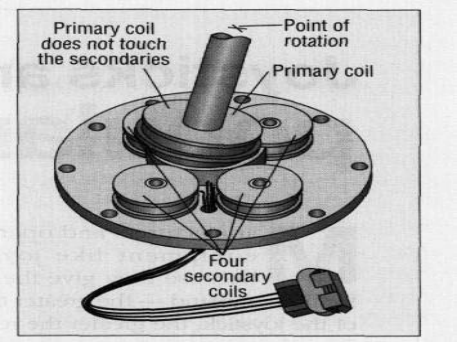


**Figure 1.4 Potentiometric movement joystick.**

The primary advantage of this mechanism over that of the potentiometric movement is that no contacting or wiping electrical parts exist. Further, the mechanical complexity is much less. The model shown in Figure 1.4 has only three moving parts (lever, centering cup, and helical compression spring), so life of the device is

significantly extended. Protection from stray electrical fields affecting the joystick's inductive field is provided by a synchronous detection system. The pickup frequency from the four secondary coils must equal the frequency of the signal applied to the primary, so the effects of adjacent electrical fields essentially are easily filtered out by synchronous detection.

### 1.5.7 Hall-Effect Technology

Development of newer joystick technology has focused on enhancing linearity and electromagnetic immunity while providing additional output capabilities within a smaller working envelope. One significant technology - the Hall effect device- has emerged as being capable of providing all these desired attributes and enhancements.

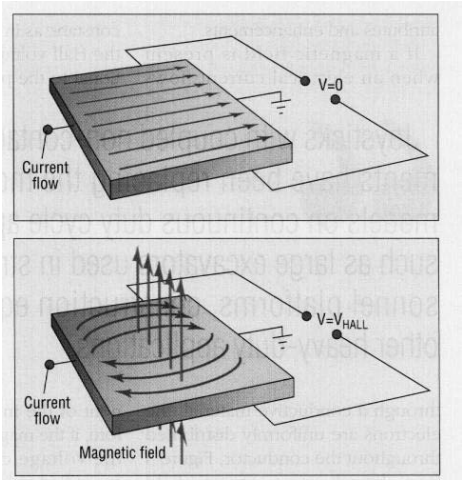


**Figure 1.5 Electromagnetism**

If a magnetic field is present when an electrical current flows through a conductive material, the electrons are uniformly distributed throughout the conductor, Figure 3 (top). Introducing a magnetic field to the electric current disrupts the current and causes its course to be changed, Figure 1.5.

When the input current is held constant, as in a joystick application, the Hall voltage is directly proportional to the perpendicular component of the magnetic field.

Therefore, if the magnets change position, the voltage changes and can be quantified as joystick movement.

The mechanical simplicity of the inductively coupled and Hall effect joystick movements lends itself to incorporation in multiple movement axes. The traditional two-axis joystick can have a third or even a fourth axis added to it, while still retaining the basic mechanical simplicity, and having no wiping contacts. For example, a twist movement of the handgrip may produce a third axis, and a thumb-operated wheel can provide a proportional fourth axis. A grip-- mounted switch could also be incorporated to add simple functionality.

Joysticks with coupled non-contact sensing elements have been replacing the more traditional models on continuous duty cycle applications - such as large excavators used in strip mines, personnel platforms, construction equipment, and other heavy-duty applications. These applications and others have found electric joysticks, particularly the inductively coupled type, to enhance their reliability.

Joysticks with inductively coupled movement have been replacing traditional joysticks on continuous duty cycle applications - such as large excavators used in strip mines and aerial basket controls for utility trucks using fibre-optic couplings. These and other applications have found electric joysticks, and more particularly the non-contact sensing element type, to enhance their operation. In addition, the electrical on input can be processed by a computer to decouple end effector commands from those required for the actuators.

### 1.5.8 Three Translational Degrees of Freedom

For multiple degree-of-freedom (DOF) systems, it is important to determine how accurately operators can control each DOF and what influence perception, information processing, and psychomotor components have on performance.

Two ideas were introduced by Chernikoff & LeMay; Fracker & Wickens [5]. First, as the number of input devices is reduced, so is the number of limbs needed. Second, control performance can be improved with integrated controls, especially when an integrated multiple-DOF display is used.

Van Erp and Oving [5] conducted two experiments one involved with positioning and another involved tracking with 3 translational DOFs. Sixteen right-handed male students were selected to participate in the 2 experiments. To separate perceptual and psychomotor effects, 2 control-display mappings were used that differed in the coupling of vertical and depth dimensions to the up-down and fore-aft control axes. Information processing effects in the positioning task were observed: Initial error correction on the vertical dimension lagged in time behind the horizontal dimension. The depth dimension error correction lagged behind both, which was ascribed to the poorer perceptual information. This perceptual effect in the tracking experiment was also observed: Tracking error along the depth dimension was 3.8 times larger than along the other dimensions. Motor effects were also present, with tracking errors along the up-down axis of the hand controller being 1.1 times larger than along the fore-aft axis. These results indicate that all 3 components contribute to control performance. Actual applications of this research include interface design for remote control and virtual reality.

One of the questions arises as to how accurately the human operator can control each translational DOF when using an integrated control device in combination with an integrated display. A common observation is that tracking accuracy in the depth dimension of the display is worse than in the vertical and horizontal dimensions. There are indications that limitations in information processing capacity may also play a role in asymmetrical control performance. For instance, Zhai et al. [9] found different learning curves for the three visual dimensions in simultaneous three-dimensional tracking tasks, with the tracking error along the vertical and depth

dimensions being higher than along the horizontal dimension in the first phase of the experiment. Zhai and colleagues ascribed the difference between the horizontal and vertical dimensions to a shortage of attentional resources in the early stages of learning when participants had difficulty in controlling all DOFs simultaneously combined with greater attention being given to the horizontal dimension. This difference disappeared in the second and subsequent phases, when more attentional resources may have been freed up because of increased experience with the control system. These results are in compliance with the notion that priority differences diminish when task execution shifts from controlled to more automatic during the course of learning. According to Zhai et al. such attentional priority differences may be the result of daily experiences, in which movement visual stimuli are distributed more often in the horizontal direction than in the vertical direction.

### 1.5.9 Gaming Joystick

Niemela et al [3] developed a user-friendly teaching system for a polishing robot using a game joystick. The teaching process is as follows. First, a zigzag path, which depends on both sizes of each object and polishing tool, was prepared. Next, the polishing robot whose control system consisted of an impedance model following force controller profiles the object's surface using the zigzag path. In this case, the operator had to control only the orientation of the polishing tool using a usual game joystick. Further, since the impedance model following force controller kept the contact force to be a desired value, the operator did not need to give attention to a sudden overload or non-contact state. Through the above process, the desired trajectory was automatically obtained as the data including both continuous information of the position and its normal vector of the object's surface along the zigzag path. The robot could achieve the polishing task without any assistance from the operator simply by referring to the obtained trajectory. The effectiveness of the proposed method was demonstrated through some experiments on polishing wood.

Invented for the video gaming market, haptic technology is now spreading to other applications, such as Web surfing, CAD model manipulation, medical design surgical training and automotive controls. Efforts to develop joysticks for cars are also being demonstrated.

The latest driving games feature haptic steering wheels that jerk with every passing bump in the road, and golf games that let you feel the thwack of club against ball.
That technology uses small motors to provide force-feedback to the user, thus reducing one more hurdle between the real world and virtual reality.

### 1.5.10 Human-induced Instability in Powered Hand Controllers

The dynamic behaviour of a hand controller when it is manoeuvred by a human was described by Kazerooni and Snyder [7]. Powered hand controllers are active multi-degree-of-freedom joystick-like haptic devices that are manoeuvred by humans to produce commands. A general control architecture that ensures various impedances on the hand controller was developed. It was demonstrated that some compliance in the hand controller or in the human arm was required to achieve stability of the hand controller and the human arm taken as a whole. The actuator's back-drivability, the dynamics of the hand controller mechanisms, and the computer sampling time were considered as they relate to system stability.

Torque in harmonic drives was transmitted by a pure couple, harmonic drives did not generate radial forces and therefore could be instrumented with torque sensors without interference from radial forces. The installation of torque sensors on the stationary component of harmonic drives (the Flexipline cup in this research work) produced the backdrivability needed for robotic and telerobotic compliant maneuvers. Backdrivability of a harmonic drive, when used as torque increaser, means that the output shaft could be rotated via finite amount of torque. A high ratio harmonic drive was non-backdrivable because its output shaft could not be turned by applying a

torque on it. Kazerooni et al [7] developed the dynamic behaviour of a harmonic drive, in particular the non-backdrivability, in terms of a sensitivity transfer function. The instrumentation of the harmonic drive with torque sensor was also considered by him. This leads to a description of the control architecture which allows modulation of the sensitivity transfer function within the limits established by the closed-loop stability.

### 1.5.11 A Mechatronic System with Force Feeling

In recent years the disappointment about the slow progress in the area of sensor-based robot intelligence and autonomy had led to an increasing interest in master-slave systems. A tele-operational solution-developed by Bencsik and Garai [6] at the Department of Mechanical Engineering of Banki Donat Polytechnic-was based on 6D force reflection. The joystick-like master arm (with the hydraulic force percolation generated by the executive mechanism) connected the signal from the force perceptors and processing electronics to the controller of the proportional valves. The proportional valves transmit pressure proportional to with the force generated at the final point of the manipulator to the force feeling valves of the master arm. The system also provided the ability to select the force feedback and also the actuator control by degrees of freedom, however the force reflection could be stopped at any time by the operator. The force was visualised by a digital display.

### 1.5.12 Joystick for Powered Wheelchair Drive

An investigation of performance while driving an electric-powered wheelchair (EPW) with an isometric joystick (IJ) and a position-sensing joystick was presented by Cooper et al.[4]. Fitt's Law for target acquisition, extended to include a continuously updated target, provided insight into the problems associated with target acquisition tasks with an EPW. The test results revealed significant differences between the 2 joystick types for information processing time, movement time, rms error, and average velocity while turning. The mean values showed that the IJ might give the

best turning performance.

The majority of electric wheelchair users were able to operate a joystick to control the chair, however many more quadriplegic users needed some other means of controlling the wheelchair. Coyle [10] developed an electronic PWM DC drive unit designed for operation by standard joystick, ultrasonic non-contact head control, and by command from a limited speech vocabulary.

There were limited interface options for electric powered wheelchairs, which resulted in the inability of some individuals to drive independently. In addition, the development of new interface technologies would necessitate the development of alternative training methods. Cooper et al. compares a conventional position sensing, 5 joystick to a novel isometric joystick during a driving task in a virtual environment and a real environment. The results revealed that there were few differences in task completion time and root-mean-square (RMS) error between the two types of 5 joysticks. There were significant correlations between the RMS error in the virtual environment and the real environment for both types of 5 joysticks. The data indicates that performance in the virtual environment was representative of driving ability in the real environment, and the isometric joystick performed similarly to the position sensing joystick.

### 1.5.13 Joystick Operated by Fuzzy Logic

Fuzzy logic[4] had been applied widely in various closed-loop control systems. In the case of a hydraulic mobile crane, the operator often had many mechanical manual valve lever arms to handle simultaneously. Niemela and Virvalo[3] used a fuzzy logic controller, to show that the operator's task of controlling independent booms could be reduced using an electrically operated joystick

A fuzzy logic controller was designed and built which is able to minimise the effect of

multiple sclerosis (MS) hand tremors. The aim of their project was to give people with MS better control of an electric wheelchair by removing tremors from the joystick signal. The system intercepted the signal from the joystick and then passed it through the fuzzy logic controller. The fuzzy logic rules identify and reduce erratic or unusual movements, by employing a history mechanism to determine what “unusual” is. The fuzzy logic then outputs a signal which most closely represents the intent of the user.

### 1.5.14 Force Feedback Controller

Force-reflected tele-operation with in-parallel devices are gaining prominence in robotics applications [8]. Although their development has been limited primarily to Gough Stewart platform type devices, many other parallel hand controllers hold promise for force-reflected manipulation. One factor prohibiting a full exploration involves the problem of their singularity analysis as the use of conventional rank determining methods are overly complicated. Singularity analysis complications arise because the Jacobian matrix has several functionally dependent variables. Collins and Long [8] has first derive the Jacobian matrix and then show its six columns can be viewed as zero-pitch wrenches (lines) acting on the top platform. The analysis then shows how line geometry and rank determining geometric constructions can be used to obtain all configuration singularities.

Wang et al. [11] carried out an experiment to analysis the control strategy for a force feed back joystick using an underwater robotic vehicle (URV). The topside controllers linked through Internet/User Datagram Protocol consist of the operator control panel, a dynamic module and a 3D virtual display developed using LabVIEW and WorldToolKit. It is well known that force feedback can be employed to enhance the touch perception in the virtual environment (VE) so they presented the control strategy for force feedback using a commercially inexpensive force feedback joystick and its implementation in LabVIEW. The pilot can steer and guide the vehicle using

the joystick with two basic force behaviour modes, namely joystick based behavioural effects and vehicle dynamic based behavioural effects. When the vehicle in the virtual environment approaches an obstacle, the operator can experience a “wall” force that will prevent the vehicle from collision. However, in the event of collision, either due to the operator's mishandling or unknown water current interference, a vibration force is used to simulate this event. All these force effects are generated to enhance haptic perceptions for the operator in the real underwater environment while interacting with the simulation. They constructed the interface design of joystick force functions in LabVIEW environment. Instead of hardwired control consoles, LabVIEW based user interfaces have been developed in the URV topside control system because LabVIEW is a powerful graphical language with friendly human interaction where prototyping and modification are easy and flexible. Operators could concentrate on commanding the vehicle while the computer interpreted the command and controlled the main electric motors that propelled and oriented the vehicle. This greatly reduced operator fatigue, improved control and with the force feedback greatly improved the sensitivity of the control.

## 1.6 Background Theory

To control a machine in $R^3$ requires six degrees of freedom (DOFs), three for translation (along the x,y, and z axes) and three for angular orientation ($\theta_x$, $\theta_y$ and $\theta_z$). Common input devices such as mouse and joystick utilise only 2 DOFs. Additional buttons are required to be able to fully operate the machine in 3D. As a consequence, designers concentrate on the development of the user interface and software development. Until 3D input devices become as ubiquitous as 2D devices, designers continue to design navigation interfaces that take advantage of only those features present in a typical 2D input device.

The mathematical theory and equations need to be studied in order to understand the linear displacement and angular displacement of a particular point for the controller.

It is important to identify a suitable geometric co-ordinate system for the mechanism. Using Jacobians for the co-ordinate exchange, the equations representing the relationship between the mechanism's co-ordinate systems can be developed. The unknown (finial displacement or angular displacement) can be found by doing row reduction of the relative matrix. For a mechanism which has one degree of freedom, this unknown will be found by solving equation such as F(x)=0. For higher DOF mechanisms, the unknowns can be obtained by solving higher power non-linear equations.

# CHAPTER 2

# DESIGN & BUILD PROTOTYPE

## 2.1 Introduction

This chapter discusses the design process for the 6DOF joystick. The model was modified many times and finally the prototype was built based on the final design. The design of the joystick is based on the structure of Gough-Stewart Platform. This structure is constructed by using two truncated triangular plates with six legs. The design process involves determining the size, the material and the shape of the platforms. The mechanism that connects the two platforms along with the attachment of strain gauges will be discussed. Prototype requires suitable computer software, to calculate the displacement of the joystick.

## 2.2 Designing the Structure

The joystick was designed based on the structure of Gough-Stewart platform, the lower platform is basically a fixed base while the upper platform is compliant and can be moved by the user. The initial idea was using six hydraulic actuators to connect the upper and lower platforms. This kind of structure has been widely used by robotic motion simulators, and there are many of such products that have been made for the robotic control market. The technology is expensive, even four small haptic systems so, it was decided to use a different mechanism to link the upper and lower platforms.

Several issues have to be considered when choosing the right mechanism. The size limitation of the joystick was one of the most important subjects to be considered. The user will have difficulty when holding or using the joystick if it is being either too

big or too small. Other aspects that should also be considered in constructing the controller are material selection, geometric, and machining of parts are also important. Strain gauges would appear to offer an inexpensive way to detect movement of the platform, and with appropriate springs, movement can provide feedback to the user. Among all, attaching strain gauges on to the joystick has to be taken into consideration before designing the structure.

### 2.2.1 Strain Gauge

Strain is the amount of deformation of a body due to an applied force. More specifically, strain (ε) is defined as the fractional change in length, as shown in the figure defining a strain gauge below.

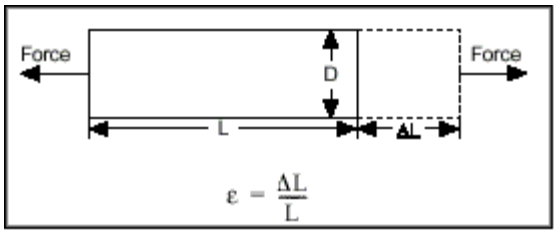


**Figure 2.1 Definition of Strain**

Strain can be positive (tensile) or negative (compressive). Although dimensionless, strain is sometimes expressed in units such as in/in or mm/mm. In practice, the magnitude of measured strain is very small. Therefore, strain is often expressed as microstrain ($\mu\varepsilon$), which is E x $10^{-6}$.

When a bar is strained with a uniaxial force, as depicted in the figure defining a strain gauge above, a phenomenon known as Poisson strain causes the girth of the bar, D, to contract in the transverse, or perpendicular, direction. While there are several methods of measuring strain, the most common is with a strain gauge. A strain gauge's electrical resistance varies in proportion to the amount of strain placed on it. The most widely used gauge is the bonded metallic strain gauge.

The metallic strain gauge consists of a very fine wire or, more commonly, metallic foil arranged in a grid pattern. The grid pattern maximizes the amount of metallic wire or foil subject to strain in the parallel direction (shown as the "active grid length" in the bonded metallic strain gauge figure). The cross sectional area of the grid is minimized to reduce the effect of shear strain and Poisson strain.

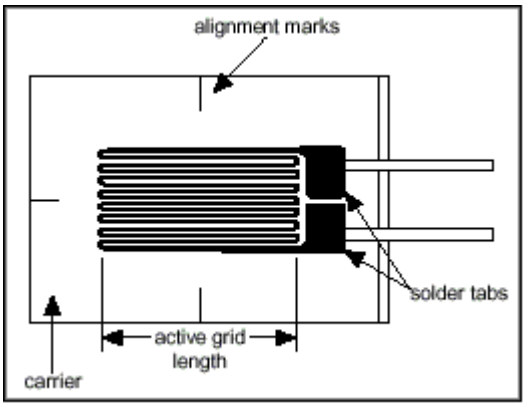


**Figure 2.2 Bonded metallic strain gauge**

A fundamental parameter of the strain gauge is its sensitivity to strain, expressed quantitatively as the gauge factor (GF). Gauge factor is the ratio of fractional change in electrical resistance to the fractional change in length (strain):

$$GF = \frac{\Delta R/R}{\Delta L/L} = \frac{\Delta R/R}{\varepsilon} \quad \textbf{(2.1)}$$

The gauge factor for metallic strain gauges is typically around two.

Ideally, the resistance of the strain gauge would change only in response to applied strain. However, strain gauge material, as well as the specimen material to which you apply the gauge, will also respond to changes in temperature. Strain gauge manufacturers attempt to minimize sensitivity to temperature by processing the gauge material to compensate for the thermal expansion of the specimen material intended for the gauge. While compensated gauges reduce the thermal sensitivity, they do not remove it completely. In practice, the strain measurements rarely involve quantities

larger than a few milli-strain (ε x 10-3). Therefore, measuring strain requires accurate measurement of very small changes in resistance.

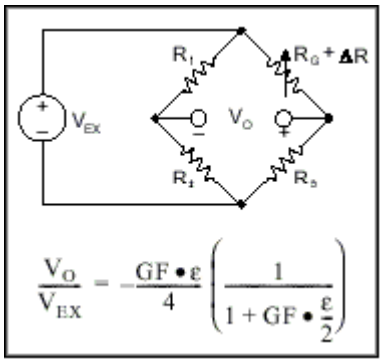


**Figure 2.3 Quarter-Bridge Circut**

The sensitivity of the bridge to strain can be doubled by making both gauges active. For example, the half-bridge circuit figure illustrates a bending beam application with one bridge mounted in tension ($R_G$ + ΔR) and the other mounted in compression ($R_G$ - ΔR). This half-bridge configuration, whose circuit diagram is also illustrated in the Half-Bridge Circuit figure, yields an output voltage that is linear and approximately double that of the single gauge circuit.

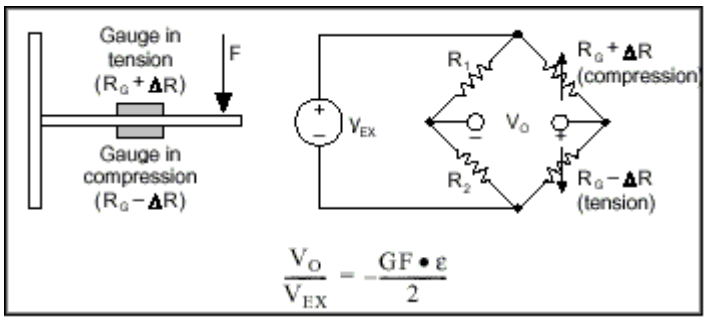


**Figure 2.4 Half-bridge circuit**

Finally, the sensitivity of the circuit can be further increased by making all four of the arms of the bridge active strain gauges and mounting two gauges in tension and two gauges in compression. The full-bridge circuit is shown in the figure below.

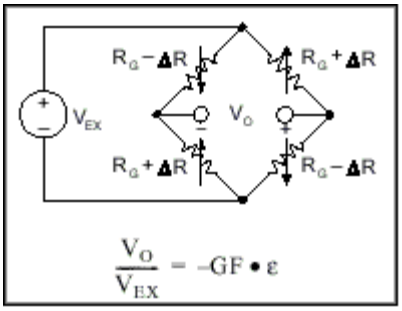


**Figure 2.5 Full-bridge circuit**

The equations given here for the Wheatstone bridge circuits assume an initially balanced bridge that generates zero output without strain. In practice however, resistance tolerances and strain induced by gauge application will generate some initial offset voltage. This initial offset voltage is typically handled in two ways. First, use a special offset-nulling, or balancing circuit to adjust the resistance on rebalance the bridge to zero output.

The two primary criteria for selecting the right type of strain gauge are sensitivity and precision. In general, if the more strain gauges, (a 4 active gauges rather than a single gauge) used the faster the response and the better precision. On the other hand, cost will also play a large part in determining the type of strain gauge selected as full-bridge strain gauges are 4 times more expensive single gauge. For a summary of the various types of strain and strain gauges, please refer to the strain gauge summary table below.

| Strain | Gauge Setup | Bridge Type | Sensitivity MV/V @ 1000 uE | Details |
|---|---|---|---|---|
| Axial | 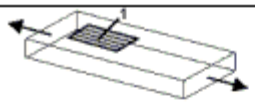 | ¼ | 0.5 | Good: Simplest to implement, but must use a dummy gauge if compensating for Temperature. Also responds to Bending Strain. |
| | 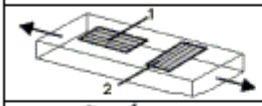 | ½ | 0.65 | Better: Temperature compensated, but it is sensitive to bending strain. |
| | 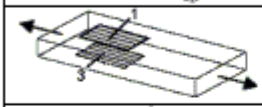 | ½ | 1.0 | Better: Rejects Bending Strain, but not temperature. Must use dummy gauges if compensating for temperature. |
| | 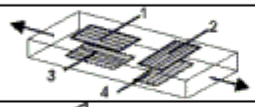 | Full | 1.3 | Best: More sensitive and compensates for both temperature and bending strain. |
| Bending | 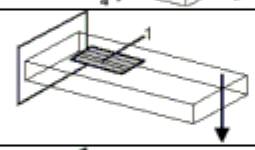 | ¼ | 0.5 | Good: Simplest to implement, but must use a dummy gauge if compensating for Temperature. Responds equally to Axial Strain. |
| | 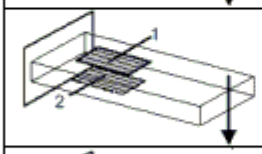 | ½ | 1.0 | Better: Rejects axial strain and is temperature compensated |
| | 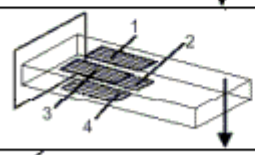 | Full | 2.0 | Best: Rejects axial strain and is temperature compensated. Most sensitive to bending strain. |
| Torsional and Shear | 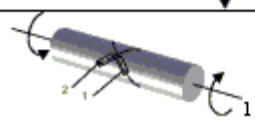 | ½ | 1.0 | Good: Gauges must be mounted at 45 degrees from centerline. Axial and Bending forces produce equal strain and are hence rejected. |
| | 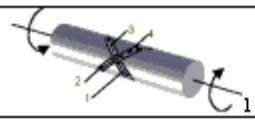 | Full | 2.0 | Best: More sensitive full-bridge version of previous setup. Rejects both axial and bending strains. |

**Figure 2.6 Strain Gauge Summary**

## 2.2.2 Joining the Platforms

Spring wire was studied and used to join the two platforms. One of the most important features of using spring wire is it will allow the upper platform to return to its natural position. Other advantages of spring wire are such as it has lightweight, it is inexpensive the length is relatively easy to adjust, and there are lots of options for the wire diameter and stiffness from the industrial market.

The first question arises in the process of making the joystick is to fix the wires to the

triangular plates. A good method for solving this problem is to drill holes at the side of the plate and insert the wires into the holes. The holes could have same diameter as the wires so it will be a ‘tight fit’ or ‘push fit’ situation in the manufacturing process. The advantage of this method is that the wires can be fixed firmly in the holes; on the other hand, close tolerance is needed for ‘push fit’ machining. Also the wires may have angles that are not normal to the surface of the platform.

Another option is to drill the hole diameter slightly lager than wire diameter, then glue is injected into the holes followed by the wires. Advantages of this method are the wires can be fixed in a natural position. Besides, it is a relatively easy procedure, this method is selected due to its advantages in manufacturing.

### 2.2.3 Design of Platforms

The problem of twisted wires is also another matter to be considered. Both platforms are triangle shaped. For discussion purposes, the three angle are named A, B, and C respectively. According to the structure of Gough-Stewart platform, two wires extend from A of the top platform will be joined to B and C of bottom platform; another two wires extend from B of the top platform will be joined to A and C of bottom platform; the last two wires extend from C or the top platform will be joined to A and B of bottom platform. This kind of arrangement will cause twist or tension in the wires, thus the design needs to be modified.

The wires need to lie in a plane in order to achieve zero twisting. Each angle of the platforms is cut as shown in Figure 2.7. This kind of arrangement allows the wires lie in the same plane thus achieving zero twist.

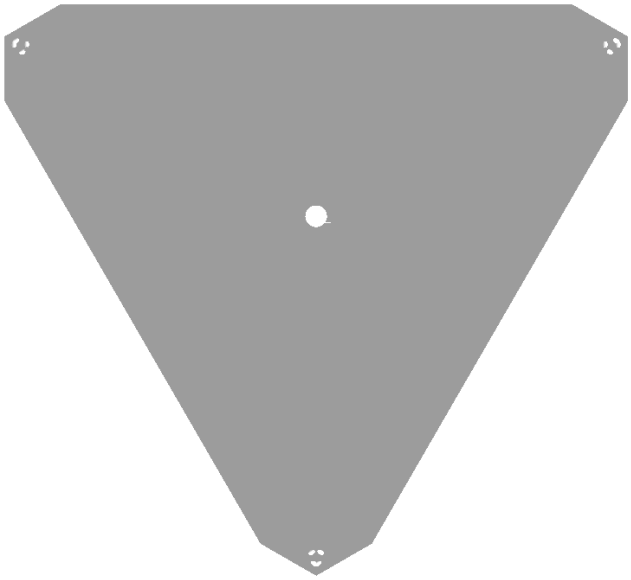

**Figure 2.7 Design of the plate.**

The size of the two platforms is the same. Materials available for the platforms are steel, aluminium and plastic. Steel has disadvantages of weight and rust. The relatively large mass of steel causes large pre-stress of the wires. Plastic is one of the good options as being lightweight and inexpensive. However the material was not as strong or as stable as aluminium and requires a similar amount of machining. Thus aluminium is chosen as the material for the two platforms as it does not rust, it is relatively lightweight (compare to steel), hard, easy to be machined, inexpensive, and reality available.

The two identical platforms were manufactured. Diameter of the spring wires is 0.9mm so the holes on the platforms are drilled as 2mm. Glue was then injected into the holes, and the wires inserted. The model was let aside in its natural position allow the glue to dry. The joystick is shown in the following Figure 2.8.

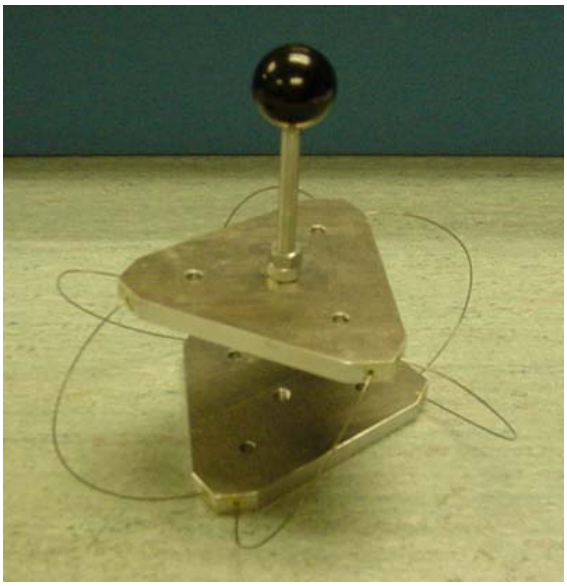

**Figure 2.8 Joystick with connected spring wire**

When force and torque are applied to the joystick, the spring wires do bring the joystick back to its initial position. The movement of the joystick can be expressed as non-linear large deflections of the 6 springs, as will be discussed in chapter 4.

After the model was constructed, the relationship between force/torque applied to the joystick and the displacement of the joystick was calculated. However for such mechanical structure it is very hard to mathematically express the relationship between force/torque applied to the joystick and the displacement. The only methods available are either using finite element or performing experiments in order to obtain numerical results. Finite element methods will be discussed in chapter 5 and ANSYS will be used. On the other hand, experiments can be performed by connecting strain gauges on to the wires in order to obtain the voltages, which represent the displacements. The smallest strain gauge available now is 1mm, whereas diameter of the wires is 0.9mm. It is impossible to attach the strain gauge on the wire. Moreover, the surface of the wire is not flat which makes the strain gauge hard to attach to the wire even though thinner wires are used. The design was then modified in order to overcome this problem.

The platform was then modified for allowing strain gauges to be attached. Figure 2.9 shows rectangular blocks being extruded from each angle, the wires are then inserted into the blocks. Strain gauges are attached to the surface of the blocks. However the disadvantage is strain gauges may not be able to measure the strain from the wires because of the large cross-section ratio between the block and the wire.

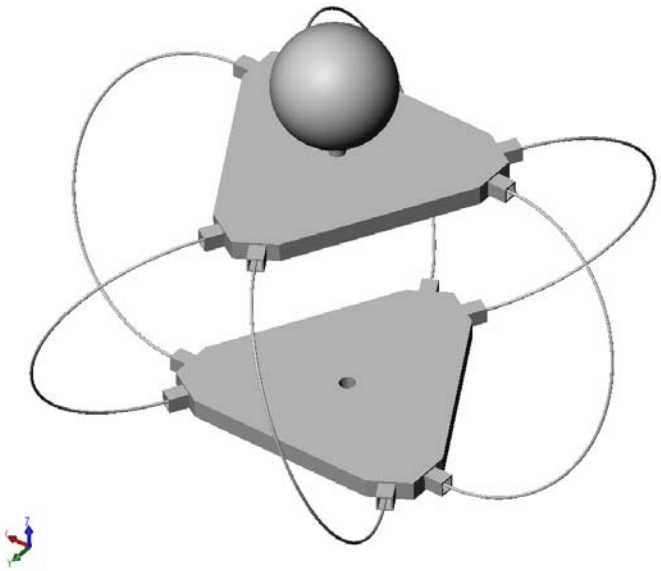

**Figure 2.9 Model with rectangular blocks.**

Another modification has been made. Each angle is cut into thin section, but still a large section is left to allow the attachment of the wires. The advantage of this design is that there is sufficient free space for the attachment of strain gauges to measure axial, bending and torsional strain. However the disadvantage is strain gauges may not be able to measure the strain from the wires because of the large cross-section ratio between the block and the wire.

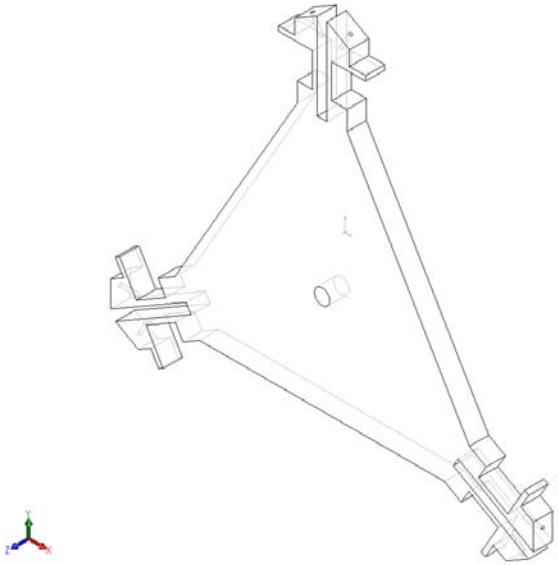

**Figure 2.10 Platform with special cut**

## 2.3 Constructing the Prototype

Another way to avoid attaching the strain gauge to the wire is to use strip with spring properties. Since strip is flat, strain gauges can be easily attached. This strip of steel has spring properties that restore the joystick to its natural position. Spring strip with different thickness, width, and length, is available from the local manufacturer.

The prototype was designed and drawn in SolidWorks. Since the spring property and hardness of the strip was unknown until several variants were tested, the size of the strips created by SolidWorks could not be precise. The result is shown in Figure 2.11.

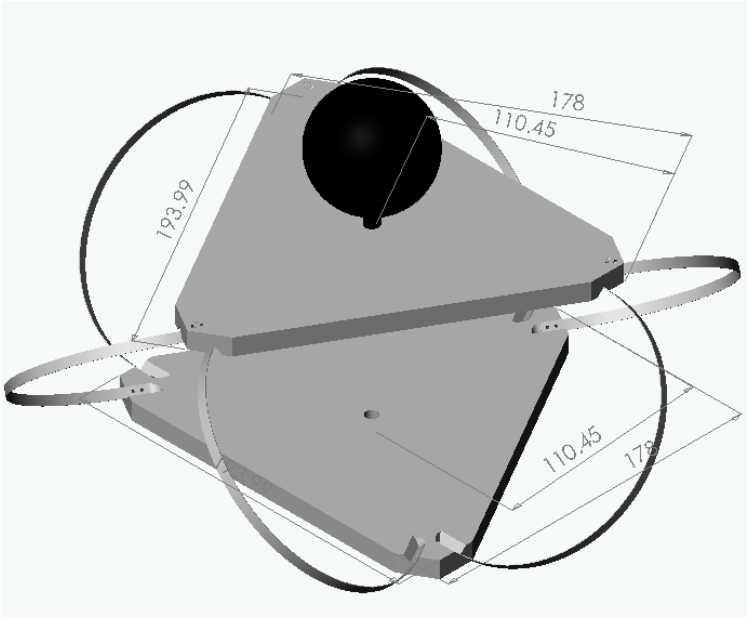


**Figure 2.11 The 6DOF hand grip (sphere) mounted on the platform that is supported by 6 spring steel strips.**

### 2.3.1 Spring Steel Strip

Spring hardness is a fix property according to the manufacturer. Stiffness of the strip depends on the thickness and the width of the strip. The chosen thickness of the strip is 0.5mm. It is the smallest thickness available from the local manufacturer. A smaller thickness makes it easier to construct the joystick, and it is discussed later. wo values of width were chosen in order to test the stiffness of the joystick, they were 4mm and 8 mm. Lengths of the strip available were250mm, 300mm, 350mm, 400mm, 450mm, 500mm, 600mm and 700mm. Unfortunately, the strips are pre-twist due to the guillotine process. This error could not be overcome as it was resulted from the manufacturing process and was very difficult to remove from spring steel without destroying the spring properties.

Several methods were considered for joining the strips to the platforms. One of the methods is to glue the strips on to the platforms. This method is the easiest way that does not require any extra machining. However the positions of the strips are hard to locate, and the glue might not be able to hold after a long period of time. Using G-clamp instead of glue is another option. However such small G-clamp is not

available in the market nor is it easy to manufacture.

Another method is to machine rectangular holes on the platforms that are slightly bigger than the size of the strip. Glue is then injected into the holes followed by the strips. This method is similar to the making of the first joystick. However, rectangular holes are very hard to machine. Hole size is also hard to decide. If the hole is made too big, it may cause twist in the strip; on the other hand, if the hole is made too small, it may not have clearance for enough glue to hold the strips.

The best method is to drill and tap holes on the platforms and also drill holes in the strips. Then fix the strips on the platforms by screwing them together. In this way, the machining process is relatively easier, and the strips can be fixed firmly to the platforms.

Two holes are to drilled at each end of the strip in order to the strip to the platforms. Spring steel is made from very hard material and it is hard to machine. The holes on the strip have to be drilled at exact locations or they will not fit those on the platform. Therefore, some other method has to be used to drill two holes at each end of spring strips in the right dimension.

A steel block is made to overcome this problem. This is shown in Figure 2.12. A slot is cut on one side of the block that will allow the strip to fit in. Two holes with exact dimension are drilled on the same side of the block. The block is then heat treated to achieve a harder status. The spring strips are then fitted in to the block, and the holes needed to be drilled on the strip could be located by the block.

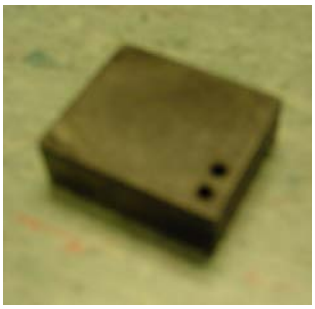

**Figure 2.12 Use of steel block to allow the strip to fit in.**

### 2.3.2 Platforms

Connecting the strips on to the two platforms causes twisting of the strip. It is necessary to connect strips and platforms so the strips are in a single plane otherwise the calculations are extraordinarily complicated and there is extra error in experiment results.

To avoid twisting the steel strips, there was a slight change in the design of the platform. Slots with an angle are machined on the platforms where they are connected with the strips. The angle is calculated so there will not be any twist in the strips due to the connection.

The dimension and structure are shown in Figure 2.13.

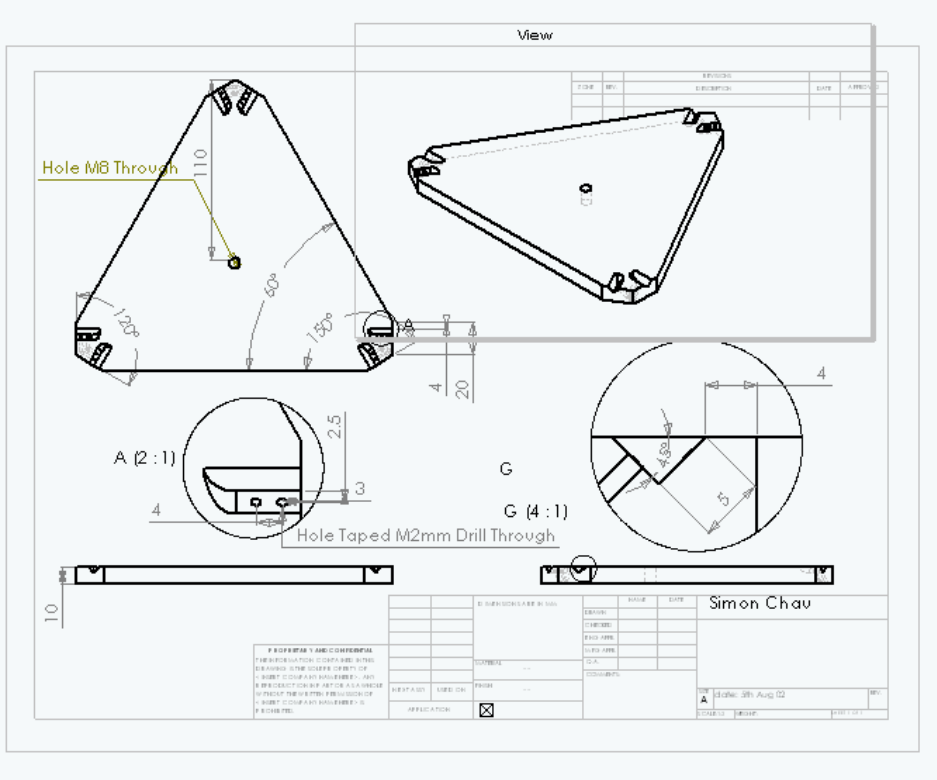


**Figure 2.13 Dimensions of the prototype platform.**

### 2.3.3 Connection Between Platforms and Strips

The strips are bolted to the platforms. Several models were made with different widths and lengths of strip.

The use of narrow and long strips results in a very flexible joystick. This is shown in Figure 2.14. This model allows large displacements, which could be an advantage, but vibration could become too large and it takes a long time to settle to its initial position. Also, if the displacement is set to a larger limit, the top platform may not be able to return to the original position after reaching certain points (permanent deformation). Increasing the width and decreasing the length of strips will result an increase in the stiffness and thus it will be harder to move the joystick. Stiff joystick using 8mm width with 200mm length proved hard to move.

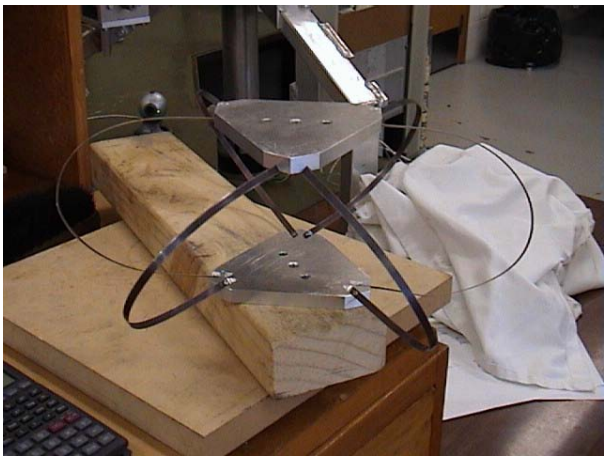

**Figure 2.14 Use of narrow long strips.**

The prototype that was finally constructed used strips of 8mm width and 400mm length. This is shown in Figure 2.15. These dimensions gave a joystick that was stiff enough, and which could return to its initial position quite easily. It is still capable of large displacements but it has small vibrations. With these dimensions, the strips formed a perfect semi-circle between the platforms; something that did not happen with other strip dimensions. This feature is important for simplifying calculations as well as for programming in ANSYS.

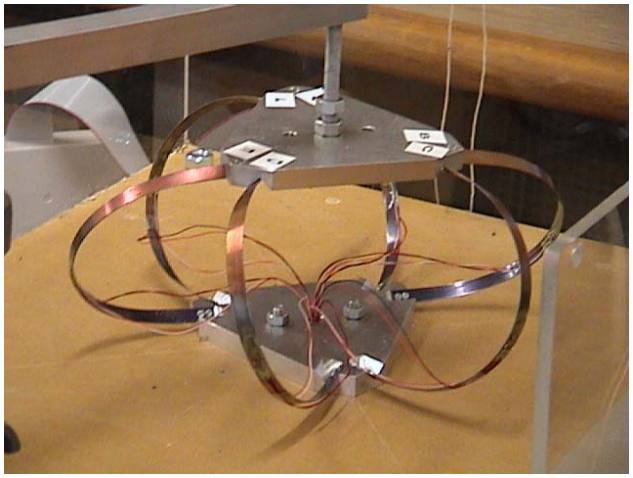

**Figure 2.15 Strips used in the prototype.**

### 2.3.4 Attaching the Strain Gauges

Two strain gauges are attached to each strip one on the inner side and one on the outer

side. It is very important that the strain gauges are properly mounted onto the spring steel strips as this ensures that the strain accurately transfers from the test specimen through the adhesive and gauge backing to the foil.

### 2.3.5 Casing of the Prototype

The strain gauges and wires are very easily damaged so some protection is required. A case was made to constrain the joystick. Dimensions of the case are 500 x 500 x 300mm. For such a large base, aluminium is costly so wood with thickness of 20mm is used to form the base. The four sides of the case are made from Perspex, which allows the users to observe the movement of the joystick. These Perspex 'walls' are drilled and counter-sunk, and then screwed on to the wooden base. The top of the case is made of wood with a 200mm diameter hole for clearance of the handle movement.

The lower platform was then bolted to the base of the case. An extra hole is drilled on the base for all the strain gauge wires to pass through. The case with prototype joystick is shown in Figure 2.16.

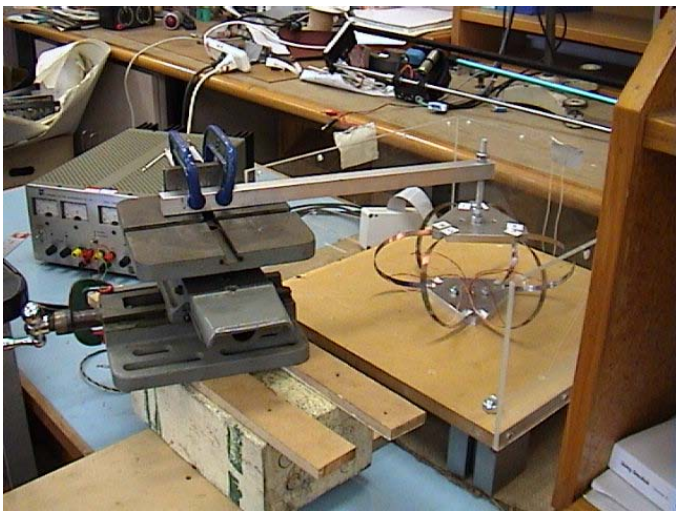

**Figure 2.16 Prototype joystick with case**

### 2.3.6 Connection Between Prototype and Computer

All the strain gauge wires are connected to bridge amplifiers. The amplifiers are shown in Figure 2.17.

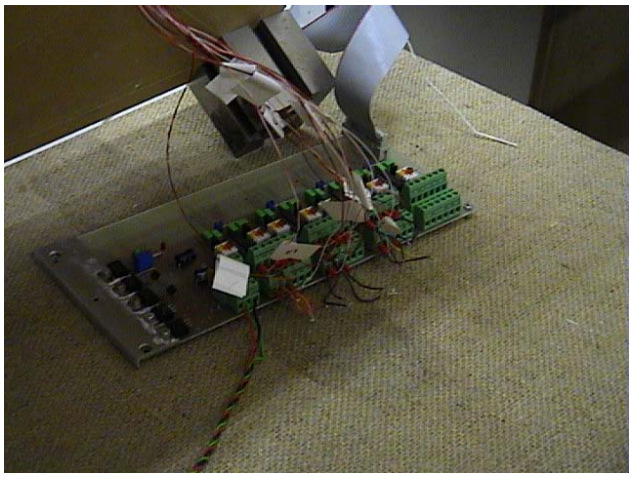

**Figure 2.17 Bridge amplifiers**

Outputs of the amplifier were then connected to a computer that was used to run DSPACE and Matlab for data collection, which shown in Figure 2.18.

**Figure 2.18 DSPACE setup for data collection.**

## 2.4 Computer Software

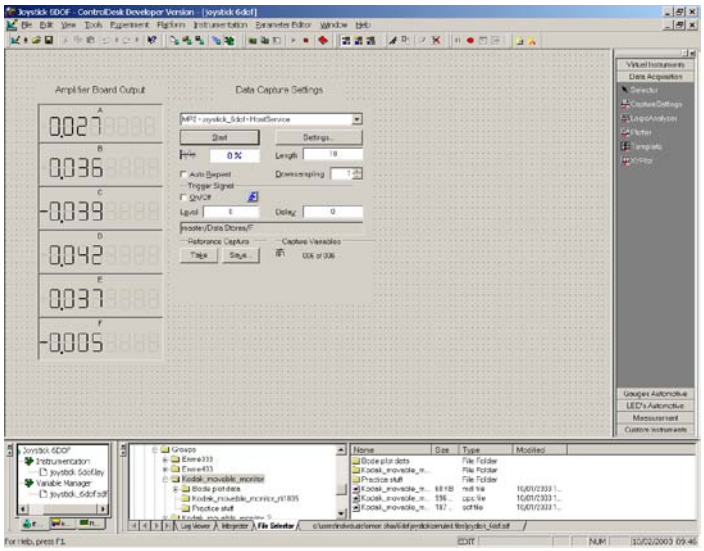


**Figure 2.19 Screen shot of the data collection**

There are two software programs for converting the measurements in to voltage readings. Simulink within the MATLAB program is used for modelling, simulating and analysing dynamic, multi-domain systems. It builds block diagram, simulates the system's behaviour, evaluates its performance, and is used to refine the design. It has a comprehensive set of features for creating models, simulating the model plus analysing and testing the model. The Simulink model was built to simulate and to analyse the analogue voltage and convert it into digital signal for display.

The main feature of the DSPACE program is that it has a real time interface that can implement Simulink diagrams on DSPACE real-time hardware with one mouse-click. It has a simple graphical I/O configuration and automatic generation of real-time code. The real-time model includes compiling, connecting and downloading, plus configuration of the real-time scheduler and the I/O. The reasons that DSPACE is selected are that it is in the laboratory and because it has the following features:

Implementation Software – implement models on DSPACE real-time hardware quickly and easily.

Experiment Software - manage, instrument and automate the experiments. (3) Production Code Generation Software – production code generation for ECU, automatic and direct from Simulink.

Single-Board Hardware – Compact prototyping systems with fast processors and comprehensive IO in one board.

Modular Hardware – Powerful platform for all requirements in the fields of function prototyping and ECU testing. Based on processor boards and I?O boards that can be extended as required.

MicroAutoBox Hardware – Compact prototyping hardware for test drives. Real time hardware, I/O and signal conditioning on board.

The virtual model for obtaining and converting the analogue readings of the strain gauges to digital signals is built using the MATLAB model. The MATLAB model is then realised using the DSPACE hardware and software.

# CHAPTER 3

# DEFLECTION THEORY

## 3.1 Introduction

Most beam deflection problems can be divided into two main category, small deflection and large deflection. Small deflection problems can be worked out mostly by solving equation using structural analysis techniques. Large deflection problems are more complicated and involved complex computations. Most large deflection problems can be solved by using finite element methods.

In this chapter, deflection theory is discussed, along with equations of calculating single beam deflections. This equation can be checked with the result obtained by using ANSYS in chapter 4.

## 3.2 Half Circular Beam

For the calculation of the single wire beam of a deflection, it is assumed the wire is a perfect circle so that only a quarter circle needs to be analysed. Constant elastic properties are assumed throughout the wire. The wire can be simulated as one end clamped. Two forces will be applied along the X and Y axes to the other end of the wire. Then the corresponding displacement at the end of the wire must be determined, as well as the strain within the beam.

### 3.2.1 Case 1

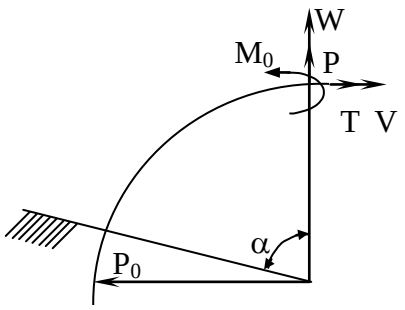


**Figure 3.1 FBD for case 1**

Displacement W =

$$\frac{R^2}{EJ}\left[ M_0(1-\cos a) + PR\left( \frac{a}{2} - \frac{\sin 2a}{4} - TR\frac{(1-\cos a)^2}{2} \right) \right]$$

**(3.1)**

Displacement V =

$$\frac{R^2}{EJ}\left[ -M_0(a-\sin a) - PR\frac{(1-\cos a)^2}{2} + TR\left( \frac{3a}{2} - 2\sin a + \frac{\sin 2a}{4} \right) \right]$$

**(3.2)**

Angular Displacement θ =

$$\frac{R}{EJ}\left[ M_0 a + PR(1-\cos a) - TR(a-\sin a) \right]$$

**(3.3)**

where M is the applied moment

R is the radius

P is the applied force

T is the applied torque

α is the angle

### 3.2.2 Case 2

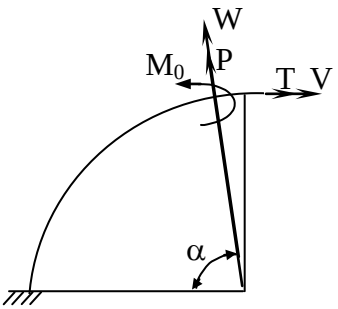


**Figure 3.2 FBD for case 2**

Displacement W =

$$\frac{R^2}{EJ}\left[\begin{array}{l} M_0(\sin a - a\cos a) + PR\left(a + \frac{1}{2}a\cos 2a - \frac{3}{4}\sin 2a\right) \\ -TR\left(\cos a - \frac{3}{4}\cos 2a - \frac{1}{2}a\sin 2a - \frac{1}{4}\right) \end{array}\right] \quad \textbf{(3.4)}$$

Displacement V =

$$\frac{R^2}{EJ}\left[\begin{array}{l} -M_0(a\sin a - 1 + \cos a) - PR\left(\cos a - \frac{3}{4}\cos 2a - \frac{1}{2}a\sin 2a - \frac{1}{4}\right) \\ +TR\left(a - \frac{1}{2}a\cos 2a + \frac{3}{4}\sin 2a - 2\sin a\right) \end{array}\right] \quad \textbf{(3.5)}$$

Angular Displacement θ =

$$\frac{R}{EJ}\left[M_0 a + PR(\sin a - a\cos a) - TR(a\sin a - 1 + \cos a)\right] \quad \textbf{(3.6)}$$

where M is the applied moment

R is the radius

P is the applied force

T is the applied torque

α is the angle

### 3.2.3 Case 3

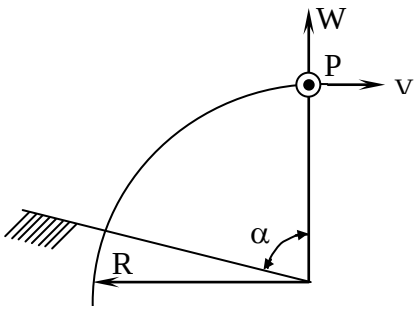


**Figure 3.3 FBD for case 3**

Displacement perpendicular to plane WV

$$\frac{PR^3}{EJ}\left(\frac{1+3\lambda}{2}a+\frac{\lambda-1}{4}\sin 2a-2\lambda\sin a\right) \tag{3.7}$$

Angular Displacement along V-axis

$$\frac{PR^3}{EJ}\left(\frac{\lambda-1}{2}\sin 2a+\frac{\lambda+1}{2}a-\lambda\sin a\right) \tag{3.8}$$

Angular Displacement along W-axis

$$\frac{PR^3}{EJ}\left(\frac{\lambda-1}{2}\sin^2 a+\lambda(1-\cos a)\right) \tag{3.9}$$

where P is the applied force

$\alpha$ is the angle

### 3.2.4 Case 4

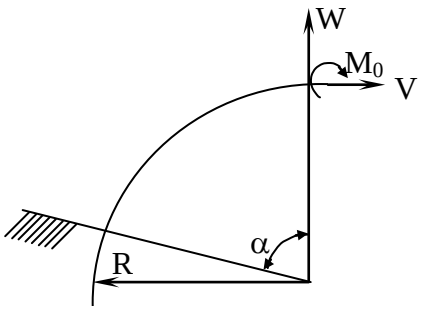


**Figure 3.4 FBD for case 4**

Displacement perpendicular to plane WV

$$\frac{M_0 R^2}{EJ}\left(\frac{\lambda-1}{4}\sin 2a+\frac{\lambda+1}{2}a-\lambda\sin a\right) \quad \textbf{(3.10)}$$

Angular Displacement along V-axis

$$\frac{M_0 R}{EJ}\left(\frac{\lambda+1}{2}+\frac{\lambda-1}{2}\sin 2a\right) \quad \textbf{(3.11)}$$

Angular Displacement along W-axis

$$\frac{M_0 R}{EJ}\left(\frac{\lambda-1}{2}\sin^2 a\right) \quad \textbf{(3.12)}$$

where M is the applied moment

R is the radius

$\alpha$ is the angle

### 3.2.5 Case 5

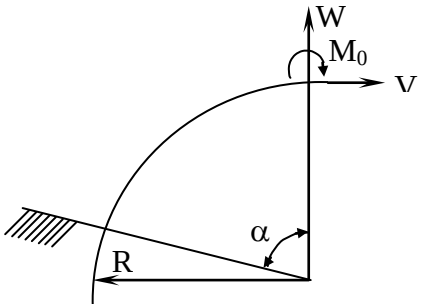


**Figure 3.5 FBD for case 5**

Displacement perpendicular to plane WV

$$\frac{M_0 R^2}{EJ}\left(\frac{\lambda-1}{2}\sin^2 a+\lambda(1-\cos a)\right) \tag{3.13}$$

Angular Displacement along V-axis

$$\frac{M_0 R}{EJ}\left(\frac{\lambda-1}{2}\sin^2 a\right) \tag{3.14}$$

Angular Displacement along W-axis

$$\frac{M_0 R}{EJ}\left(\frac{\lambda+1}{2}a-\frac{\lambda-1}{4}\sin 2a\right) \tag{3.15}$$

where M is the applied moment

R is the radius

α is the angle

### 3.2.6 Results

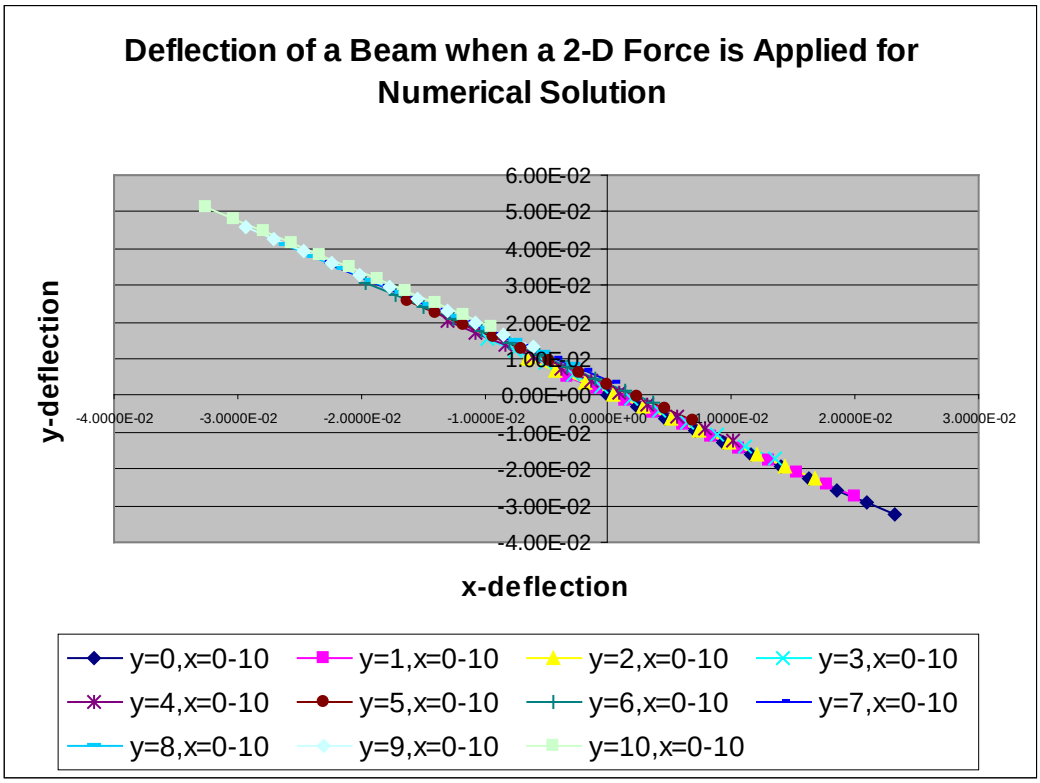


**Figure 3.6 Results of a 2-D Force beam deflection.**

This result will be compared to result obtain from ANSYS in section 4.5.2

## 3.3 Large Deflection of Beams

Large deflections problem continues to be researched. The problem here is to develop methods and equations to calculate the beam deflection under three forces and three torques. However, three dimensional deflection is extremely hard to modelling using mathematical methods.

In this section, beam deflection under two forces and a moment is discussed, which is the current state of this field. As this topic continues to be researched for doctoral theses, a full solution is outside the scope of this thesis. A simplified approach is

used here as beam theory only contributes to rather than defines the objectives of this master thesis.

To develop a model for large deflections of a flexural section, the actual deflections are determined (in closed form if possible, otherwise numerically), and appropriate dimensions for a pseudo rigid body model are determined through optimization. The Benoulli-Euler beam equation, which states that the moment at any point in a beam is proportional to its curvature at that point, can be used to solve large deflection problems. The Bernoulli-Euler equation can be written as

$$M = EI\frac{d\theta}{ds} = EI\frac{\frac{d^2y}{dx^2}}{(1+(\frac{dy}{dx})^2)^{3/2}} \tag{3.16}$$

where M is the moment, dθ/ds is the rate of change of angular deflection along the beam, EI is the flexural rigidity of the beam, x is the distance along the undeflected beam axis, and y is the transverse deflection. For small deflections, dy/dx is small, and so $(dy/dx)^2$ can be neglected, leading to the standard linearized beam theory. However, in large deflections such as are seen in compliant mechanisms, this term is large and may not be neglected. In this case, Eq. 3.16 may be solved either through a classical method using elliptic integrals [3,8 – 10] or numerically [4,5]. The elliptic integral solutions are used here, as they provide a simple method of determining when an inflection point will occur.

Equation 3.16 can be rewritten as

$$\frac{d\theta}{ds} = \pm\sqrt{2\frac{P}{EI}(-\sin\theta + n\cos\theta + \sin\theta_o - n\cos\theta_o) + (\frac{M_o}{EI})^2} \tag{3.17}$$

the loads P, $P_n$, and $M_o$, and n defines the ratio between the horizontal and vertical forces. In the following discussion, P is assumed to be positive, and $M_o$ is assumed to be negative. The arc length s is measured from the fixed end of the beam, the angle θ(s) is measured from the x axis at a distance s along the beam, and $\theta_o$ is the angle of the free end of the beam. The sign of dθ/ds is determined by $\theta_o$ and the loading conditions. If no inflection point exists, the slope is either monotonically increasing or decreasing, dθ/ds must always be positive or negative, respectively. In this case, the sign of dθ/ds is equal to the sign of $\theta_o$. If an inflection point exists, then dθ/ds is positive before the inflection point and negative after. Separating variables, Eq. 3.17 can be written as

$$\sqrt{\frac{P}{EI}}ds = \pm\frac{d\theta}{\sqrt{2(-\sin\theta + n\cos\theta + \sin\theta_o - n\cos\theta_o) + \frac{M_o^2}{PEI}}} \tag{3.18}$$

Defining the following non-dimensional constants,

$$\alpha = \sqrt{\frac{Pl^2}{EI}} \qquad \kappa = \frac{1}{2}\frac{M_o^2}{PEI} \tag{3.19}$$

Eq.3.18 may be written as:

$$\frac{\alpha}{l}ds = \pm\frac{d\theta}{\sqrt{2}\sqrt{-\sin\theta + n\cos\theta + \sin\theta_o - n\cos\theta_o + \kappa}} \tag{3.20}$$

Integrating Eq. 3.20 and defining:

$$\lambda = \sin\theta_o - n\cos\theta_o + \kappa \tag{3.21}$$

yields a relationship between the angle of the free end of beam $\theta_o$, and the applied factor $\alpha$,

$$\alpha = \pm \frac{1}{\sqrt{2}} \int_0^{\theta_o} \frac{d\theta}{\sqrt{\lambda - \sin\theta + n\cos\theta}}$$

**(3.22)**

The plus or minus sign is chosen as follows: positive for monotonically increasing slope and negative for monotonically decreasing slope. This sign convention ensures that $\alpha$ is always positive (when is $\theta_o$ negative, because the upper limit of integration is less than the lower). This is consistent with the definition of a $\alpha$ given in Eq. 3.19, where $\alpha$ is a square root which must always be positive.

To find the x and y displacements of the beam tip, $d\theta/ds$ can be rewritten as:

$$\frac{d\theta}{ds} = \frac{d\theta}{dx}\frac{dx}{ds} = \frac{d\theta}{dx}\cos\theta,$$
$$\frac{d\theta}{ds} = \frac{d\theta}{dy}\frac{dy}{ds} = \frac{d\theta}{dy}\sin\theta$$

**(3.23)**

Using Eq. 3.23 and Eq. 3.21, Eq. 3.20 can be written as:

$$\frac{x_o}{l} = \pm \frac{1}{\alpha\sqrt{2}} \int_0^{\theta_o} \frac{\cos\theta d\theta}{\sqrt{\lambda - \sin\theta + n\cos\theta}}$$

**(3.24)**

$$\frac{y_o}{l} = \pm \frac{1}{\alpha\sqrt{2}} \int_0^{\theta_o} \frac{\sin\theta d\theta}{\sqrt{\lambda - \sin\theta + n\cos\theta}}$$

**(3.25)**

where $(x_o,y_o)$ represent the deflected position of the free end of the beam, as shown

in Figure 3.7.

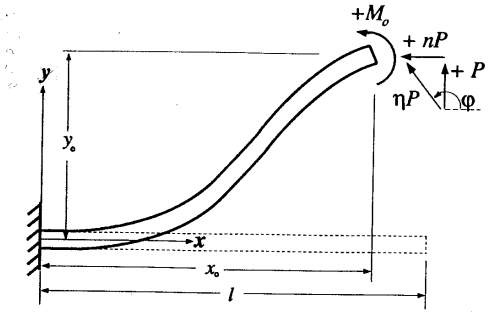


**Figure 3.7 Cantilever Beam**

Equations 3.22, 3.24 and 3.25 are functions of θ. If no inflection point exists, θ(s) is either a monotonically increasing or monotonically decreasing function. However, if an inflection point exists, θ(s) is no longer a monotonic function. That is θ(s) increases from zero to $\theta_i$ , and then decreases from $\theta_i$ to $\theta_o$, where $\theta_i$ is always greater than $\theta_o$. In this case, the integrals must be split into two parts. Specifically, dθ/ds is positive from the fixed end until the inflection point, where dθ/ds=0. After the inflection point, dθ/ds is negative. Therefore, in the first part of the integral, the positive signs of Equations 3.22, 3.24 and 3.25 are taken, whereas for the second part, the negative signs are taken. Even if no inflection point exists in the beam, the inflection point angle can still be defined mathematically. It will be shown in the next section that the above integrals must still be split into two parts, integrating from zero to the inflection point, and from the inflection point to the end of the beam. It should be noted that in the solution procedure, the inflection point never actually needs to be calculated; it drops out of the equations. By splitting integrals into two parts and taking into account the sign conventions described above, Equations 3.22, 3.24 and 3.25 can be written as follows:

Inflection Point Exists | No Inflection Point Exists

$$\alpha = \frac{1}{\sqrt{2}}\left(\int_0^{\theta_i}\frac{d\theta}{f(\theta)} + \int_{\theta_o}^{\theta_i}\frac{d\theta}{f(\theta)}\right) \qquad \alpha = \pm\frac{1}{\sqrt{2}}\left(\int_0^{\theta_i}\frac{d\theta}{f(\theta)} + \int_{\theta_o}^{\theta_i}\frac{d\theta}{f(\theta)}\right) \tag{3.26}$$

$$\frac{x_o}{l} = \frac{1}{\alpha\sqrt{2}}\left(\int_0^{\theta_i}\frac{\cos\theta}{f(\theta)}d\theta + \int_{\theta_o}^{\theta_i}\frac{\cos\theta}{f(\theta)}d\theta\right) \text{ or } \frac{x_o}{l} = \pm\frac{1}{\alpha\sqrt{2}}\left(\int_0^{\theta_i}\frac{\cos\theta}{f(\theta)}d\theta + \int_{\theta_o}^{\theta_i}\frac{\cos\theta}{f(\theta)}d\theta\right) \tag{3.27}$$

$$\frac{y_o}{l} = \frac{1}{\alpha\sqrt{2}}\left(\int_0^{\theta_i}\frac{\sin\theta}{f(\theta)}d\theta + \int_{\theta_o}^{\theta_i}\frac{\sin\theta}{f(\theta)}\right) \qquad \frac{y_o}{l} = \pm\frac{1}{\alpha\sqrt{2}}\left(\int_0^{\theta_i}\frac{\sin\theta}{f(\theta)}d\theta + \int_{\theta_o}^{\theta_i}\frac{\sin\theta}{f(\theta)}\right) \tag{3.28}$$

where

$$f(\theta) = \sqrt{\lambda - \sin\theta + n\cos\theta} \tag{3.29}$$

At the inflection point, the moment and the rate of change of slope dθ/ds, are both zero. Setting Eq 3.17 to zero gives the following relationship that must be satisfied at the inflection point:

$$\lambda - \sin\theta_i + n\cos\theta_i = 0 \tag{3.29}$$

Using equation 3.26, 3.27 and 3.28, $\alpha$, $x_o$ and $y_o$ can be determined. However, these equations are valid for two dimensional calculations. The actual movement of the wire is three dimensional, there are also 6 of them interact with each other. Using large beam deflection theory to calculate the deflection of the platform is not possible at this stage. The alternative is to use finite element method to do the calculation, and it will be discussed in the next chapter.

# CHAPTER 4

# FINITE ELEMENT SOFTWARE

## 4.1 Introduction

In chapter 3, theoretical methods for solving the beam problem were discussed, and it was concluded that calculating the deflection of a beam subject to 3 forces and 3 torques could not be done. In this chapter, a finite element package is used to model the prototype, as well as a single beam that was calculated mathematically in last chapter.

The ANSYS finite element analysis (FEA) software enables engineers to perform the following tasks:

- Build computer models in FEA by transferring CAD models of structures, products, components, or systems.
- Apply operating loads or other design performance conditions.
- Study physical responses, such as stress levels, temperature distributions, or electromagnetic fields.
- Optimize a design early in the development process to reduce production costs.
- Do prototype testing in environments where it otherwise would be undesirable or impossible (for example, biomedical applications).

## 4.2 Finite Element Overview

The ultimate purpose of a finite element analysis is to re-create mathematically the behaviour of an actual engineering system. In other words, the analysis must be an accurate mathematical *model* of a physical prototype. In the broadest sense, this

model comprises all the nodes, elements, material properties, real constants, boundary conditions, and other features that are used to represent the physical system.

The ANSYS program has many finite element analysis capabilities, ranging from a simple, linear, static analysis to a complex, nonlinear, transient dynamic analysis. The analysis guide manuals in the ANSYS documentation set describe specific procedures for performing analyses for different engineering disciplines.

The following subsections detail some basic operations of ANSYS to construct a typical model.

### 4.2.1 Build the Model

Building a finite element model requires more time than any other part of the analysis. First, specify a jobname and analysis title. Then, use the PREP7 preprocessor to define the element types, element real constants, material properties, and the model geometry.

### 4.2.2 Defining Element Types

The ANSYS element library contains more than 150 different element types. Each element type has a unique number and a prefix that identifies the element category: beam4, beam 24, beam188.

The element type determines, among other things:

- The degree-of-freedom set (which in turn implies the discipline--structural, thermal, magnetic, electric, quadrilateral, brick, etc.)
- Whether the element lies in two-dimensional or three-dimensional space.

The ANSYS model being built for modelling the prototype used beam 4 and shell 43.

BEAM 4 is a uniaxial element with tension, compression, torsion, and bending capabilities. The element has six degrees of freedom at each node: translations in the nodal x, y, and z directions and rotations about the nodal x, y, and z axes. Stress stiffening and large deflection capabilities are included. A consistent tangent stiffness matrix option is available for use in large deflection (finite rotation) analyses.

Shell 43 is well suited to model linear, warped, moderately-thick shell structures. The element has six degrees of freedom at each node: translations in the nodal x, y, and z directions and rotations about the nodal x, y, and z axes. The deformation shapes are linear in both in-plane directions. For the out-of-plane motion, it uses a mixed interpolation of tensorial components.

### 4.2.3 Defining Element Real Constants

Element real constants are properties that depend on the element type, such as cross-sectional properties of a beam element. For example, beam 4 is defined by two or three nodes, the cross-sectional area, two area moments of inertia (IZZ and IYY), two thicknesses (TKY and TKZ), an angle of orientation (θ) about the element x-axis, the torsional moment of inertia (IXX), and the material properties. If IXX is not specified or is equal to 0.0, it is assumed equal to the polar moment of inertia (IYY+IZZ). IXX should be positive and is usually less than the polar moment of inertia. The element torsional stiffness decreases with decreasing values of IXX. An added mass per unit length may be input with the ADDMAS value.

### 4.2.4 Defining Material Properties

Most element types require material properties. Depending on the application,

material properties can be linear or non-linear. Linear material properties can be constant or temperature-dependent, and isotropic or orthotropic. Nonlinear material properties are usually tabular data, such as plasticity data (stress-strain curves for different hardening laws), magnetic field data (B-H curves), creep data, swelling data, hyperelastic material data, etc.

As with element types and real constants, each set of material properties has a material reference number. The table of material reference numbers versus material property sets is called the material table. Within one analysis, it may have multiple material property sets (to correspond with multiple materials used in the model). ANSYS identifies each set with a unique reference number.

### 4.2.5 Creating the Model Geometry

There are two methods to create the finite element model: solid modeling and direct generation. With solid modelling, the geometric shape of the model is described, then the ANSYS program instructed to automatically *mesh* the geometry with nodes and elements. The size and shape can be controlled in the elements that the program creates. With direct generation, the location of each node and the connectivity of each element is ‘manually’ defined. Several convenience operations, such as copying patterns of existing nodes and elements, symmetry reflection, etc. are available. The model of prototype is created by solid modelling.

### 4.2.6 Keypoints

When building a model from the bottom up, it starts with defining the lowest-order solid model entities, keypoints. Keypoints are defined within the currently active coordinate system. Lines, areas, and volumes can then be defined to connect to these keypoints. There is no need to explicitly define all entities in ascending order to create higher-order entities: areas and volumes can be defineed directly in terms of

the keypoints at their vertices. The intermediate entities will then be generated automatically as needed.

### 4.2.7 Lines

Lines are mainly used to represent the edges of an object. As with keypoints, lines are defined within the currently active coordinate system. It is no need to define all lines explicitly, because the program will generate the necessary lines in many instances when an area or volume is defined. Lines are required to generate line elements (such as beams) or to create areas from lines.

### 4.2.8 Areas

Flat areas are used to represent 2-D solid objects (such as flat plates or axisymmetric solids). Curved as well as flat areas are used to represent 3-D surfaces, such as shells, and the faces of 3-D solid objects. Areas are required to use area elements or to create volumes from areas. Most commands that create areas will also automatically generate the necessary lines and keypoints; similarly, many areas can be conveniently generated by defining volumes.

### 4.2.9 Meshing

Before meshing the model, and even before building the model, it is important to think about whether a free mesh or a mapped mesh is appropriate for the analysis. A free mesh has no restrictions in terms of element shapes, and has no specified pattern applied to it. Compared to a free mesh, a mapped mesh is restricted in terms of the element shape it contains and the pattern of the mesh. A mapped area mesh contains either only quadrilateral or only triangular elements, while a mapped volume mesh contains only hexahedron elements. In addition, a mapped mesh typically has a regular pattern, with obvious rows of elements.

### 4.2.10 Applying Loads

The word loads as used in ANSYS documentation includes boundary conditions (constraints, supports, or boundary field specifications) as well as other externally and internally applied loads. Loads in the ANSYS program are divided into six categories:

- DOF Constraints
- Forces
- Surface Loads
- Body Loads
- Inertia Loads
- Coupled-field Loads

Most of these loads can be applied either on the solid model (keypoints, lines, and areas) or the finite element model (nodes and elements).

### 4.2.11 DOF Constraints

DOF constrain shows the degrees of freedom that can be constrained in each discipline and the corresponding ANSYS labels. Any directions implied by the labels (such as UX, ROTZ, AY, etc.) are in the nodal coordinate system.

In the modelling of the prototype, all 6 spring strip are constrained to where they connect to the bottom platform.

### 4.2.12 Forces (Concentrated Loads)

Forces available in each discipline show a list of forces available in each discipline and the corresponding ANSYS labels. Any directions implied by the labels (such as FX, MZ, CSGY, etc.) are in the nodal coordinate system. In the modelling of the prototype, forces are applied at the top of the platforms.

### 4.2.13 Getting resolution

In the solution phase of the analysis, the computer takes over and solves the simultaneous set of equations that the finite element method generates. The results of the solution are:

- Nodal degree-of-freedom values, which form the primary solution
- Derived values, which form the element solution

The element solution is usually calculated at the elements' integration points. The ANSYS program writes the results to the database as well as to the results file.

Several methods of solving the system of simultaneous equations are available in the ANSYS program: sparse direct solution, frontal direct solution, Jacobi Conjugate Gradient (JCG) solution, Incomplete Cholesky Conjugate Gradient (ICCG) solution, Preconditioned Conjugate Gradient (PCG) solution, and an automatic iterative solver option (ITER) . The sparse direct solver is the default , except for the generation pass of a substructure analysis and for electromagnetic analyses (which use the frontal direct solver).

## 4.3 Basic Information about Nonlinear Analysis

ANSYS employs the "Newton-Raphson " approach to solve nonlinear problems. In this approach, the load is subdivided into a series of load increments. The load increments can be applied over several load steps. Newton-Raphson Approach illustrates the use of Newton-Raphson equilibrium iterations in a single DOF nonlinear analysis.

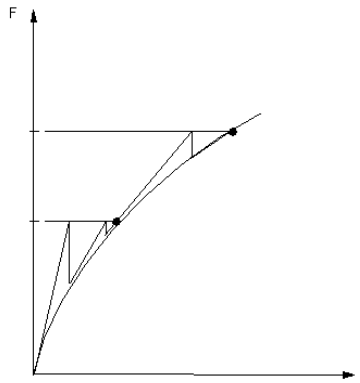


**Figure 4.1 Use of Newton-Raphson Method**

Before each solution, the Newton-Raphson method evaluates the out-of-balance load vector, which is the difference between the restoring forces (the loads corresponding to the element stresses) and the applied loads. The program then performs a linear solution, using the out-of-balance loads, and checks for convergence. If convergence criteria are not satisfied, the out-of-balance load vector is re-evaluated, the stiffness matrix is updated, and a new solution is obtained. This iterative procedure continues until the problem converges.

A number of convergence-enhancement and recovery features, such as line search, automatic load stepping, and bisection, can be activated to help the problem to converge. If convergence cannot be achieved, then the program attempts to solve with a smaller load increment.

In some nonlinear static analyses, if you use the Newton-Raphson method alone, the tangent stiffness matrix may become singular (or non-unique), causing severe convergence difficulties. Such occurrences include nonlinear buckling analyses in which the structure either collapses completely or "snaps through" to another stable configuration. For such situations, an alternative iteration scheme, the arc-length method, is activated to help avoid bifurcation points and to track unloading.

The arc-length method causes the Newton-Raphson equilibrium iterations to

converge along an arc, thereby often preventing divergence, even when the slope of the load vs. deflection curve becomes zero or negative.

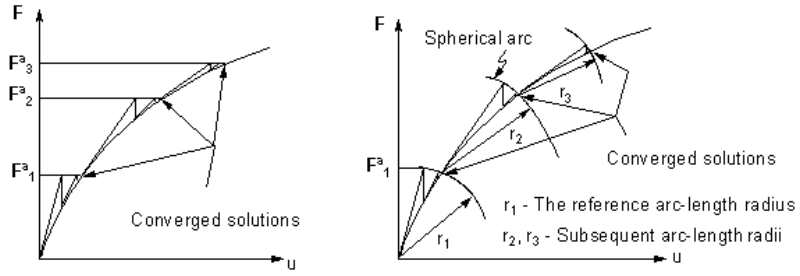


**Figure 4.2 Traditional Newton-Raphson Method vs. Arc-Length Method**

To summarize, a nonlinear analysis is organized into three levels of operation:

- The "top" level consists of the load steps that are defined explicitly over a "time" span. Loads are assumed to vary linearly within load steps.
- Within each load step, the program can be directed to perform several solutions (substeps or time steps) to apply the load gradually.

At each substep, the program will perform a number of equilibrium iterations to obtain a converged solution

## 4.4 Limitation of ANSYS

If a simple canti lever beam is consider. It has square cross section of 0.1m widths, 2m length, with E=207x$10^9$, is subject to a load of 10N at the end. Using the numerical solution:

$$Displacement = \frac{Pl^3}{3E\left(\frac{bd^3}{12}\right)} = 1.5458937198 * 10^{-5} \quad \textbf{(4.1)}$$

Using ANSYS, with 100 mesh, the result is $-1.5459 \times 10^{-5}$. However, with 1000 mesh, the result becomes $-1.5439 \times 10^{-5}$. The results is shown in the following table:

| Mesh | Result |
|---|---|
| 100 | -1.5459000000E-05 |
| 500 | -1.5457000000E-05 |
| 750 | -1.5459000000E-05 |
| 850 | -1.5465000000E-05 |
| 950 | -1.5458000000E-05 |
| 990 | -1.5488000000E-05 |
| 991 | -1.5423000000E-05 |
| 992 | -1.5454000000E-05 |
| 993 | -1.5466000000E-05 |
| 994 | -1.5476000000E-05 |
| 995 | -1.5474000000E-05 |
| 996 | -1.5465000000E-05 |
| 997 | -1.5470000000E-05 |
| 998 | -1.5475000000E-05 |
| 999 | -1.5443000000E-05 |
| 1000 | -1.5439000000E-05 |

**Table 4.1 Limitations of using ANSYS**

Notice that from 750 mesh to 995 mesh there is an increase in displacement value. However the result drops at 996 mesh and increase again at 997 mesh.

From the above result, it shows that there are errors in ANSYS, when the number of mesh hits a certain lvel, it will not converge. The users of ANSYS should keep that in mind while using this program.

## 4.5 Modelling Sample: Single beam

This model is one half of a circular beam, with one end clamped, and two forces (X, Y directions) are applied to another end. This model is constructed for checking if the theoretical results match the ANSYS results.

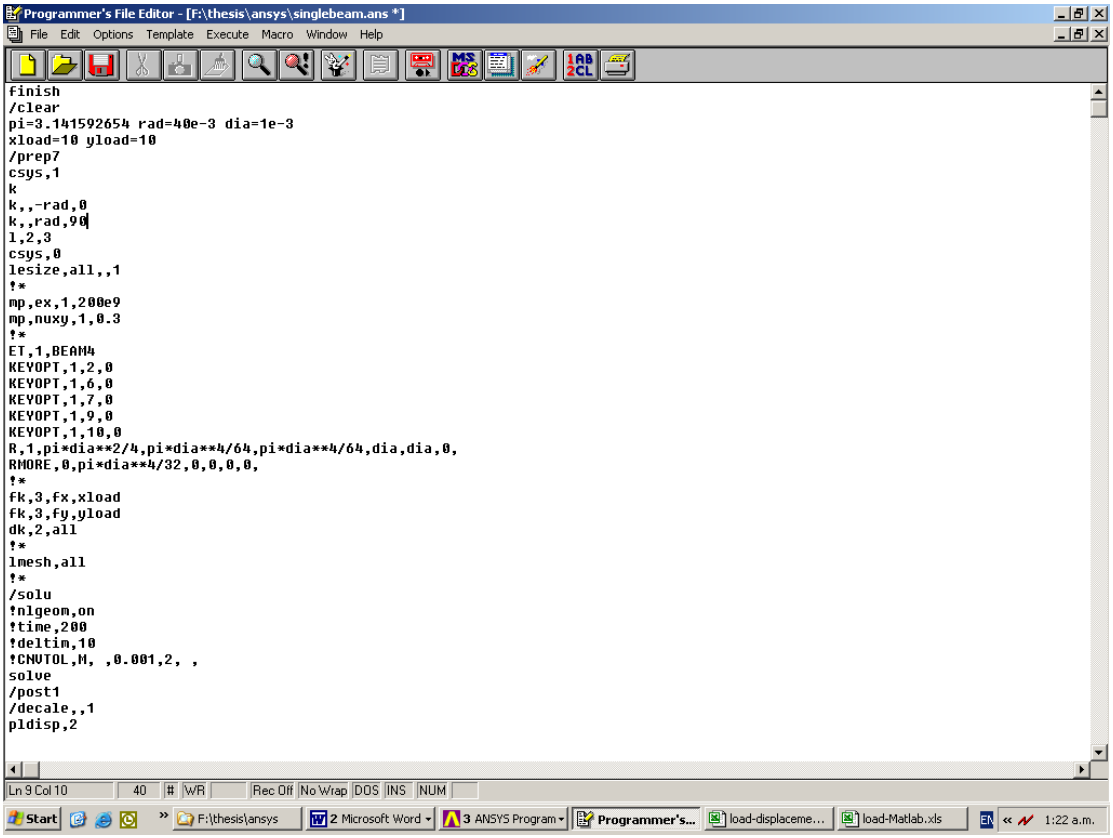


**Figure 4.3 Scripts of ANSYS to create the model**

Figure 4.3 shows the program created for constructing the beam model. The model is constructed base on joining a line of quarter of a circle thru 2 key points. The key points are at (0,0,0) and (-40,40,0). The curve beam has a radius of curvature of 40mm. The cross-section diameter of the beam is 1mm. Thus the cross-section area of the beam is $\pi(0.001)^2/4$, and the second moment of area is $\pi(0.001)^4/64$.

The element type being used for this particular case is BEAM 4 Element. BEAM4 is a uniaxial element with tension, compression, torsion, and bending capabilities. The element has six degrees of freedom at each node: translations in the nodal x, y, and z directions and rotations about the nodal x, y, and z axes. Stress stiffening and large deflection capabilities are included. A consistent tangent stiffness matrix option is available for use in large deflection (finite rotation) analyses. The Young's Modules of the beam is set to be $210 \times 10^9$ with Possion Ratio of 0.3. These are standard properties values for steel elements.

Two forces are applied at key point two, with co-ordinate (-40,40,0). The initial magnitudes of the forces are set to be both 2 x 9.81 N. The directions of the forces are one in positive X-direction and one in negative Y-direction. The magnitude of the forces applied are then vary so the data obtained by ANSYS can then be compared to the data obtain by the numerical method. The values of forces range from 0N to 10N. Displacement constrains are added to key point one, with co-ordinate (0,0,0) in the X, Y, Z direction.

The default mesh controls that the ANSYS program uses sometimes produce a mesh that is adequate for the model being analysing in which there is no need to specify any mesh controls. However, if mesh control is needed, it must be set before meshing the solid model. Mesh controls establish such factors as the element shape, midside node placement, and element size to be used in meshing the solid model. This step is one of the most important of the entire analysis, since decisions being made at this stage in the model development can profoundly affect the accuracy and economy of the analysis.

The beam under investigation was meshed with 90 elements, and 91 nodes.

### 4.5.1 Result

The results are shown below in tabulated form.

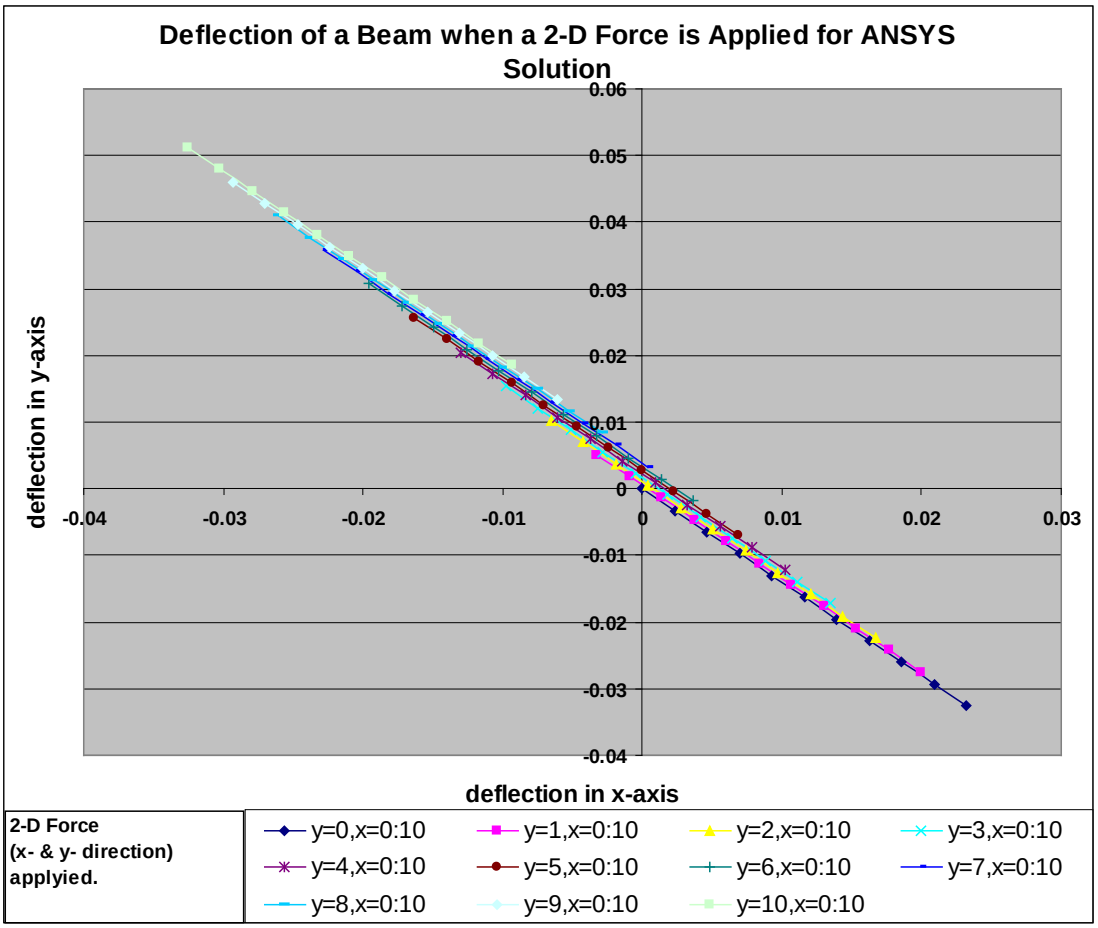


**Figure 4.4 Results of the ANSYS analysis of a 2-D Force Beam deflection**

### 4.5.2 Discussion

The above result shows the exact results obtained from numerical solution as discussed in chapter 3. It proved that the equations that were used are valid.

ANSYS simulation results are illustrated in the following figures. Figure 4.5 shows the deflections of a curved beam when a 2-dimensional force is applied at the tip of the beam. Axes of the graph correspond to the deviations in the x- and y- directions respectively (difference of the original bent position). The plotted data are a series of

forces applied to the beam. For instance, y=0,x=0:10 indicates a force of 0 N in y direction and a force in x direction (gradually from 0 to 10 N are applied).

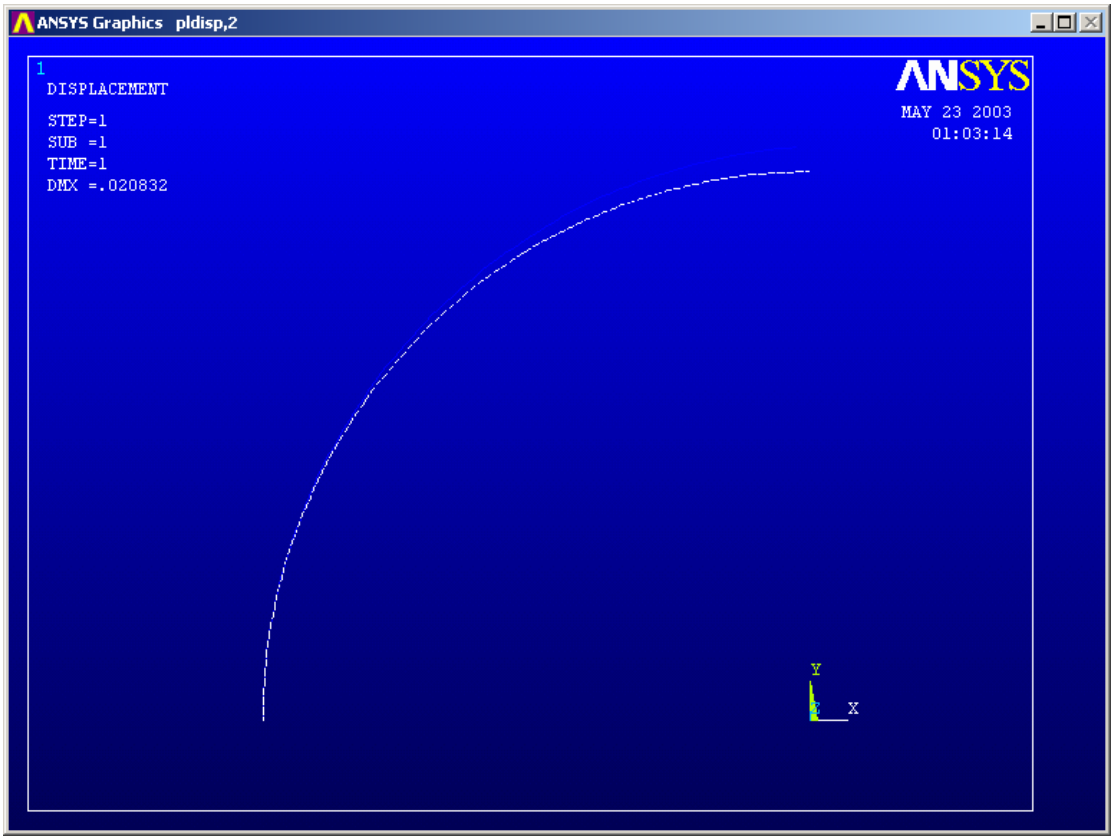


**Figure 4.5 Simulation model of ANSYS**

It is interesting to note that some of the deviations have negative values even though only 'positive' forces were applied. As an illustration, when a force of 1 N is applied in the x-direction while $F_y$= 0 N, the displacement deviation in the x-direction is positive, but the deviation in the y-direction is negative. This is because as force is applied along the positive x-direction, the beam will deflect toward the positive x-direction. The length of the beam is fixed, so to increase deflection in x-direction the beam has to deflect along the negative y-direction.

The result also shows that the beam will deflect either in the positive x-direction or in the positive y-direction, but will never deflect in both directions. The expansion case is similar to above. There are deflections alone both positive x and y-direction,

meaning that the beam has extended its own length, but that is not going to be happen since the length of the beam is fixed

## 4.6 Prototype Modelling

The prototype model was constructed according to the actual size and geometric of the joystick. Figure4. shows the model that was constructed by using ANSYS. The dotted white line is the original position of the joystick, the solid blue line is the deflected shape after a displacement constrain has been added.

In the actually experiment of the prototype, strain gauges are attached to the 6 stripes, and it gives an output voltage that will be display on screen. The voltage cannot be calculated using ANSYS, the closest relate to voltage is strain. Therefore, the graphs of displacement of the top plate against the strain of 6 strips will be drawn, as shown in Figure 4.6. The ANSYS script is listed in Appendix B.2

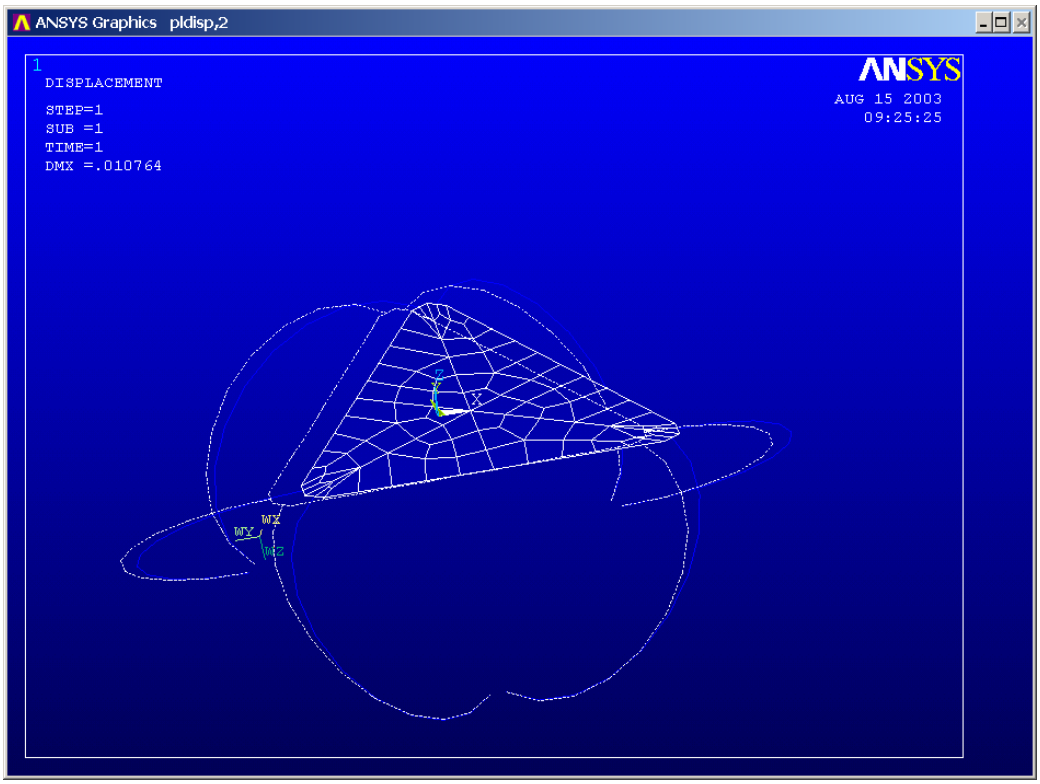


**Figure 4.6 Prototype Model constructed by using ANSYS**

### 4.6.1 Result

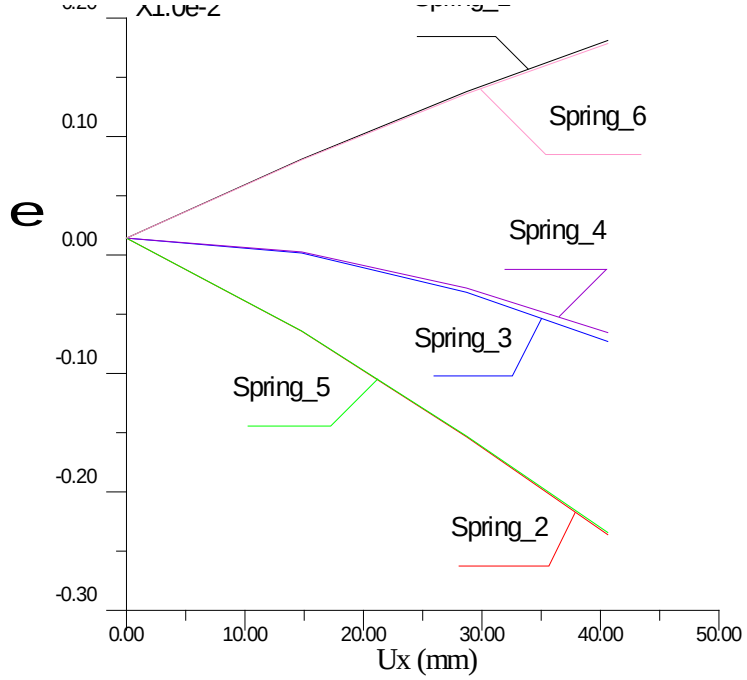


**Figure 4.7 Graph of Displacement VS Strain in X-Axis**

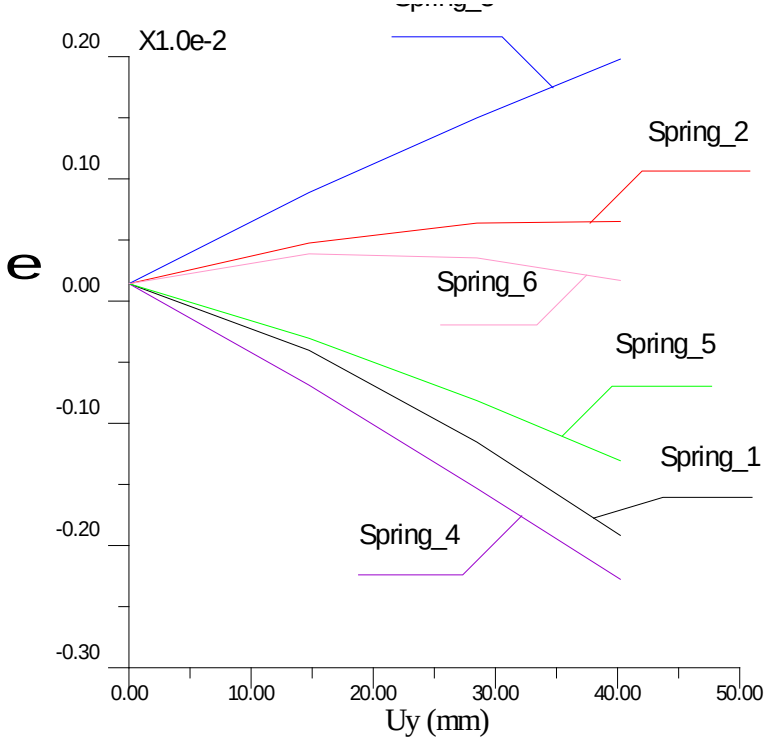


**Figure 4.8 Graph of Linear Displacement VS Strain in Y-Axis**

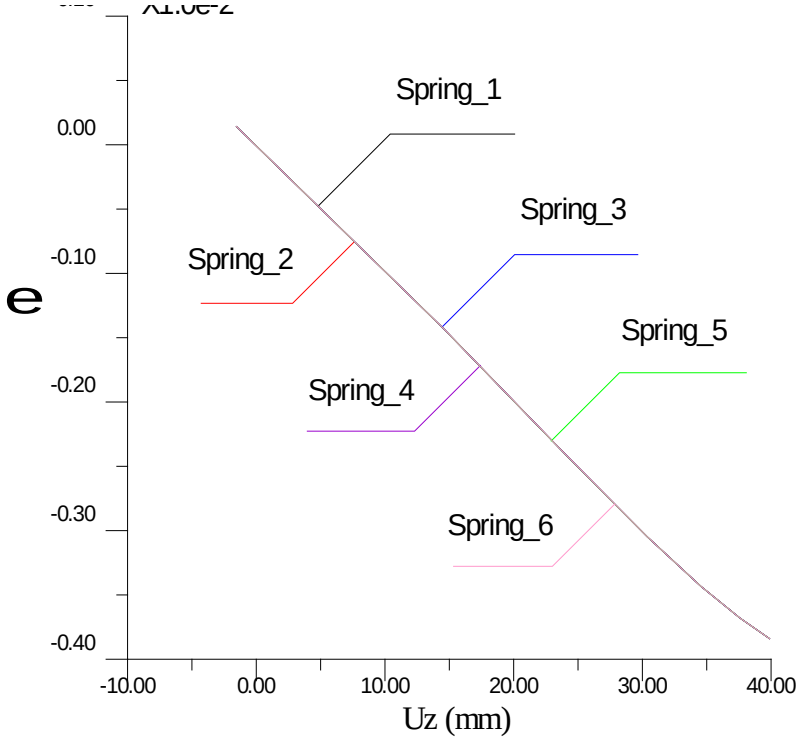


**Figure 4.9 Graph of Linear Displacement VS Strain in Z-Axis**

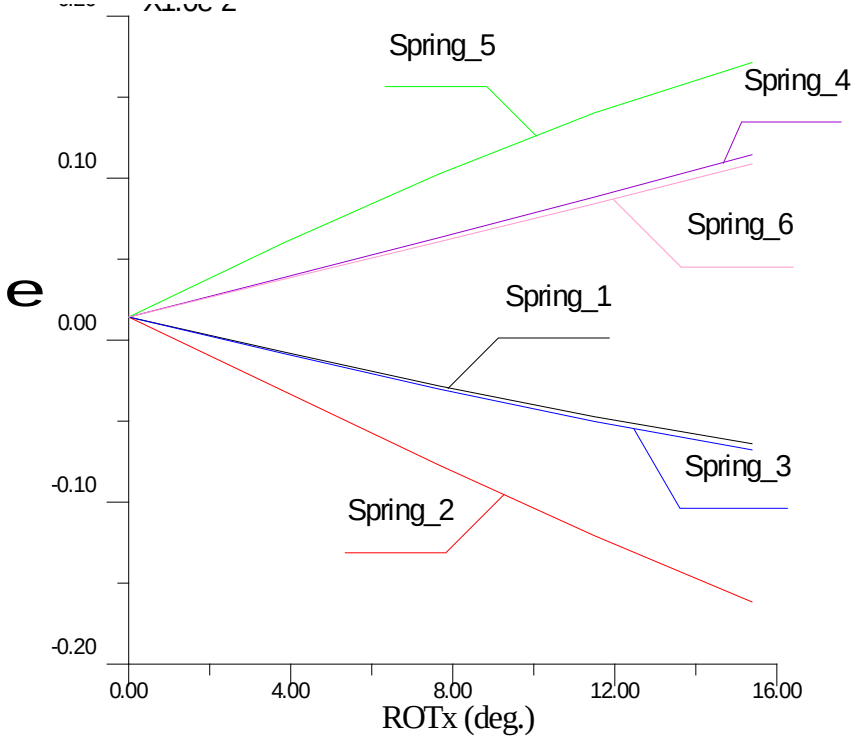


**Figure 4.10 Graph of Angular Displacement VS Strain in X-Axis**

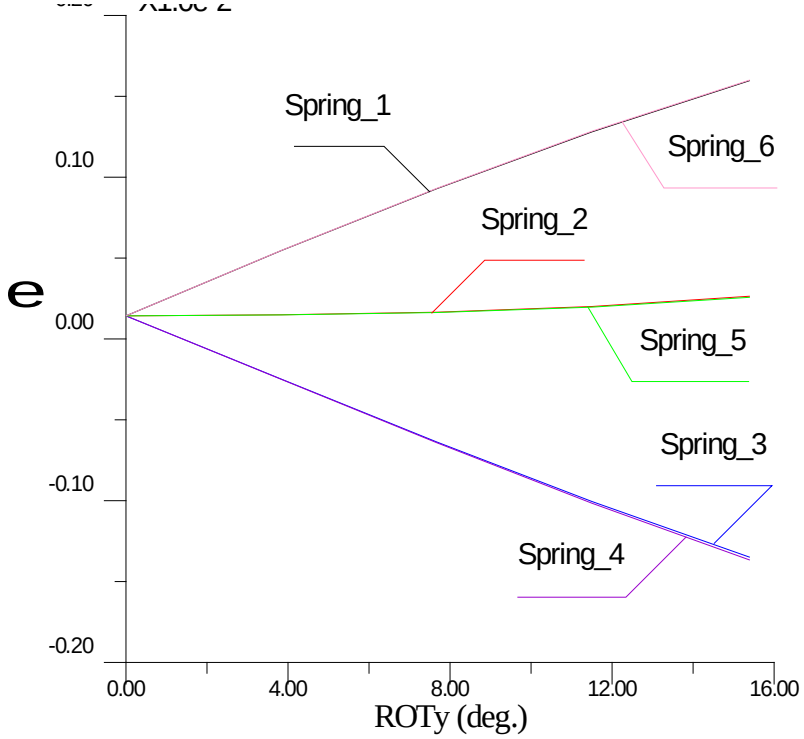


**Figure 4.11Graph of Linear Displacement VS Strain in Y-Axis**

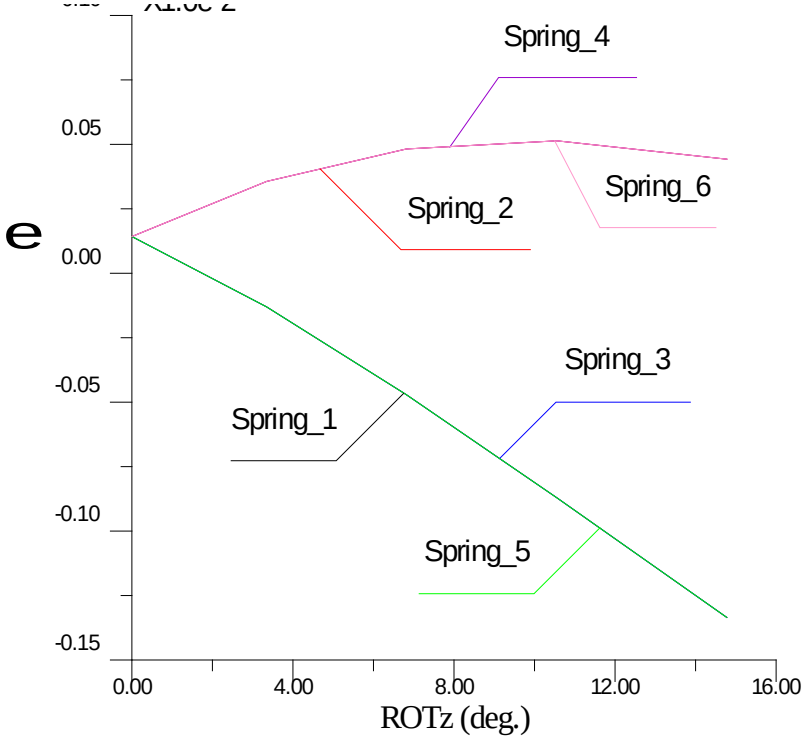


**Figure 4.12 Graph of Angular Displacement VS Strain in Z-Axis**

### 4.6.2 Discussion

All the above figures are drawn according to the experiment data in Chapter 5. For all the data obtained by linear displacement, the constrain displacements were set from 0mm to 40mm, $0^o$ to $15^o$ for all angular displacements. All the graphs are plotted displacement against strain, whereas it is displacement against voltage while doing the actual experiment.

From Figure 4.7 and 4.8, displacement in Y and X axis, it shows that the relationship between displacement and strain may not be linearly. The figures also show that the range of strain is from $-20x10^{-2}$ to $20x10^{-2}$. It was expected the two graphs should be very similar, however, they are not. For linear displacement in X-axis, strip 1 and 6, 3 and 4, 2 and 5 are overlapping each other, while they are all separated in linear displacement in Y-axis. This result shows that even the model shows symmetric in geometric, it is not.

Figure 4.9 shows the expected result, that all the lines should be overlapping each other. This is because the model was pulled upward, and all the 6 strips should perform the same as they are acting at the same direction and having the same displacement.

Figure 4.10 and 4.11 show a linear relationship between strain and displacement. However, if a ruler is measure against the lines, it shows that the relationship is not exactly linear. The lines are more likely to be in curve shape.

Figure 4.12 suggests that the relationship between strain and displacement is not linear. The lines are more likely to be polynomial.

From the above results, it concludes that the relationship between strain of the strips and displacement of the top platform is not linear. It is important to find out the

relationship between the two variables so that the position of joystick can be calculated with a given position.

For non-linear relationship, super-position cannot be applied. That means with a given displacement, voltage can be calculated if and only if the change of displacement is limited to be one degree of freedom. This effect will limit the usage of the joystick. However, this can be check by testing the prototype experimentally. In next chapter, a test rig will be set up for the testing of the prototype.

The ANSYS models and pseudo-codes for both cases are attached in Appendix B.

## 4.7 Reference data obtained from PATRAN

The prototype model can be constructed by using another program PATRAN. This program uses the same fundamental theory as ANSYS does. In this part, only reference data will be given. The model will be constructed; force and moment will be applied at the top and bottom of the joystick, the corresponding displacement will be calculated. The PATRAN parameters to generate the model are attached in Appendix C.

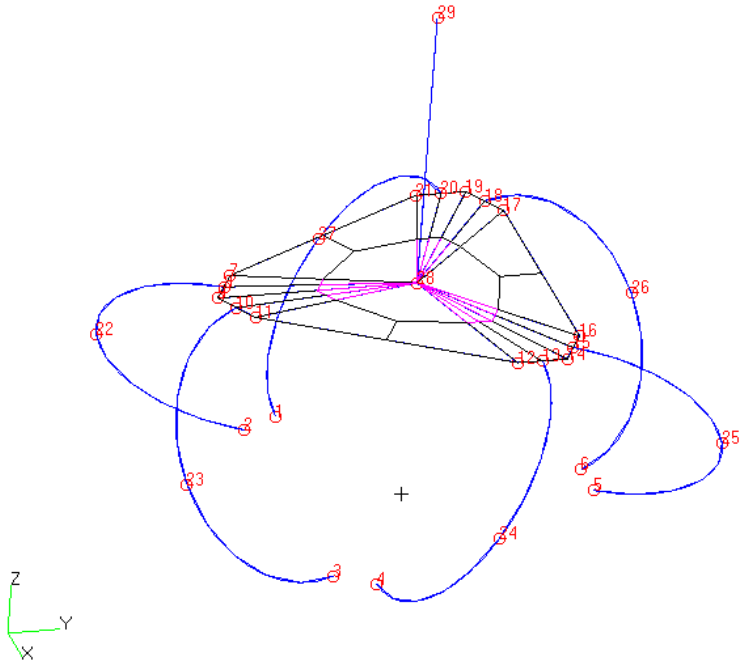


**Figure 4.13 Model generated using PATRAN**

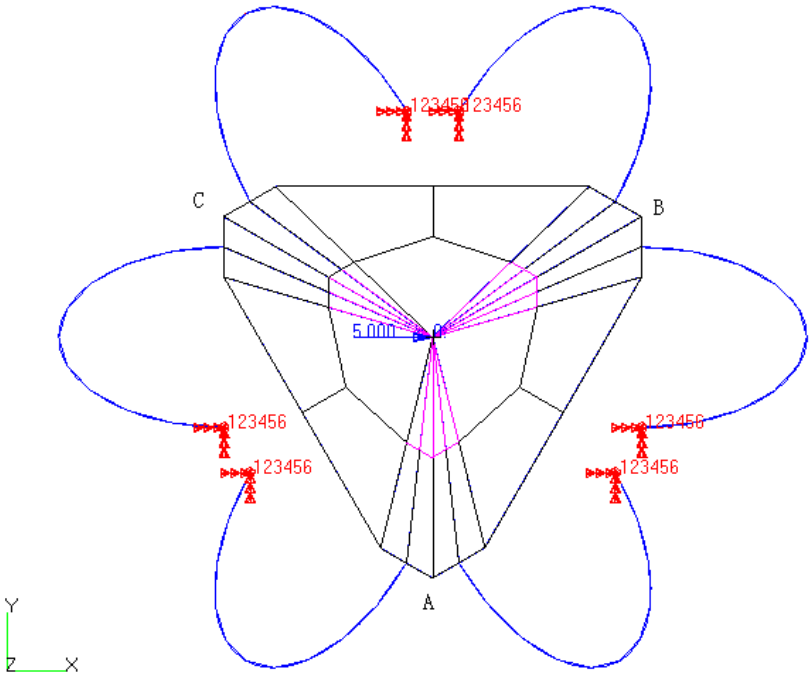


**Figure 4.14 Plain view of the model generated using PATRAN**

# CHAPTER 5

# EXPERIMENTS

## 5.1 Introduction

In this chapter, the experimental procedure and method of testing are discussed. The relationship between the 6 DOF and the 6 output channels is included in the background theory section, along with the method of getting the 6 x 6 matrix. The technique developed is based on the slopes of line of the best fit in the graphs.

Experimental data was collected and analysed with the results presented in this chapter. In particular, the analysis checks whether linearity holds for all 6 channels in all 6 DOF, and also will construct the Jacobian matrix.

Testing will ensure that the matrix works for all combinations of movement so that the inverse Jacobian can be determined, calculated and hence the 6 DOF movements from the 6 strain gauge voltage outputs.

## 5.2 Background theory

As detailed in chapter 2, movements of the spring steel strips are recorded and translated into six voltages by using strain gauges. A given displacement in a particular degree of freedom will cause changes in all 6 strain gauge bridge voltages. It is suggested that there is a linear relationship between the recorded voltages and the displacements in all 6 DOF. Hence, it can be written mathematically as:

$$V \propto D$$
$$V = KD \tag{5.1}$$

where $D$ is the 6 DOF displacement matrix

$V$ is the voltage matrix

$K$ is the constant Jacobian matrix $[k_1\ k_2\ k_3\ \ldots\ k_6]$

where $k_i = [k_{1i}\ k_{2i}\ k_{3i}\ \ldots\ k_{6i}]$

The equation in matrix form is as follow:

$$V = KD$$
$$\begin{bmatrix} V_1 \\ V_2 \\ V_3 \\ V_4 \\ V_5 \\ V_6 \end{bmatrix} = \begin{bmatrix} k_{11} & . & . & . & . & k_{16} \\ k_{21} & . & & & & . \\ . & & . & & & . \\ . & & & . & & . \\ . & & & & . & . \\ k_{61} & . & . & . & . & k_{66} \end{bmatrix} \begin{bmatrix} u \\ v \\ w \\ \theta_x \\ \theta_y \\ \theta_z \end{bmatrix} \tag{5.2}$$

$u$, $v$, $w$ are the displacements of x-axis, y-axis, z-axis respectively, while $\theta_x$, $\theta_y$, $\theta_z$ are the rotational displacements along x-axis, y-axis and z-axis respectively. $M_{11}$ to $M_{66}$ are the constants, $V_1$ to $V_6$ are the voltage readings from each strain gauge bridge.

While equation 5.1 is used to determine the elements of [K] from experimental measurements. The voltages are recorded for each single displacement while the other displacements are kept at zero. Doing this results in the following equations:

$$\textit{when} \quad D = \begin{bmatrix} u \\ 0 \\ 0 \\ 0 \\ 0 \\ 0 \end{bmatrix}, \quad \begin{aligned} V_1 &= k_{11}u \Rightarrow k_{11} = V_1 / u \\ V_2 &= k_{21}u \Rightarrow k_{21} = V_2 / u \\ V_3 &= k_{31}u \Rightarrow k_{31} = V_3 / u \\ V_4 &= k_{41}u \Rightarrow k_{41} = V_4 / u \\ V_5 &= k_{51}u \Rightarrow k_{51} = V_5 / u \\ V_6 &= k_{61}u \Rightarrow k_{61} = V_6 / u \end{aligned}$$

$$\textit{when} \quad D = \begin{bmatrix} 0 \\ v \\ 0 \\ 0 \\ 0 \\ 0 \end{bmatrix}, \quad \begin{aligned} V_1 &= k_{12}v \Rightarrow k_{12} = V_1 / v \\ V_2 &= k_{22}v \Rightarrow k_{22} = V_2 / v \\ V_3 &= k_{32}v \Rightarrow k_{32} = V_3 / v \\ V_4 &= k_{42}v \Rightarrow k_{42} = V_4 / v \\ V_5 &= k_{52}v \Rightarrow k_{52} = V_5 / v \\ V_6 &= k_{62}v \Rightarrow k_{62} = V_6 / v \end{aligned}$$

$$\textit{when} \quad D = \begin{bmatrix} 0 \\ 0 \\ w \\ 0 \\ 0 \\ 0 \end{bmatrix}, \quad \begin{aligned} V_1 &= k_{13}w \Rightarrow k_{13} = V_1 / w \\ V_2 &= k_{23}w \Rightarrow k_{23} = V_2 / w \\ V_3 &= k_{33}w \Rightarrow k_{33} = V_3 / w \\ V_4 &= k_{43}w \Rightarrow k_{43} = V_4 / w \\ V_5 &= k_{53}w \Rightarrow k_{53} = V_5 / w \\ V_6 &= k_{63}w \Rightarrow k_{63} = V_6 / w \end{aligned}$$

$$\textit{when} \quad D = \begin{bmatrix} 0 \\ 0 \\ 0 \\ \theta_x \\ 0 \\ 0 \end{bmatrix}, \quad \begin{aligned} V_1 &= k_{14}\theta_x \Rightarrow k_{14} = V_1 / \theta_x \\ V_2 &= k_{24}\theta_x \Rightarrow k_{24} = V_2 / \theta_x \\ V_3 &= k_{34}\theta_x \Rightarrow k_{34} = V_3 / \theta_x \\ V_4 &= k_{44}\theta_x \Rightarrow k_{44} = V_4 / \theta_x \\ V_5 &= k_{54}\theta_x \Rightarrow k_{54} = V_5 / \theta_x \\ V_6 &= k_{64}\theta_x \Rightarrow k_{64} = V_6 / \theta_x \end{aligned}$$

$$\textit{when} \quad D = \begin{bmatrix} 0 \\ 0 \\ 0 \\ 0 \\ \theta_y \\ 0 \end{bmatrix}, \quad \begin{aligned} V_1 &= k_{15}\theta_y \Rightarrow k_{15} = V_1 / \theta_y \\ V_2 &= k_{25}\theta_y \Rightarrow k_{25} = V_2 / \theta_y \\ V_3 &= k_{35}\theta_y \Rightarrow k_{35} = V_3 / \theta_y \\ V_4 &= k_{45}\theta_y \Rightarrow k_{45} = V_4 / \theta_y \\ V_5 &= k_{55}\theta_y \Rightarrow k_{55} = V_5 / \theta_y \\ V_6 &= k_{65}\theta_y \Rightarrow k_{65} = V_6 / \theta_y \end{aligned}$$

$$when \quad D = \begin{bmatrix} 0 \\ 0 \\ 0 \\ 0 \\ 0 \\ \theta_z \end{bmatrix}, \qquad \begin{aligned} V_1 &= k_{16}\theta_z \Rightarrow k_{16} = V_1/\theta_z \\ V_2 &= k_{26}\theta_z \Rightarrow k_{26} = V_2/\theta_z \\ V_3 &= k_{36}\theta_z \Rightarrow k_{36} = V_3/\theta_z \\ V_4 &= k_{46}\theta_z \Rightarrow k_{46} = V_4/\theta_z \\ V_5 &= k_{56}\theta_z \Rightarrow k_{56} = V_5/\theta_z \\ V_6 &= k_{66}\theta_z \Rightarrow k_{66} = V_6/\theta_z \end{aligned}$$

**(5.3)**

The Jacobian matrix is obtained from the constant matrix column elements. In order to reduce errors when determining the Jacobian elements, average values of the elements are obtained by taking several displacement values of the same DOF. This is done by fitting a straight line though the graphs of voltage plotted against the single DOF input. The Jacobian is inverted to accurately compute the displacements of the joystick from he measured voltages.

$$V = KD$$
$$D = K^{-1}V$$

**(5.4)**

The above method assumes a relationship between voltages and displacements behave linearly, and also there is no initial strain or displacement in the system. In this case, if graph of voltage Vs displacement is drawn, all line should be straight and pass through the origin. Due to the experimental set-up, the joystick was clamped by a dividing head and an X-Y table. The dividing head moved the joystick slightly away from its natural position, which cause an initial strain in the system. The following method may be used to find the initial strain.

Assume a graph of voltage against displacement was drawn, the slope of this graph will give the ***k*** values where the voltage caused by the initial strain will be represented by the Y-intercept of the lines, thus we call that value ***b***.

Once all slopes of the best fit lines are determined, a matrix can be formed using

these k values. Similarly, another matrix is formed using the b values or offset voltages from the 6 strain gauge bridges when they are not start from zero input displacements.

$$\begin{bmatrix} V_1 \\ V_2 \\ V_3 \\ V_4 \\ V_5 \\ V_6 \end{bmatrix} = \begin{bmatrix} k_{11} & k_{12} & . & . & . & k_{16} \\ k_{21} & . & & & & . \\ & & . & & & . \\ & & & . & & . \\ & & & & . & k_{56} \\ k_{61} & . & . & . & k_{65} & k_{66} \end{bmatrix} \begin{bmatrix} x \\ y \\ z \\ \theta_x \\ \theta_y \\ \theta_z \end{bmatrix} + \begin{bmatrix} b_1 \\ b_2 \\ b_3 \\ b_4 \\ b_5 \\ b_6 \end{bmatrix}$$

$$V = Kx + B \quad \Rightarrow \quad V - B = Kx$$

**(5.5)**

where V1 to V6 (represents values of y-axis of the best fit line graph) are the voltage readings obtained from the strain gauges; the k values are the slopes of all the best fit lines; The linear and rotational displacements along the x, y, z axes are *x*, *y*, *z* and the $\theta_x$, $\theta_y$, $\theta_z$. The term ***b*** contains the intercepts of y-axis for each best-fit line respectively. Therefore, the equation written in matrix form is as follow:

$$V = KD + b$$

**(5.6)**

Using this equation with a given displacement in a particular DOF, the voltage output can be determined. By inverting K it is possible to determine the displacement from the voltages measured:

$$D = K^{-1}V - K^{-1}b = K^{-1}(V - b)$$

**(5.7)**

The above equations assume a linear relationship between voltage and displacement. If we look at the strips and consider it measures the bending strain in the strip, the above relationship can be considered as between that lateral displacement and axial displacement of the beam. Since the strain gauges measure the bending strain in

the strip, which will be related to the lateral displacement of the beam. The displacement is applied at the top platform, and hence the end of the strip, it is related to the axial displacement of the beam.

The relationship between the lateral and axial displacement is not linear at least in one case as described below. Consider a beam subject to an axial load P, with initial deflection $Y_0$, as shown in Figure 5.1

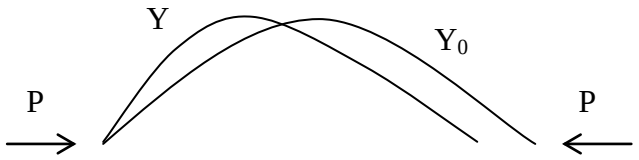


**Figure 5.1 Example of Non-linear later and axial displacements.**

$$Y_0 = \sum a_i \sin \frac{i\pi x}{L} \tag{5.8}$$

If we are interested in calculating the difference Y and $Y_0$, consider:

$$Y - Y_0 = ds\left(1 - \frac{\theta^2}{2}\right) - ds\left(1 - \frac{\theta_0^2}{2}\right)$$
$$= \frac{ds}{2}\left(\theta_0^2 - \theta^2\right) \tag{5.9}$$

The slope θ is proportional to lateral displacement which is proportional to V. This shows the relationship between V and lateral displacement has at least one non-linear component.

## 5.3 Method of testing

The joystick has six degree of freedom, so it is important to develop some

mechanisms for testing all six input values. A device that can vary all six DOF at the same time would be ideal but even a device to apply three calibrated displacements and rotations simultaneously is difficult to make. The experiment is divided into several parts in order to test the uniaxially determined Jacobian matrix values.

## 5.4 Experiment Setup

An X-Y table was used to obtain linear displacements on the X and Y axes. Turning the lead screw handle for one revolution on either the X or Y axis represents a 2mm movement. A dividing head was used to obtain the angular displacements about the X and Y axes. Each hole on the dividing head represents a five-degree increment. Four DOFs (linear and angular displacement for the X and Y axes) can be obtained by combining these two devices.

**Figure 5.2 Work area**

Special connection had to be constructed to join the dividing head to the X-Y table.. An L-beam and a rectangular-beam were cut and bolted together to form a frame. The dividing head was bolted on to a connection beam, which was then bolted to the X-Y table. This is shown in Figure 5.2

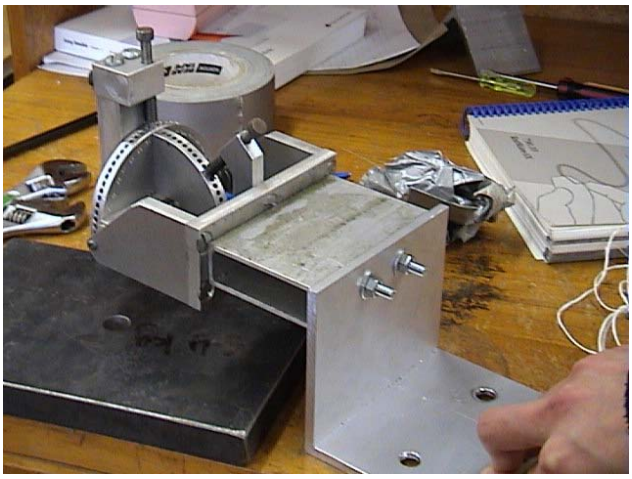

**Figure 5.3 Dividing head with L-beam**

The handle of joystick was then clamped by the dividing head. This device was designed to be exactly the same height as the top surface of the platform, so that the dividing head was sitting just above the top platform. It was important to do this even though it did not matter when testing the linear displacement, but it could cause uncertainty when working on the angular displacement. This set-up would allow the device to rotate about the X and Y axes on the same plane as the upper platform. Attaching the dividing head anywhere else shifts the points of rotation, which causes a displacement, which in turn causes errors.

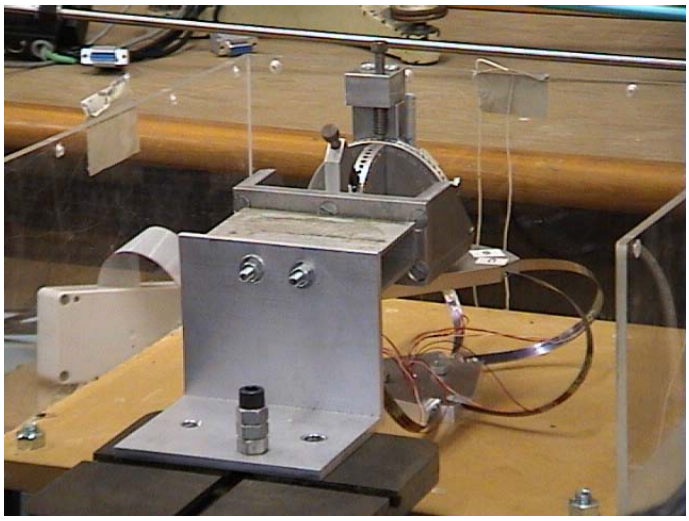

**Figure 5.4 The joystick is connected to the dividing head and X-Y table**

## 5.5 Experiment Procedure

The experiment procedure allows only one degree freedom to be tested while all the other 5 degrees of freedom will be restrained.

The joystick was placed in the dividing head and to the attached X-Y table. The initial voltages were recorded. The Y-axis on the X-Y table was adjusted to 10mm while X-axis was fixed. The readings of voltages were again taken. This procedure was repeated with 20mm and 30mm. The same procedure was repeated with Y-axis while X-axis was fixed.

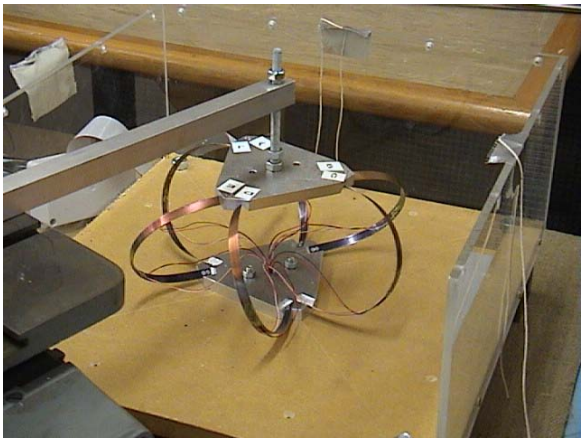

**Figure 5.5 Testing linear displacement in Z-axis**

**Figure 5.6 The top platform is rotated by the dividing head**

The X-Y table was located back to its original position. The X-axis on dividing head was turned 5 degrees, while the Y-axis was fixed. The voltages were recorded, and this procedure was repeated at 10 degree and 15 degrees. The same procedure was repeated with Y-axis while X-axis was fixed.

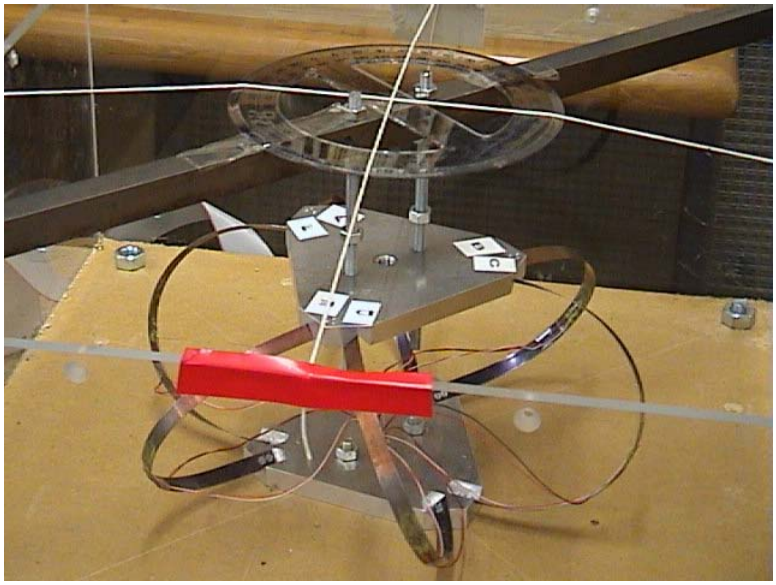

**Figure 5.7 Testing angular displacement in Z-axis**

## 5.6 Result

| Voltage | zero | -30 | -25 | -20 | -15 | -10 | -5 | 5 | 10 | 15 | 20 | 25 | 30 |
|---|---|---|---|---|---|---|---|---|---|---|---|---|---|
| V1 | -0.842 | -0.837 | -0.873 | -0.893 | -0.895 | -0.883 | -0.854 | -0.782 | -0.667 | -0.573 | -0.471 | -0.346 | -0.219 |
| V2 | -1.61 | -1.274 | -1.351 | -1.414 | -1.467 | -1.51 | -1.541 | -1.613 | -1.549 | -1.526 | -1.487 | -1.438 | -1.374 |
| V3 | -0.449 | -0.167 | -0.247 | -0.308 | -0.349 | -0.38 | -0.399 | -0.439 | -0.376 | -0.343 | -0.297 | -0.231 | -0.158 |
| V4 | -0.351 | -0.167 | 0.067 | -0.029 | -0.117 | -0.192 | -0.257 | -0.383 | -0.348 | -0.349 | -0.332 | -0.303 | -0.254 |
| V5 | -0.426 | -0.439 | -0.472 | -0.487 | -0.478 | -0.461 | -0.423 | -0.354 | -0.217 | -0.117 | -0.007 | -0.118 | -0.256 |
| V6 | -0.461 | 0.025 | -0.075 | -0.188 | -0.243 | -0.308 | -0.364 | -0.491 | -0.444 | -0.446 | -0.43 | -0.396 | -0.349 |

**Table 5.1 Linear Displacements in X-axis**

| Voltage | zero | -30 | -25 | -20 | -15 | -10 | -5 | 5 | 10 | 15 | 20 | 25 | 30 |
|---|---|---|---|---|---|---|---|---|---|---|---|---|---|
| V1 | -0.813 | -0.438 | -0.531 | -0.612 | -0.683 | -0.741 | -0.786 | -0.825 | -0.806 | -0.791 | -0.764 | -0.726 | -0.674 |
| V2 | -1.551 | -1.513 | -1.563 | -1.592 | -1.606 | -1.605 | -1.587 | -1.503 | -1.445 | -1.366 | -1.274 | -1.165 | -1.044 |
| V3 | -0.41 | -0.34 | -0.394 | -0.434 | -0.457 | -0.457 | -0.443 | -0.362 | -0.3 | -0.216 | -0.119 | -0.009 | 0.155 |
| V4 | -0.302 | 0.181 | 0.071 | -0.029 | -0.115 | -0.191 | -0.252 | -0.325 | -0.327 | -0.325 | -0.309 | -0.277 | -0.226 |
| V5 | -0.368 | -0.004 | -0.092 | -0.173 | -0.24 | -0.299 | -0.344 | -0.398 | -0.421 | -0.419 | -0.4 | -0.367 | -0.322 |
| V6 | -0.404 | 0.118 | 0.005 | -0.1 | -0.195 | -0.28 | -0.352 | -0.456 | -0.501 | -0.523 | -0.525 | -0.512 | -0.483 |

**Table 5.2 Linear Displacements about Y-axis**

| Voltage | Zero | -20 | -15 | -10 | -5 | 5 | 10 | 15 | 20 |
|---|---|---|---|---|---|---|---|---|---|
| V1 | 0.143 | -0.303 | -0.202 | -0.1 | 0.013 | 0.287 | 0.439 | 0.575 | 0.709 |
| V2 | -1.146 | -1.618 | -1.513 | -1.396 | -1.293 | -1.015 | -0.845 | -0.7 | -0.575 |
| V3 | -0.025 | -0.537 | -0.417 | -0.29 | -0.159 | 0.13 | 0.308 | 0.457 | 0.62 |
| V4 | -0.39 | -0.927 | -0.805 | -0.686 | -0.543 | -0.236 | -0.065 | 0.082 | 0.239 |
| V5 | -0.135 | -0.59 | -0.491 | -0.372 | -0.273 | -0.008 | 0.173 | 0.311 | 0.435 |
| V6 | -0.108 | -0.508 | -0.42 | -0.327 | -0.23 | 0.008 | 0.175 | 0.303 | 0.436 |

**Table 5.3 Linear Displacements about Z-axis**

| Voltage | Zero | -5degree | 5 degree | 10degree |
|---|---|---|---|---|
| V1 | -0.57 | -0.152 | 0.046 | 0.182 |
| V2 | -1.231 | -1.402 | -1.052 | -0.836 |
| V3 | -0.045 | 0.258 | -0.334 | -0.593 |
| V4 | -0.575 | -0.483 | -0.654 | -0.7 |
| V5 | -0.123 | -0.19 | -0.078 | -0.01 |
| V6 | -0.116 | 0.109 | -0.35 | -0.58 |

**Table 5.4 Angular Displacements about X-axis**

| Voltage | Zero | 5 degree | 10degree | 15degree |
|---|---|---|---|---|
| V1 | -0.063 | 0.07 | 0.189 | 0.312 |
| V2 | -1.233 | -1.396 | -1.566 | -1.747 |
| V3 | -0.05 | -0.084 | -0.109 | -0.128 |
| V4 | -0.576 | -0.374 | -0.169 | 0.016 |
| V5 | -0.132 | -0.41 | -0.639 | -0.793 |
| V6 | -0.122 | -0.311 | -0.438 | -0.517 |

**Table 5.5 Angular Displacements about Y-axis**

| Voltage | Zero | -15 | -10 | -5 | 5 | 10 | 15 |
|---|---|---|---|---|---|---|---|
| V1 | 0.016 | 0.207 | 0.123 | 0.054 | 0.006 | 0.073 | 0.148 |
| V2 | -1.232 | -1.194 | -1.241 | -1.249 | -1.22 | -1.124 | -1.046 |
| V3 | -0.052 | 0.167 | 0.05 | -0.013 | -0.062 | -0.051 | 0.043 |
| V4 | -0.439 | -0.318 | -0.398 | -0.432 | -0.399 | -0.324 | -0.323 |
| V5 | -0.111 | -0.038 | -0.083 | -0.123 | -0.091 | 0.01 | 0.085 |
| V6 | -0.154 | -0.04 | -0.098 | -0.161 | -0.142 | -0.073 | 0.009 |

**Table 5.6 Angular Displacement about Z-axis**

## 5.7 Data analysis

Having obtained all the above data, linearity was then checked. The graphs showing the relationship between displacement and voltage were drawn for each channel and are in the following figures.

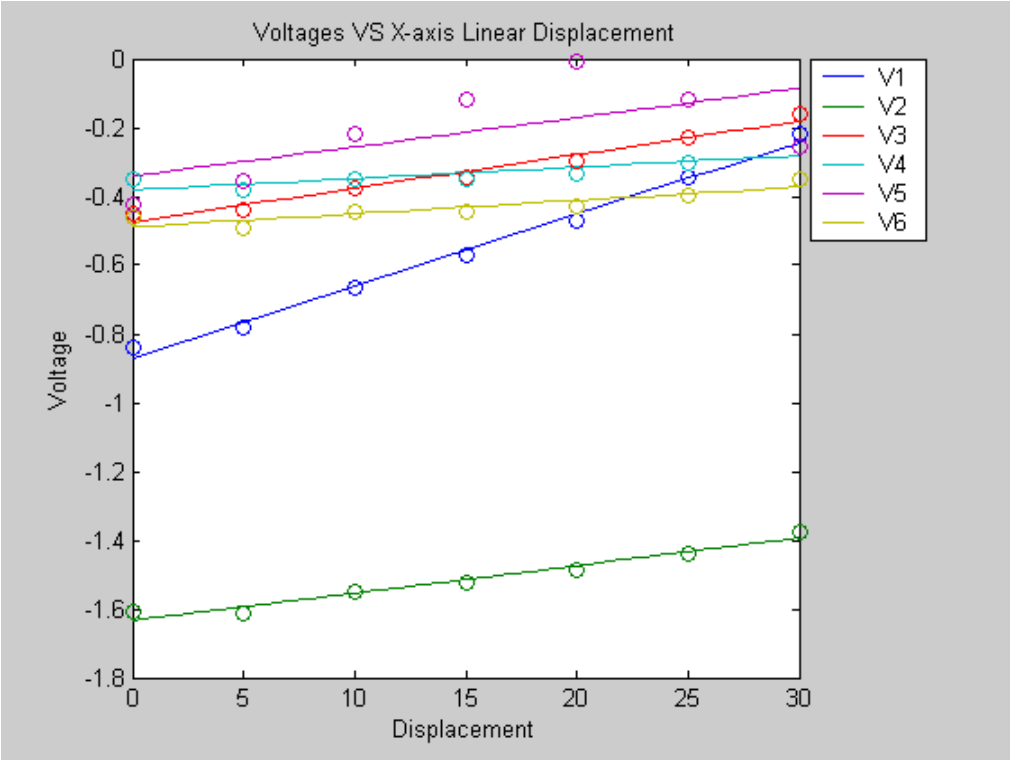


**Figure 5.8 Linear Displacement in X-axis in 1st order polynomial**

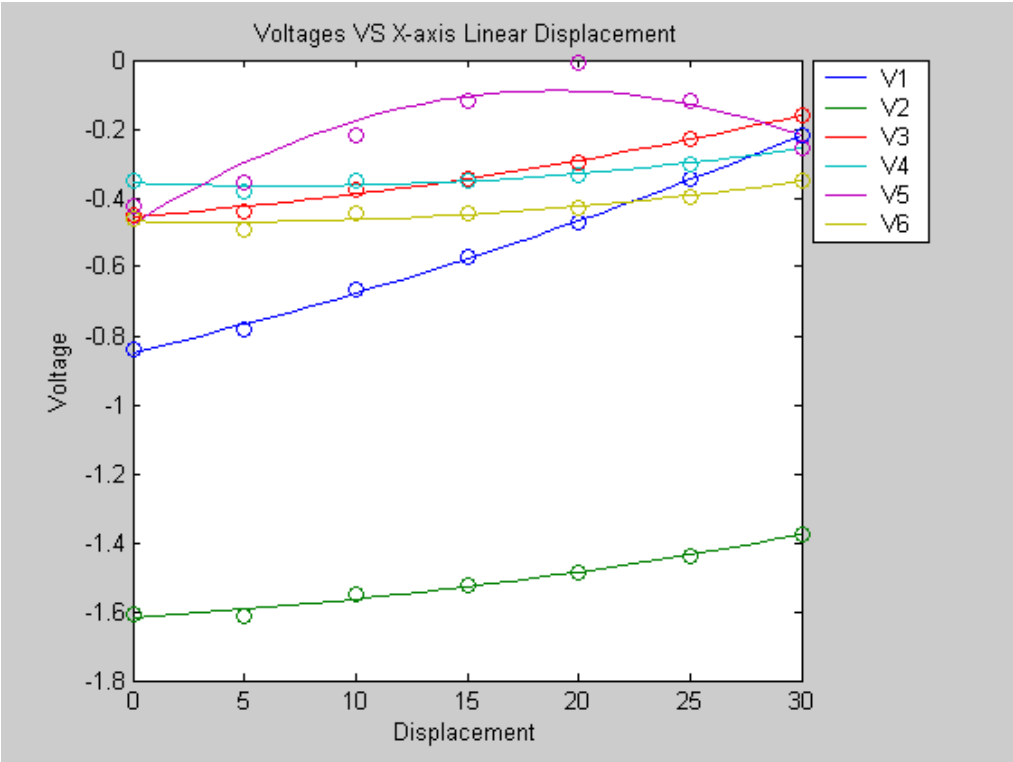


**Figure 5.9 Linear Displacement in X-axis in 2nd order polynomial**

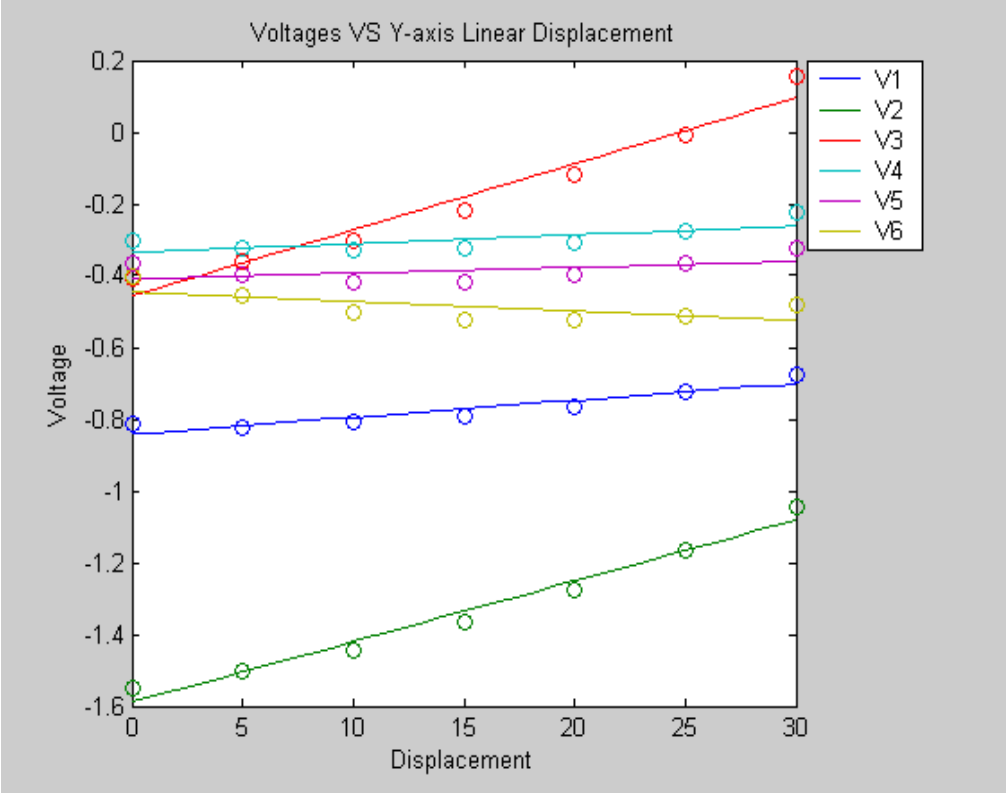


**Figure 5.10Linear Displacement in Y-axis in 1st order polynomial**

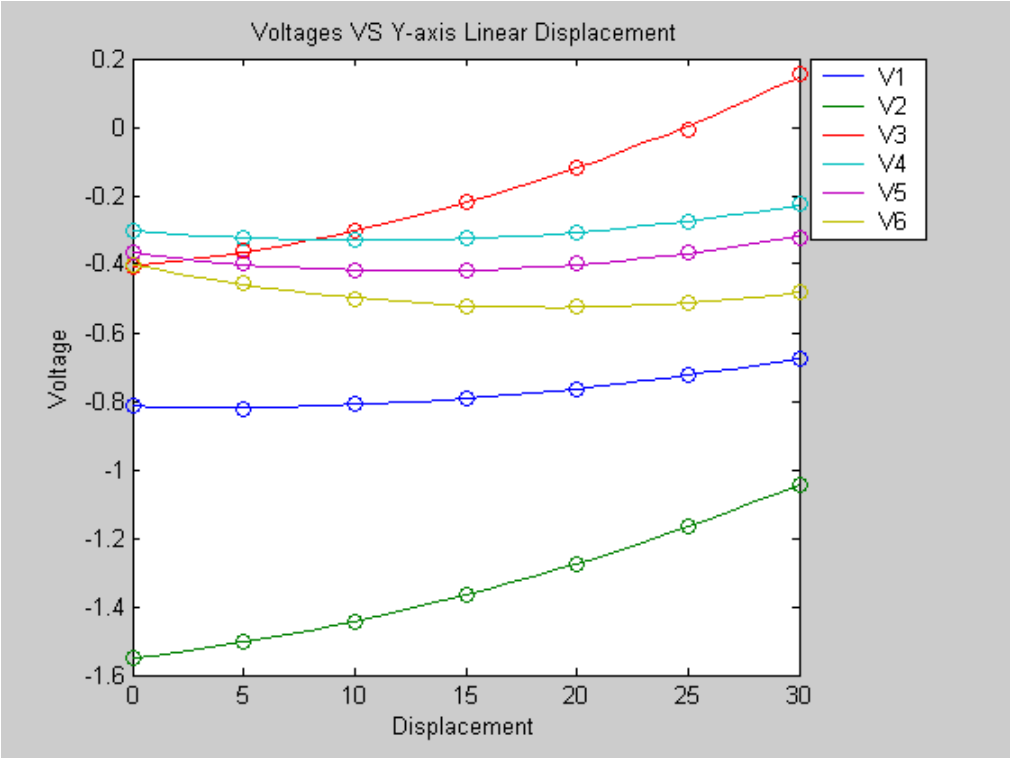


**Figure 5.11 Linear Displacement in Y-axis in 2nd order polynomial**

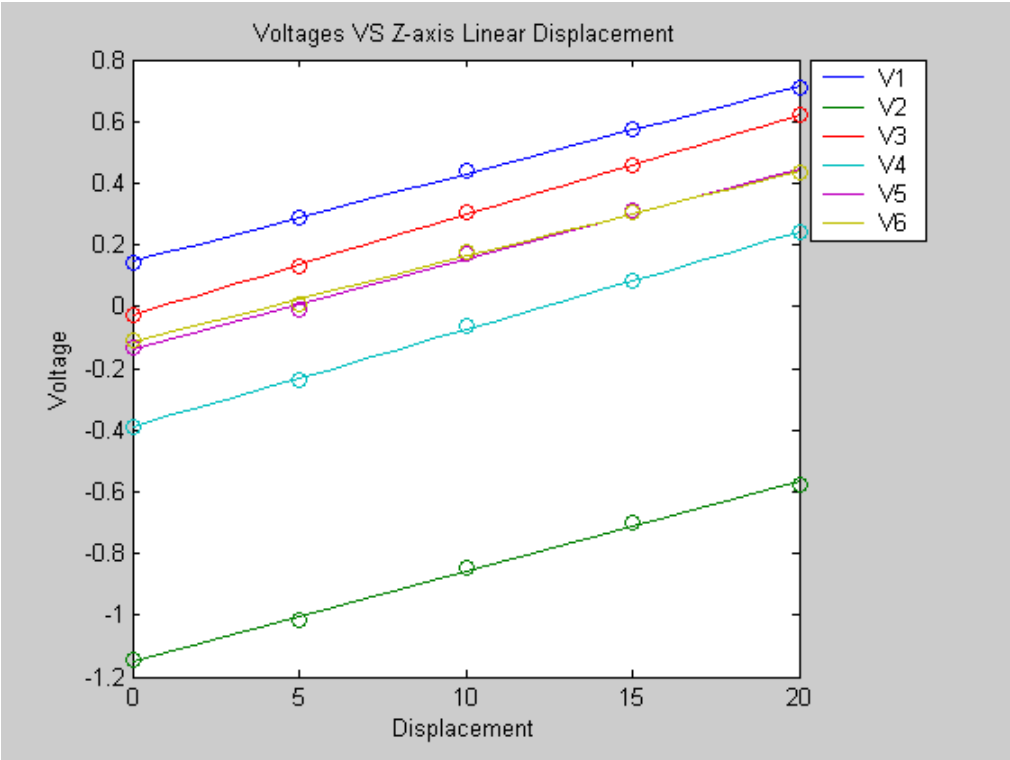


**Figure 5.12 Linear Displacement in Z-axis in 1st order polynomial**

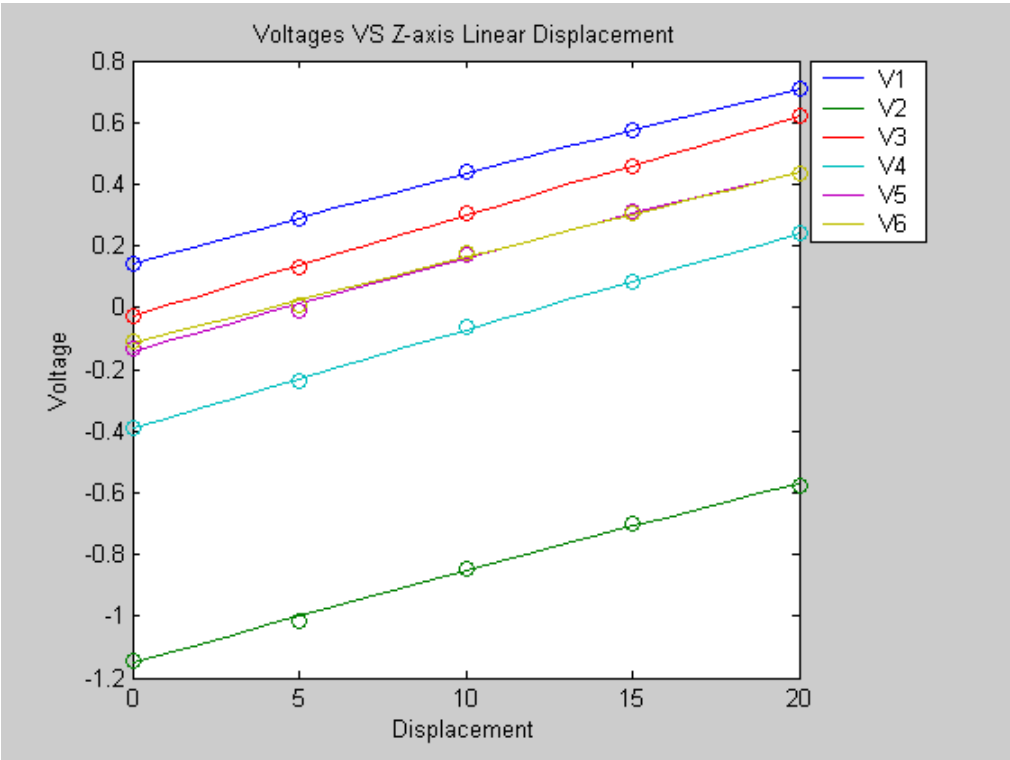


**Figure 5.13 Linear Displacement in Z-axis in 2nd order polynomial**

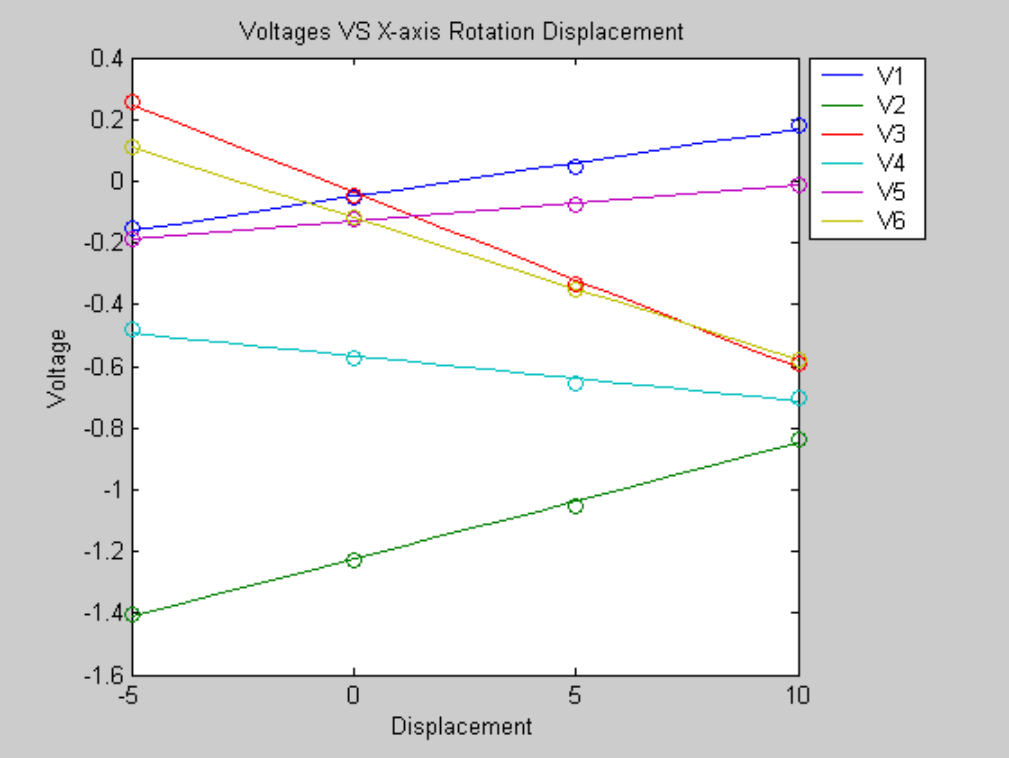


**Figure 5.14 Rotational Displacement about X-axis in 1st order polynomial**

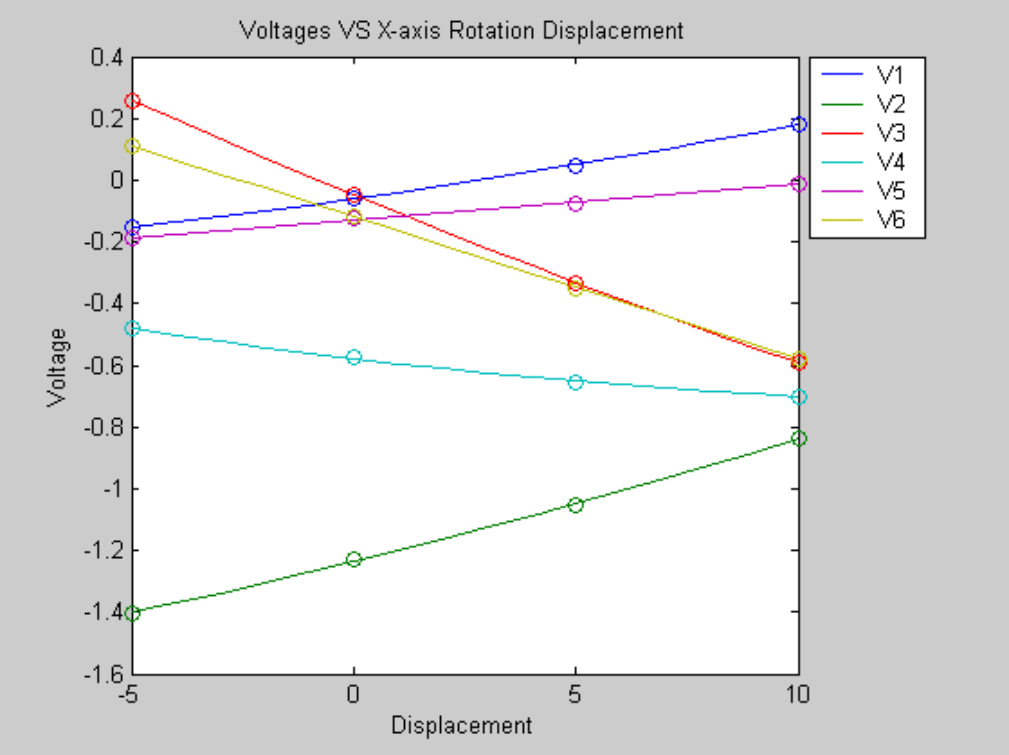


**Figure 5.15 Rotational Displacement about X-axis in 2nd order polynomial**

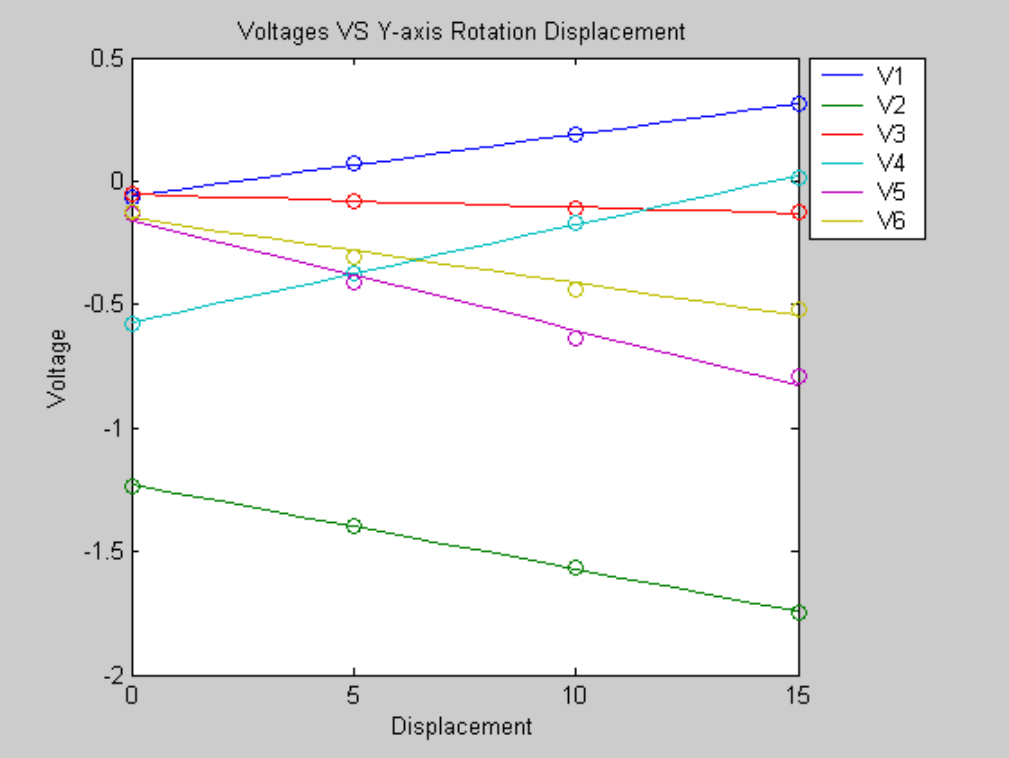


**Figure 5.16 Rotational Displacement about Y-axis in 1st order polynomial**

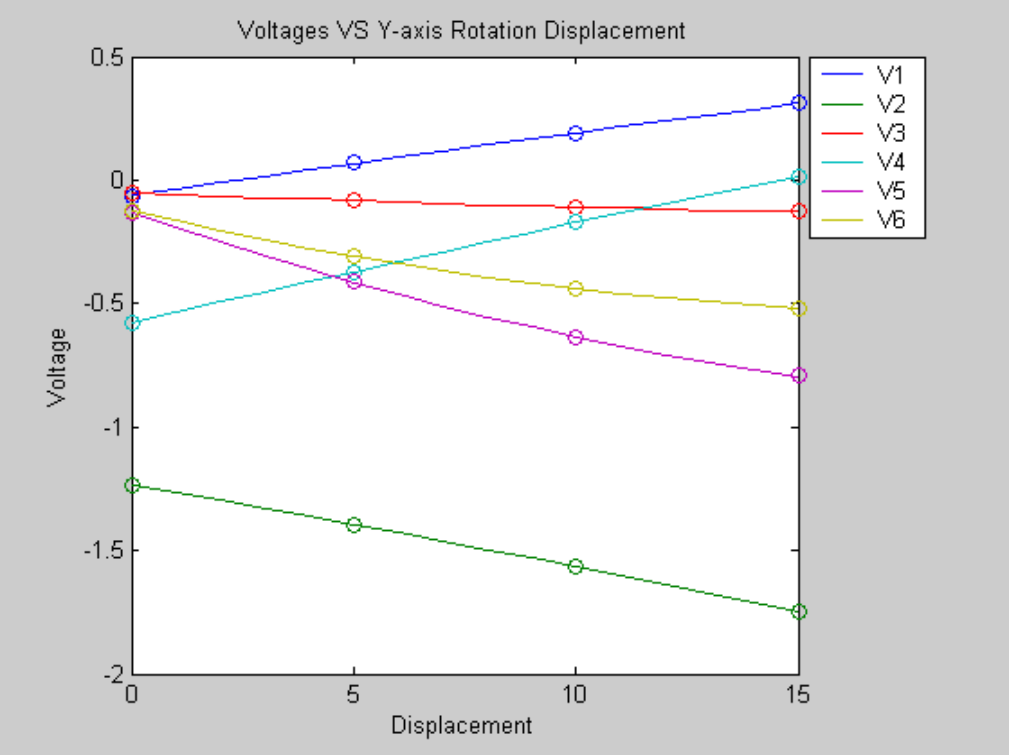


**Figure 5.17 Rotational Displacement aboout Y-axis in 2nd order polynomial**

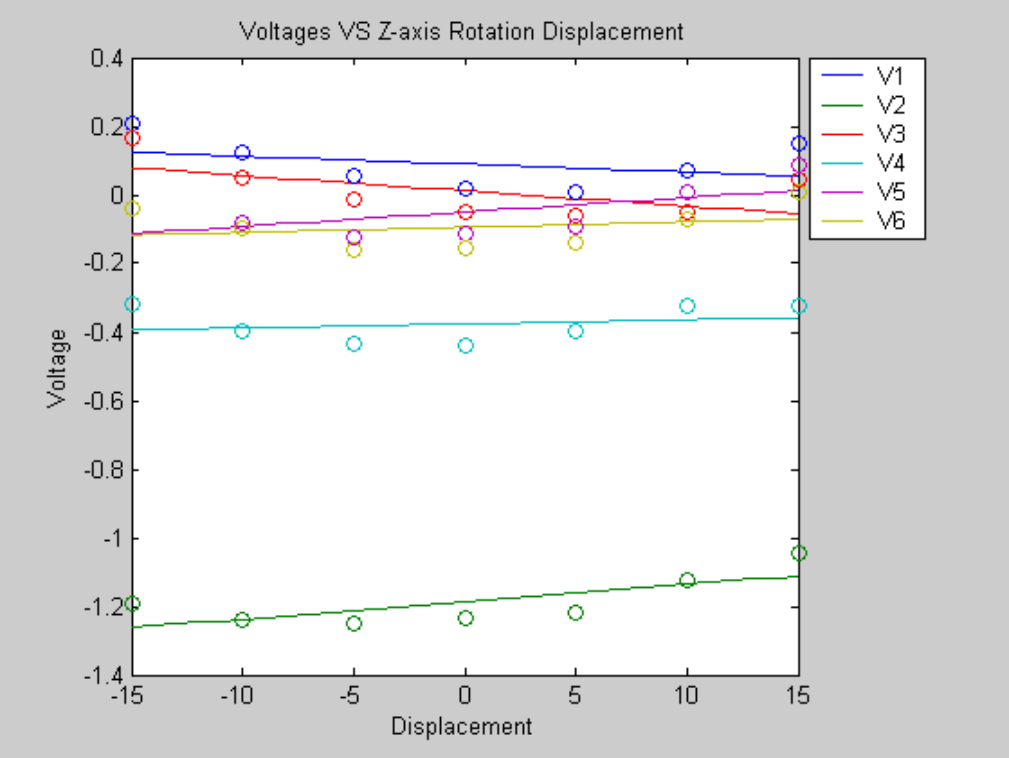


**Figure 5.18 Rotational Displacement about Z-axis in 1st order polynomial**

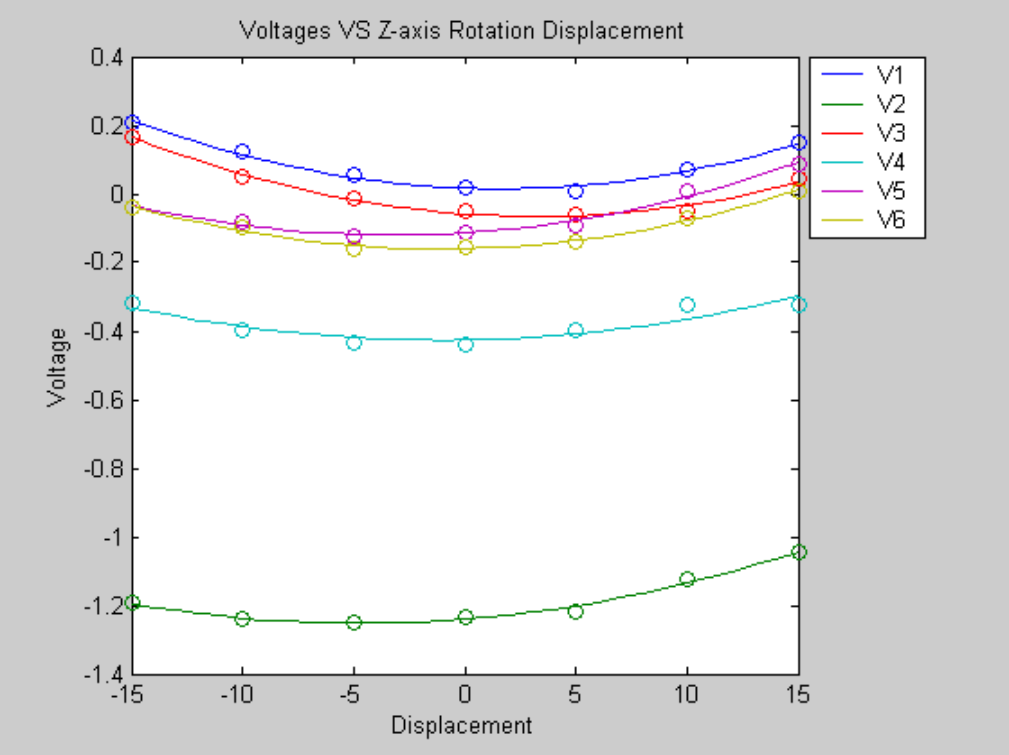


**Figure 5.19 Rotational Displacement about Z-axis in 2nd order polynomial**

Figure 5.8 and Figure 5.9 show the difference between 1st order and 2nd polynomial using the same data. Figure 5.8 shows most of data lie on the best-fit line, but we can't conclude that the relationship between displacement and voltage behaves linearly. At least the line of V5 doesn't agree with all the corresponding data. Figure 5.9 shows the line of best-fit lie more accurate on the data points. It may show that the best fit line for V5 does not lie precisely on the data points, but the line fits better as a 2nd order polynomial rather than a 1st order polynomial.

Similar to the displacements in X axis. The 2nd order polynomial for Y-displacements fits the data better than the 1st order poly. Although in Figure 5.10 most data correspond to the best fit line, V3 is the particular line that doesn't agree with the data. On the other hand, V3 fits better using 2nd order polynomial, and so as all the other lines.

From Figure 5.12 and Figure 5.13, data was collected by pulling the controller upward (+) and push downward (-). It is important to do that in order to check whether linearity will hold for both tension and compression of the controller. It is also an indication whether there are fault on any channels of strain gauges, and it is shown that all channels work are functional and without fault. As expected, all the 6 channels lie almost on the same line. The linear relationship is true for all 6 channels and it shows that there are no faulty in the channels since from symmetry, all should output the same voltage. Both 1st order and 2nd order polynomial should come up with the same result as they should be all straight lines.

Figure 5.14 and Figure 5.15 indicate the results of the rotational displacements in X-axis. Data is slightly different from the data collected from angular displacement in Y-direction. This is because the dividing head is connected to the root of the joystick, where it almost touched the surface of the upper platform of the controller. The upper platform had blocked the movement of the dividing head in the X-direction, so the dividing head could not be adjusted to 15 degree. Instead of

taking a reading at 15 degrees, the dividing head was rotated the other way and was placed at –5 degrees. This experimental procedure caused the above Figure to be slightly different from the other graph. Both figures show all the best-fit lines lie on the data. However, best-fit line of V2 and V4 fit better for $2^{nd}$ order than $1^{st}$ order polynomial. It is interesting that in Figure 5.14 even though the best-fit lines are in $2^{nd}$ order polynomial, they look like straight lines. The reason is if we take a small fraction of a curve line, it should appear to be a straight line.

Figure 5.16 and 5.17 show the results of rotational displacements in Y-axis. Both figures show similar trend, except for V5 for which a $2^{nd}$ order would fit better than a $1^{st}$ order polynomial.

Figure 5.18 and 5.19 show the results of rotational displacements in Z-axis. The result show clearly $2^{nd}$ order polynomial fits the data a lot better than $1^{st}$ order. But for this particular set of results, it should be noted that V2 has a mush lower value then other channels. But its shape is consistent.

### 5.7.1 Second Order Polynomial Functions for V

Second order polynomials are fitted using the LSM for the six imposed displacements for each voltage reading. These are given below:

From linear displacement in X axis

$V1 = 0.002D^2 + 0.0153D - 0.848$

$V2 = 0.001D^2 + 0.0038D - 1.6165$

$V3 = 0.002D^2 + 0.0047D - 0.453$

$V4 = 0.002D^2 – 0.0025D - 0.357$

$V5 = -0.0011D^2 + 0.0409D - 0.4764$

$V6 = 0.0002D^2 -0.0012D - 0.4677$

**(5.11)**

From linear displacement in Y axis

$V1 = 0.0002D^2 - 0.0016D - 0.8155$

$V2 = 0.0003D^2 + 0.0077D - 1.5507$

$V3 = 0.0004D^2 + 0.0064D - 0.4064$

$V4 = 0.0003D^2 - 0.0057D - 0.3015$

$V5 = 0.0003D^2 - 0.0083D - 0.3677$

$V6 = 0.0004D^2 - 0.0132D - 0.4026$

**(5.12)**

From linear displacement in Z axis

$V1 = -0.0001D^2 + 0.0305D + 0.1415$

$V2 = -0.0001D^2 + 0.0313D - 1.1529$

$V3 = 0.0000D^2 + 0.0331D - 0.0273$

$V4 = -0.0001D^2 + 0.0325D - 0.3918$

$V5 = -0.0001D^2 + 0.0320D - 0.1436$

$V6 = 0.0000D^2 + 0.0279D - 0.1145$

**(5.13)**

From angular displacement in X axis

$V1 = 0.0004D^2 + 0.0201D - 0.0607$

$V2 = 0.0005D^2 + 0.0353D - 1.2354$

$V3 = 0.0004D^2 - 0.0590D - 0.0474$

$V4 = 0.0005D^2 - 0.0169D - 0.5780$

$V5 = 0.0000D^2 + 0.0116D - 0.1297$

$V6 = -0.0001D^2 - 0.0458D - 0.1180$

**(5.14)**

Form angular displacement in Y axis

$V1 = -0.0001D^2 + 0.0264D - 0.0621$

$V2 = -0.0002D^2 - 0.0315D - 1.2332$

$V3 = 0.0002D^2 - 0.0074D - 0.0501$

$V4 = -0.0002D^2 + 0.0422D - 0.5771$

$V5 = 0.0012D^2 - 0.0628D - 0.1307$

$V6 = 0.0011D^2 - 0.0427D - 0.1227$

**(5.15)**

From angular displacement in Z axis

$V1 = 0.0007D^2 - 0.0023D + 0.0167$

$V2 = 0.0005D^2 + 0.0051D - 1.2406$

$V3 = 0.0007D^2 - 0.0045D - 0.0589$

$V4 = 0.0005D^2 + 0.0012D - 0.4259$

$V5 = 0.0006D^2 + 0.0042D - 0.1130$

$V6 = 0.0007D^2 + 0.0015D - 0.1594$

**(5.16)**

If we use matrix form to represent the above data, we will have

$$\{V\} = [a]\{D^2\} + [b]\{D^1\} + [C]\{D^0\}$$

**(5.17)**

where

$$a = \begin{bmatrix} 0.0002 & 0.0002 & -0.0001 & 0.0004 & -0.0001 & 0.0007 \\ 0.001 & 0.0003 & -0.0001 & 0.0005 & -0.0002 & 0.0005 \\ 0.002 & 0.0004 & 0 & 0.0004 & 0.0002 & 0.0007 \\ 0.002 & 0.0003 & -0.0001 & 0.0005 & -0.0002 & 0.0005 \\ -0.0011 & 0.0003 & -0.0001 & 0 & 0.0012 & 0.0006 \\ 0.0002 & 0.0004 & 0 & -0.0001 & 0.0011 & 0.0007 \end{bmatrix}$$

$$b = \begin{bmatrix} 0.0153 & -0.0016 & 0.0305 & 0.0201 & 0.0264 & -0.0023 \\ 0.0038 & 0.0077 & 0.0313 & 0.0353 & -0.0315 & 0.0051 \\ 0.0047 & 0.0064 & 0.0331 & -0.0590 & -0.0074 & -0.0045 \\ -0.0025 & -0.0057 & 0.0325 & -0.0169 & 0.0422 & 0.0012 \\ 0.0409 & -0.0083 & 0.032 & 0.0116 & -0.0628 & 0.0042 \\ -0.0012 & -0.0132 & 0.0279 & -0.0458 & -0.0427 & 0.0015 \end{bmatrix}$$

$$c = \begin{bmatrix} -0.848 & -0.8155 & 0.1415 & -0.0607 & -0.0621 & 0.0167 \\ -1.1615 & -1.5507 & -1.1529 & -1.2354 & -1.2332 & -1.2406 \\ -0.453 & -0.4064 & -0.0273 & -0.0474 & -0.0501 & -0.0589 \\ -0.357 & -0.3015 & -0.3918 & -0.5780 & -0.5771 & -0.4259 \\ -0.4764 & -0.3677 & -0.1436 & -0.1297 & -0.1307 & -0.1130 \\ -0.4677 & -0.4026 & -0.1145 & -0.118 & -0.1227 & -0.1594 \end{bmatrix}$$

Substitute $D = \begin{bmatrix} 10 \\ 0 \\ 0 \\ 0 \\ 0 \\ 0 \end{bmatrix}$ we get $V = \begin{bmatrix} -0.680 \\ -1.50 \\ -0.375 \\ -0.344 \\ -0.217 \\ -0.440 \end{bmatrix}$

Comparing to the Voltage we get form experiment $V_{(\exp)} = \begin{bmatrix} -0.667 \\ -1.549 \\ -0.376 \\ -0.348 \\ -0.217 \\ -0.444 \end{bmatrix}$

The results are very close to each other. Now the linear displacement is correct and will check for angular displacement.

Using $D = \begin{bmatrix} 0 \\ 0 \\ 0 \\ 5 \\ 0 \\ 0 \end{bmatrix}$ the calculated $V = \begin{bmatrix} 0.046 \\ -1.044 \\ -0.334 \\ -0.650 \\ -0.080 \\ -0.361 \end{bmatrix}$

Comparing to the Voltage we get form experiment $V_{(\exp)} = \begin{bmatrix} 0.046 \\ -1.052 \\ -0.334 \\ -0.654 \\ -0.078 \\ -0.35 \end{bmatrix}$

Now it is found that the above equation will work for input for a single DOF. The next step is to check whether it will work if there are more than two input of DOF. For example, using data of X = 20mm and Y = 10 mm i.e.

$D = \begin{bmatrix} 20 \\ 10 \\ 0 \\ 0 \\ 0 \\ 0 \end{bmatrix}$

The calculated $V = \begin{bmatrix} -1.2381 \\ -6.9913 \\ -0.0451 \\ -1.9083 \\ -1.0361 \\ -1.4209 \end{bmatrix}$ and the actual experimental $V_{(\exp)} = \begin{bmatrix} -0.054 \\ -1.4 \\ -0.123 \\ -0.412 \\ -0.06 \\ -0.138 \end{bmatrix}$

The two V values are totally different. And if we consider another case where

$$D = \begin{bmatrix} 10 \\ 10 \\ 0 \\ 10 \\ 10 \\ 0 \end{bmatrix}$$

The calculated $V = \begin{bmatrix} -0.9561 \\ -7.2613 \\ -1.2961 \\ -2.2003 \\ -1.5071 \\ -2.2539 \end{bmatrix}$ whereas the experimental $V_{(\exp)} = \begin{bmatrix} -0.043 \\ -0.652 \\ -0.60 \\ -0.654 \\ 0.548 \\ -0.21 \end{bmatrix}$

As to be expected, the two Voltage values are totally different, there must be some fundamental theory that is not true for this set up. The super-position theory is applicable on if the relationship between the lateral displacement and axial displacement is linear. This will be discussed further in the discussion section.

## 5.8 Discussion

From the experiment, it shows that the relationship between voltage and displacement may not necessary be linear. Parabolic relationship can be found between the two variables. Because of this fact, superposition cannot be applied. Only one degree of freedom is varied at a time.

One of the errors in this experiment is the initial strain and initial displacement. Because the joystick is very flexible, when it is clamped by the dividing head, there will always be a very small deflection, and thus change the boundary conditions. I try to design a better system in order to overcome this problem, but was unable to do so. Therefore this error will be there when measuring the displacement.

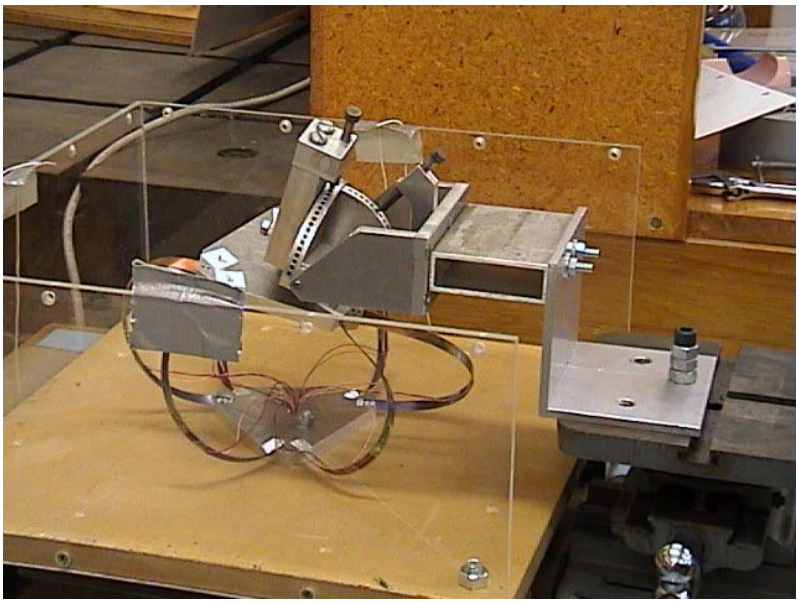

**Figure 5.20 The base platform is not parallel to the X-Y table**

Another error of concern is the direction of the constrained displacement, which is shown in Figure 5.20. The joystick can be considered as symmetric, but if we applied constrained displacement on X and Y axes, where they are $90^o$ offset, then the system will not be symmetric because all the strips are $120^o$ offset. This problem will affect the result when more than two degrees of freedom are being varied.

Further work can be done on placement of the strain gauges. There maybe be some place on the joystick where the relationship between voltage and displacement is linear. In this case, the original K matrix can be determined. With a given displacement, the corresponding voltage can be calculated.

# CHAPTER 6

# CONCLUSION

This chapter summarises each chapter and presents a brief discussion and conclusion for each chapter.

The following sections summarise each chapter respectively and described the achieved objectives.

## 6.1 Design and Build of the Prototype Model

This part of thesis discusses the design process for the 6DOF joystick. The model was modified many times. The design of the joystick is based on the structure of Gough-Stewart Platform. This structure is constructed by using two truncated triangular plates with six legs. The design process involves determining the size, the material and the shape of the platforms. Two mechanisms were considered to connect the two platforms, spring wire and spring strip. They both have their own advantages and disadvantages. One of the most important features of using spring wire is that it will allow the upper platform to return to its natural position. Other advantages of spring wire are such as it has lightweight, easy to install, inexpensive, the length is relatively easy to adjust, and there are lots of options for the wire diameter and stiffness from the industrial market. The biggest disadvantage was that the strain gauge could not be able to attach on the wire. Therefore spring strip was used. It has almost all the advantages of spring wire except that it is not easy to install, and it has torsional strain introduced during manufacture. The strip has flat surface that allows the installation of the standard strain gauges, which being the biggest advantage of using spring strip.

All the strain gauge wires are connected to bridge amplifiers. Outputs of the amplifier were then connected to a computer that was used to run DSPACE and MATLAB for data collection. There are two software programs for converting the measurements in to voltage readings. Simulink within the MATLAB program is used for modelling, simulating and analysing dynamic, multidomain systems.

## 6.2 Deflection theory

Since the prototype model is constructed by two platforms and 6 strips. It is necessary to develop a set of equations to calculate the deflection of these strips subject to 3 forces and 3 moments in three dimensions under large deflection theory. The Three-dimensional beam deflection is extremely difficult especially with large deflection. The equations of large deflection are derived as follow.

Inflection Point Exists

$$\alpha = \frac{1}{\sqrt{2}}\left(\int_0^{\theta_i}\frac{d\theta}{f(\theta)} + \int_{\theta_o}^{\theta_i}\frac{d\theta}{f(\theta)}\right) \tag{6.1}$$

$$\frac{x_o}{l} = \frac{1}{\alpha\sqrt{2}}\left(\int_0^{\theta_i}\frac{\cos\theta}{f(\theta)}d\theta + \int_{\theta_o}^{\theta_i}\frac{\cos\theta}{f(\theta)}d\theta\right) \tag{6.2}$$

$$\frac{y_o}{l} = \frac{1}{\alpha\sqrt{2}}\left(\int_0^{\theta_i}\frac{\sin\theta}{f(\theta)}d\theta + \int_{\theta_o}^{\theta_i}\frac{\sin\theta}{f(\theta)}\right) \tag{6.3}$$

No Inflection Point Exists

$$\alpha = \pm\frac{1}{\sqrt{2}}\left(\int_0^{\theta_i}\frac{d\theta}{f(\theta)} + \int_{\theta_o}^{\theta_i}\frac{d\theta}{f(\theta)}\right) \tag{6.1}$$

or

$$\frac{x_o}{l} = \pm\frac{1}{\alpha\sqrt{2}}\left(\int_0^{\theta_i}\frac{\cos\theta}{f(\theta)}d\theta + \int_{\theta_o}^{\theta_i}\frac{\cos\theta}{f(\theta)}d\theta\right) \tag{6.2}$$

$$\frac{y_o}{l} = \pm\frac{1}{\alpha\sqrt{2}}\left(\int_0^{\theta_i}\frac{\sin\theta}{f(\theta)}d\theta + \int_{\theta_o}^{\theta_i}\frac{\sin\theta}{f(\theta)}\right) \tag{6.3}$$

As the joystick has six beams interacting with each other, it is beyond the scope of this project to determine the detailed calculations of the interactions. Alternatively, further analysis should be performed using finite element software such as ANSYS.

## 6.3 ANSYS

ANSYS as the finite element package is used to model the prototype, as well as a single beam that was calculated mathematically.

The ultimate purpose of a finite element analysis is to re-create mathematically the behaviour of an actual engineering system. In other words, the analysis must be an accurate mathematical model of a physical prototype.

The first model is one half of a circular beam, with one end clamped, and two forces (X, Y directions) are applied to another end. This model is constructed for checking if the theoretical results match the ANSYS results. Comparing the result obtained from theory and ANSYS, they are exactly the same. Therefore ANSYS proved that the formulas used to calculate the deflection of singular beam is correct.

The prototype model was constructed according to the actual size and geometry of the joystick. In the actually experiment of the prototype, strain gauges are attached to the 6 stripes, and it gives an output voltage that will be display on screen. The voltage cannot be calculated using ANSYS, the closest relate to voltage is strain. Therefore, the graphs of displacement of the top plate against the strain of 6 strips were determined.

## 6.4 Testing

The experiment procedure and method of testing are discussed in this section. The relationship between the 6 DOF and the 6 output channels is included in the background theory section, along with the method of getting the 6 x 6 matrix. In particular, the analysis checks whether linearity holds for all 6 channels in all 6 DOF, and also will construct the Jacobian matrix.

Base on the experimental evidence, non-linearity relationships are found to apply for combined multi-DOF inputs. Thus super-position theory cannot be used to precisely separate the various displacements input to the joystick. However, in the case of varying only 1 DOF, the Jacobian gives a good approximation to the answer. In

other words, the simulation model is able to accurately compute the displacements if only one force or one moment is applied. If combinations of moments and forces are applied, the model is unable to predict the displacements, although it can determine crude approximations of the multiple values.

To conclude, the joystick prototype is successfully designed and built. Extensive analysis has been performed to simulate the movements of the wire strips by using finite element analysis.

## 6.5 Further Work

The priority for future work will be investigating and applying the beam deflection theory on the 3-dimensional model subject to 3-forces and 3-moments, as well as large deflections. This is not a trivial task and is the subject of continuing research in this field. By doing so, the exact relation could be identified and hence the control interface could be investigated.

It is also important to optimise the calibration process by means of minimizing the b matrix and defining the process of calibration.

# APPENDIX A

# PROTOTYPE DRAWINGS

A.1 SolidWorks Drawings of Designs

A.2 SolidWorks Drawings of Prototype

# A.1 SolidWorks Drawings of Designs

### Design Model 1: Overall Model

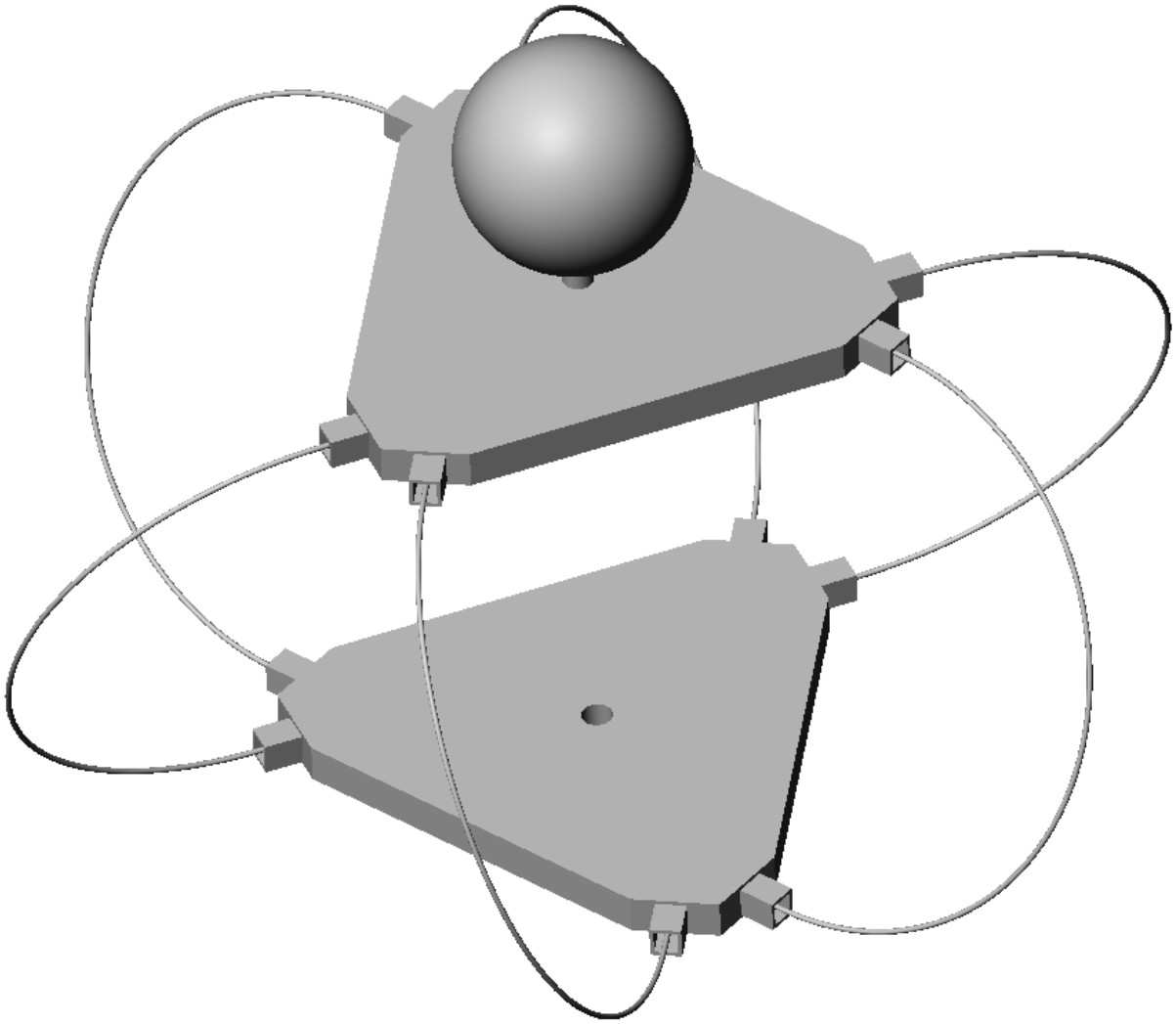

**Design Model 1: Platform Design**

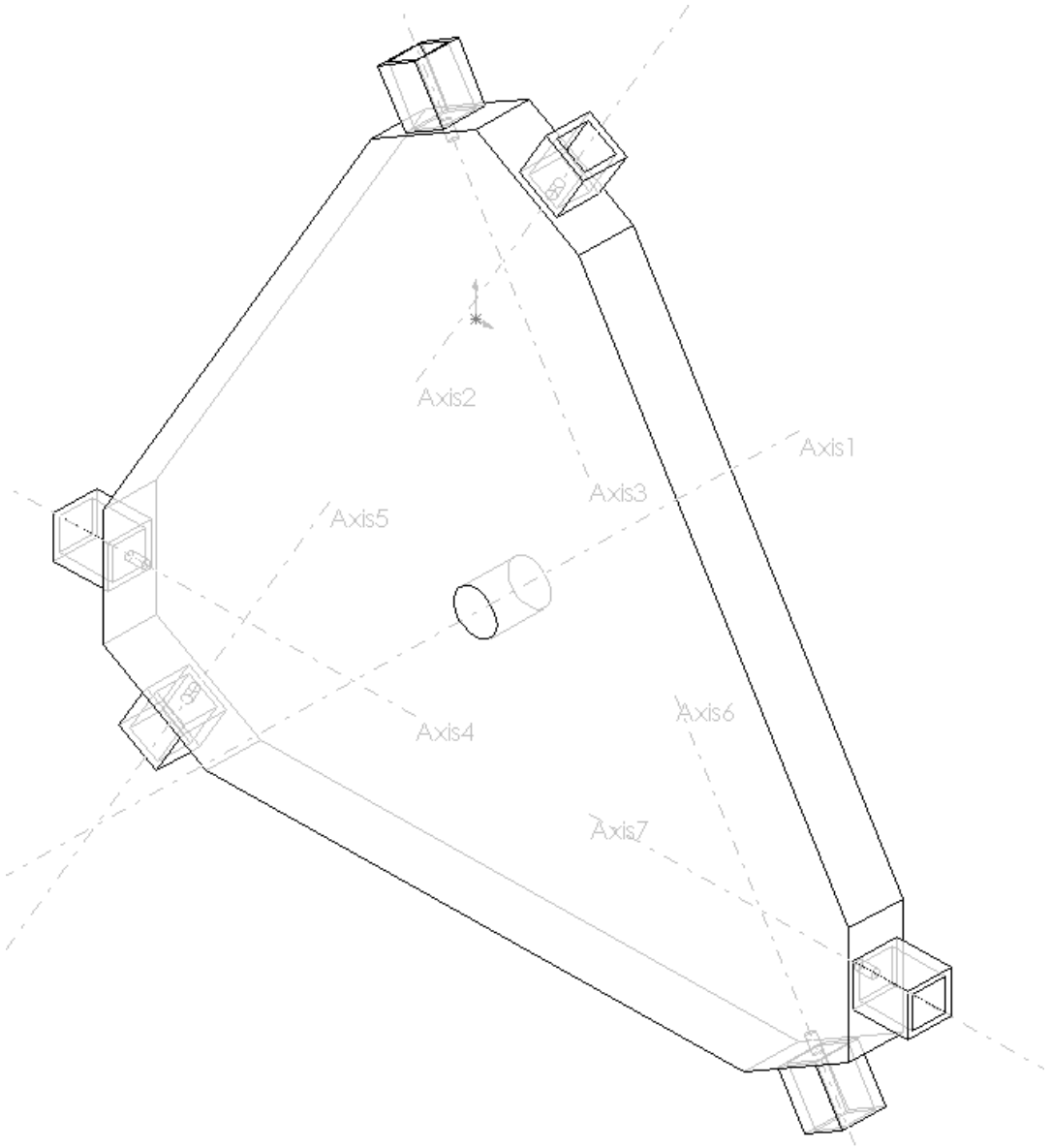

## Design Model 1: Dimension of the platform

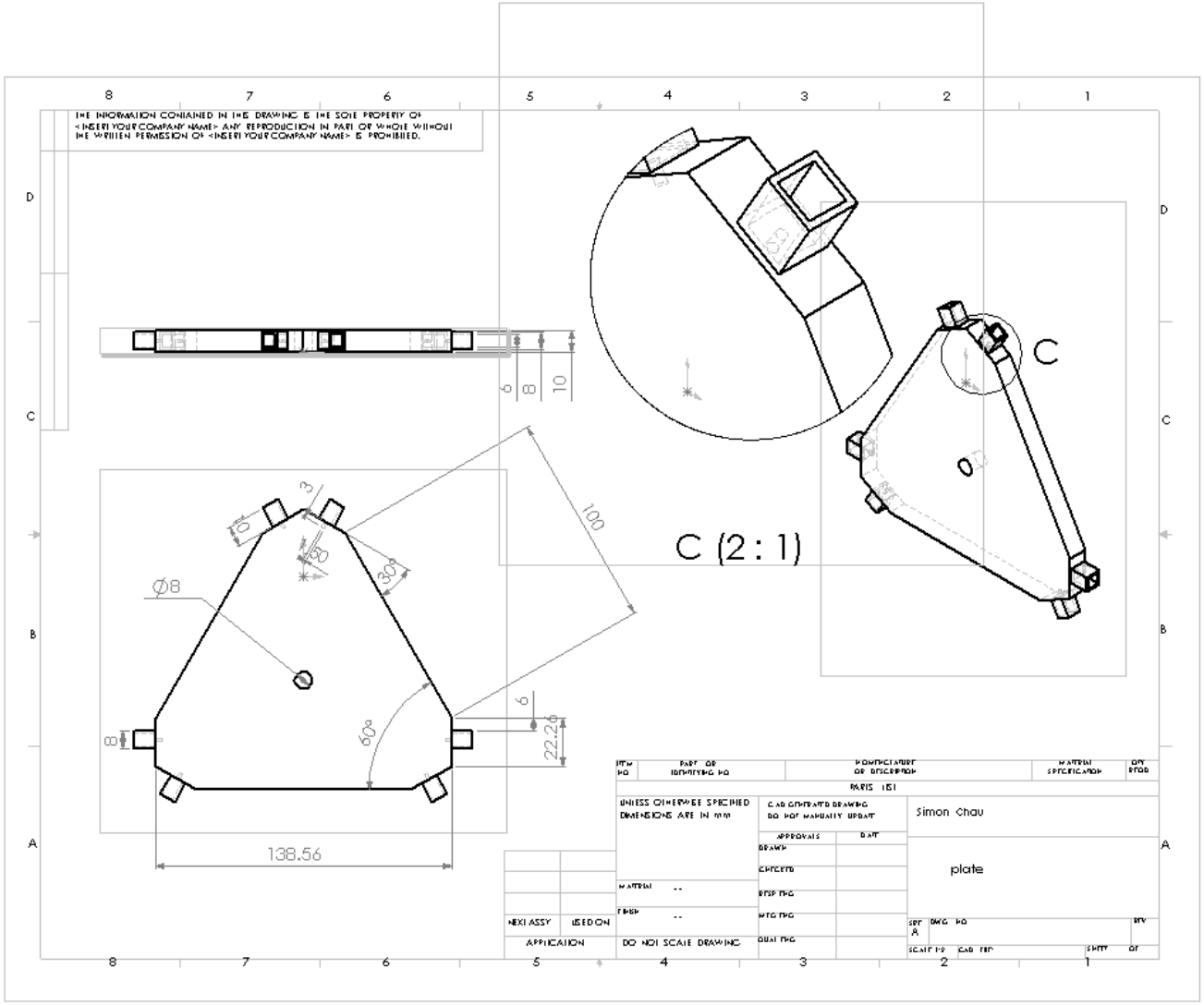

**Design Model 2: Platform Design**

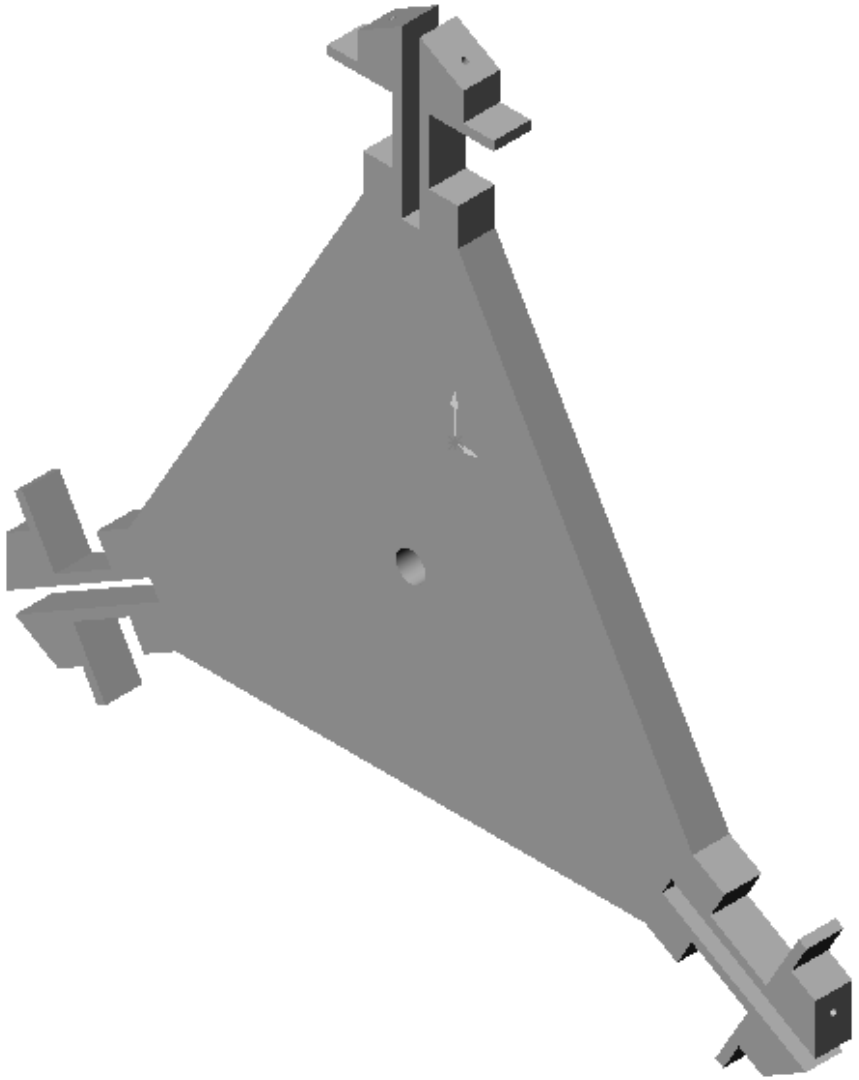

**Design Model 2: Dimension of the platform**

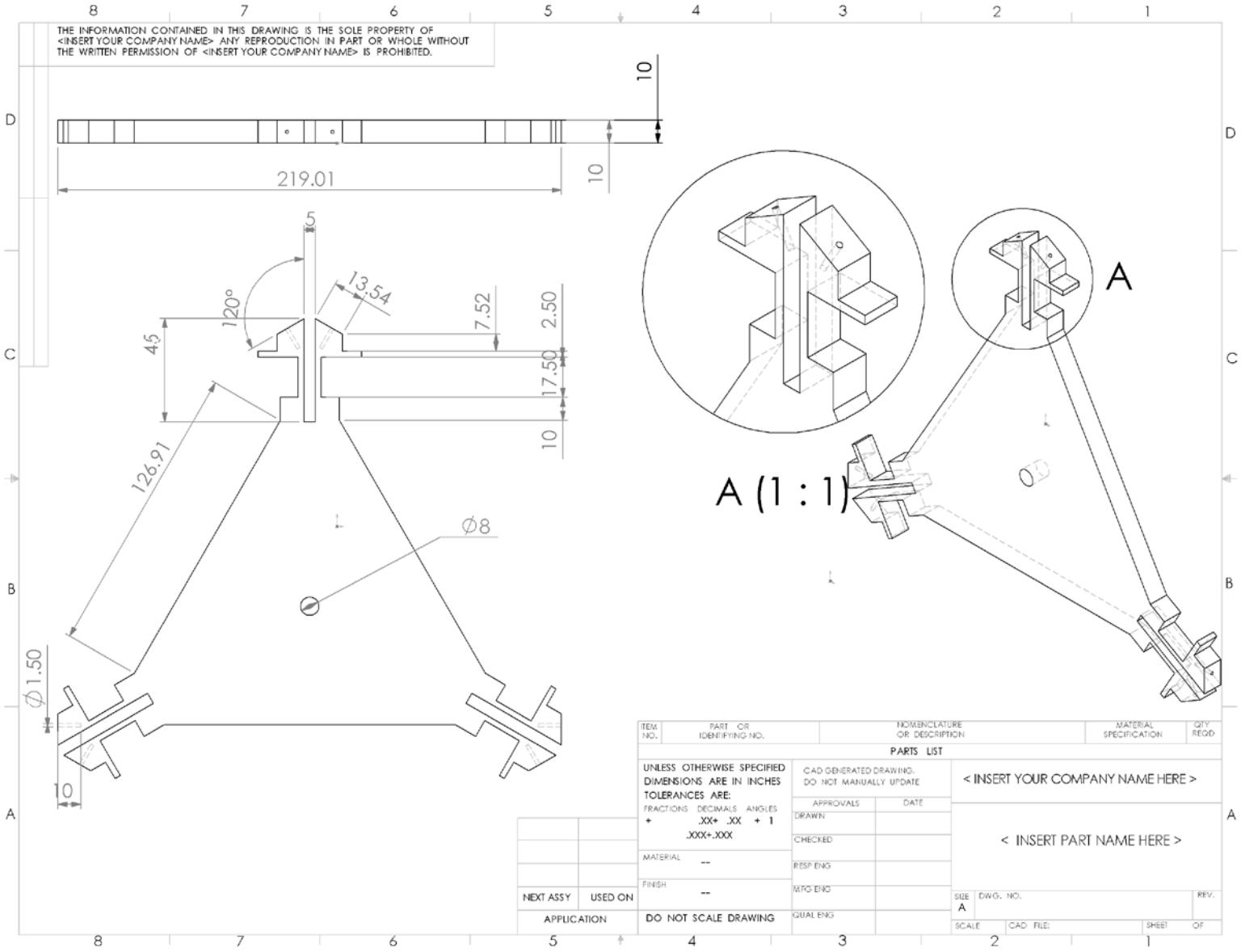
THE INFORMATION CONTAINED IN THIS DRAWING IS THE SOLE PROPERTY OF <INSERT YOUR COMPANY NAME> ANY REPRODUCTION IN PART OR WHOLE WITHOUT THE WRITTEN PERMISSION OF <INSERT YOUR COMPANY NAME> IS PROHIBITED.
10
219.01
10
5
120°
13.54
7.52
2.50
45
17.50
10
126.91
Ø8
Ø1.50
10
A
A (1 : 1)
ITEM NO.
PART OR IDENTIFYING NO.
NOMENCLATURE OR DESCRIPTION
MATERIAL SPECIFICATION
QTY REQD
PARTS LIST
UNLESS OTHERWISE SPECIFIED DIMENSIONS ARE IN INCHES TOLERANCES ARE:
FRACTIONS DECIMALS ANGLES
+ .XX+ .XX + 1
.XXX+.XXX
MATERIAL --
FINISH --
DO NOT SCALE DRAWING
CAD GENERATED DRAWING. DO NOT MANUALLY UPDATE
APPROVALS DATE
DRAWN
CHECKED
RESP ENG
MFG ENG
QUAL ENG
< INSERT YOUR COMPANY NAME HERE >
< INSERT PART NAME HERE >
SIZE A
DWG. NO.
REV.
SCALE
CAD FILE:
SHEET OF
NEXT ASSY
USED ON
APPLICATION

**Design Model 3: Platform Design**

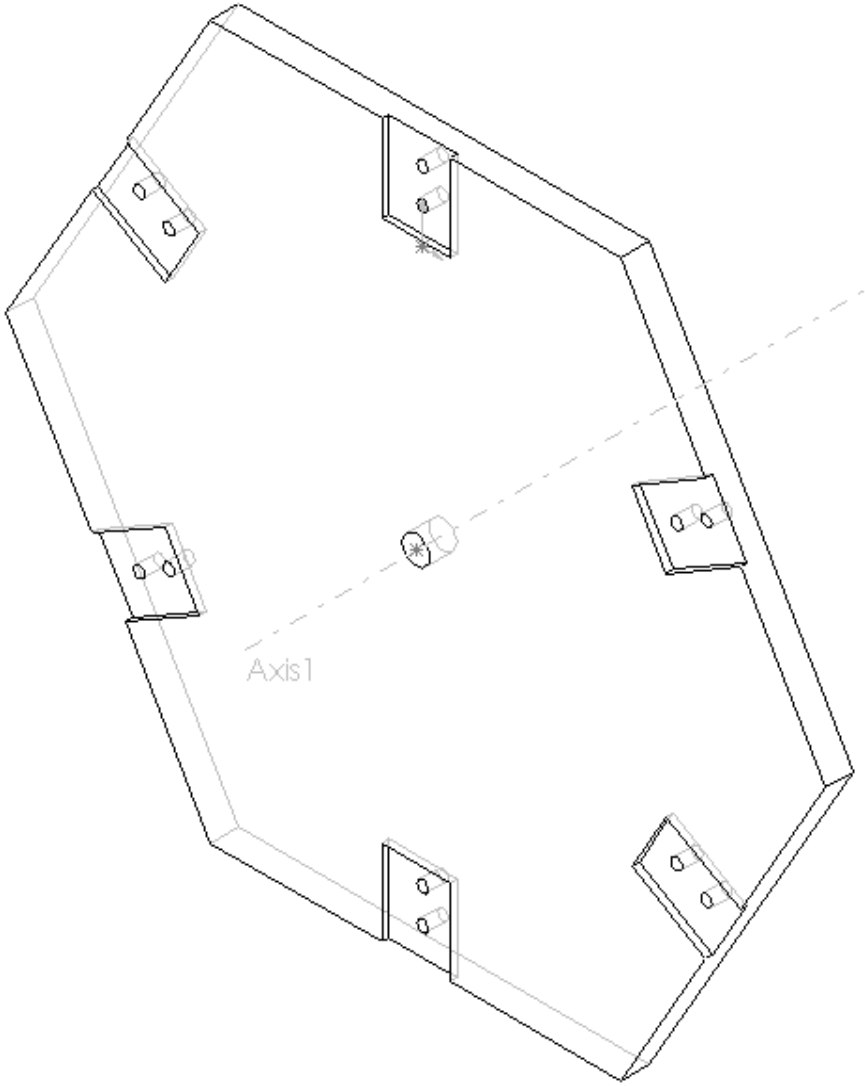

**Design Model 3: Overall Design**

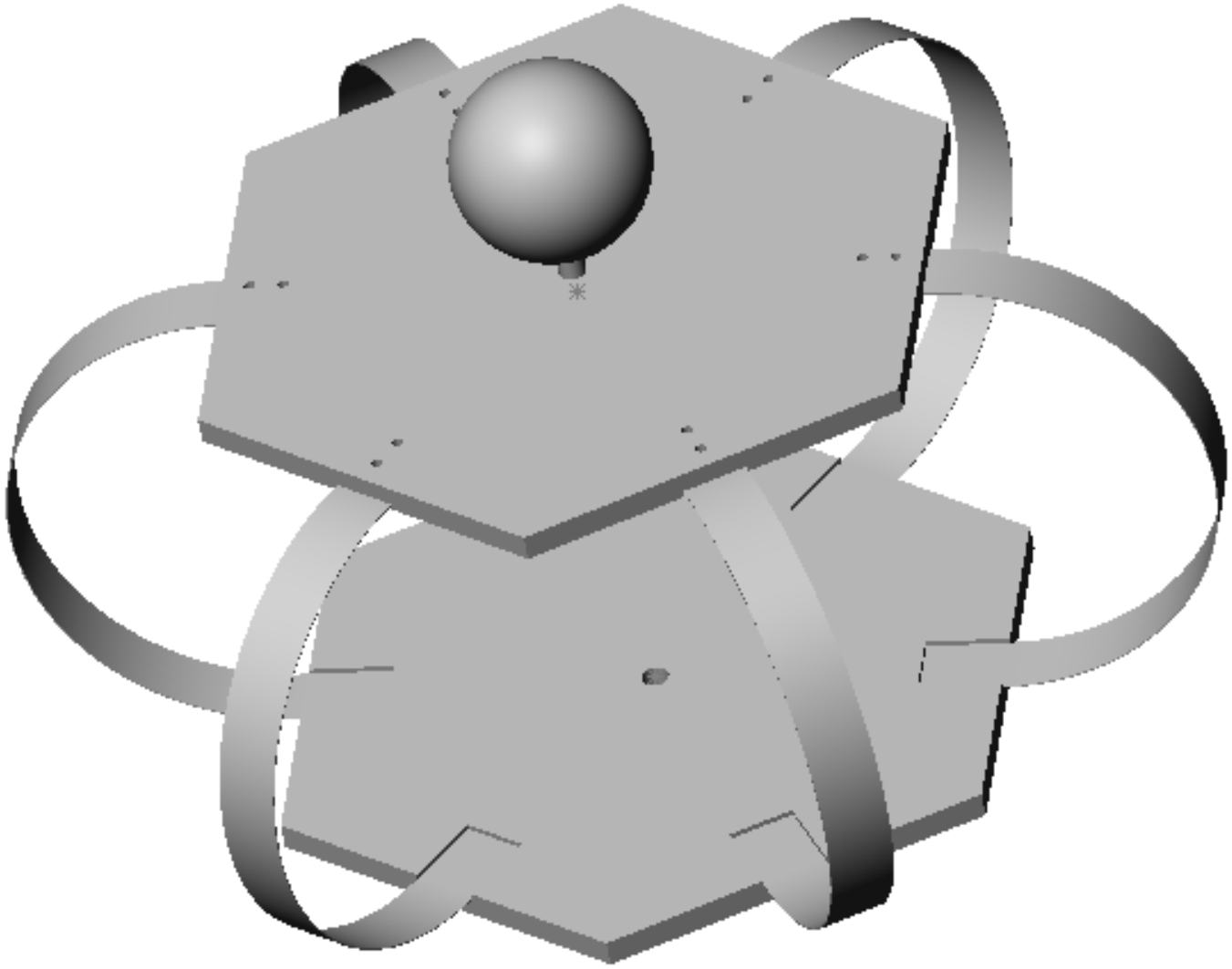

**Design Model 3: Dimension of the platform**

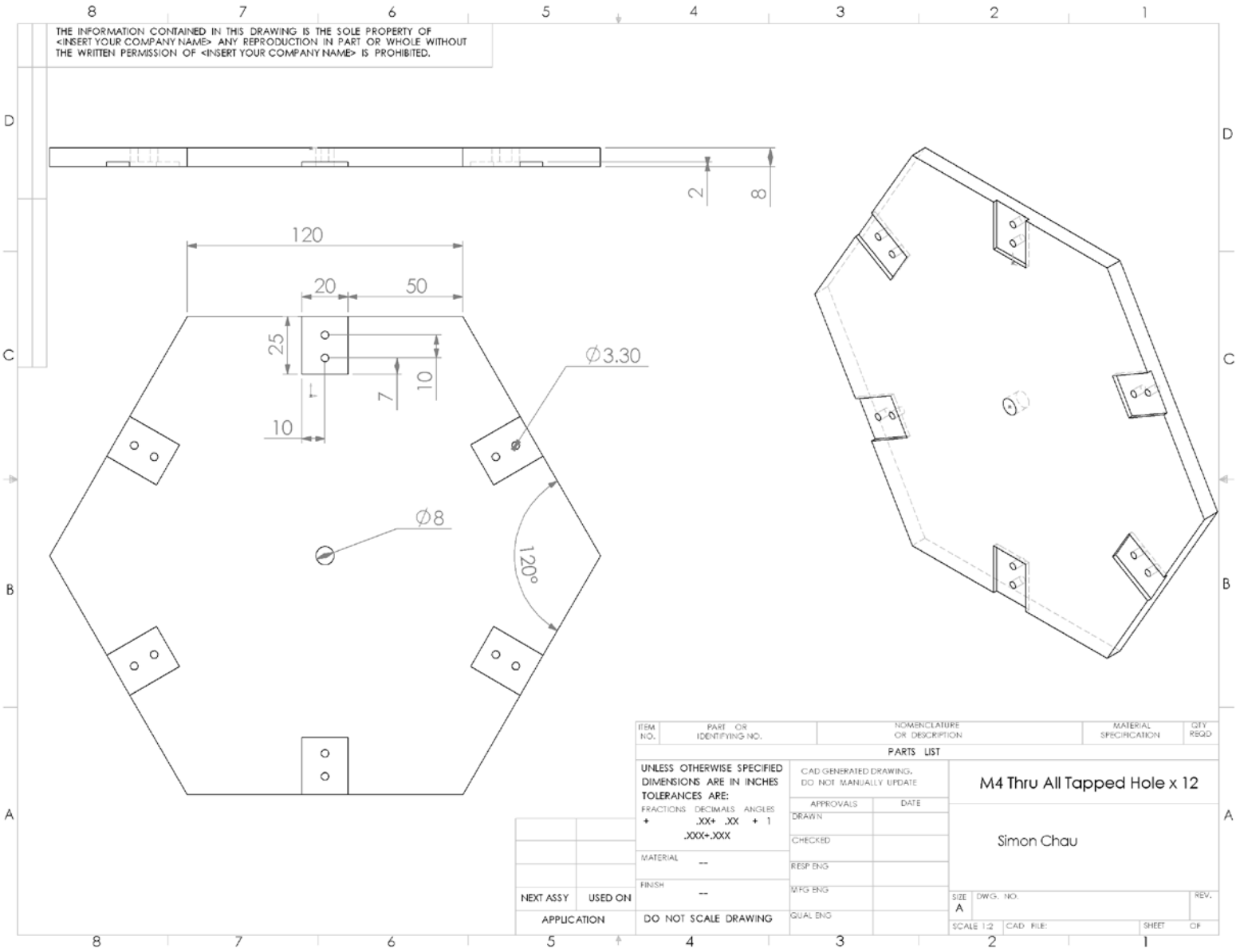
THE INFORMATION CONTAINED IN THIS DRAWING IS THE SOLE PROPERTY OF <INSERT YOUR COMPANY NAME> ANY REPRODUCTION IN PART OR WHOLE WITHOUT THE WRITTEN PERMISSION OF <INSERT YOUR COMPANY NAME> IS PROHIBITED.
2
8
120
20
50
25
10
7
10
Ø3.30
Ø8
120°
ITEM NO.
PART OR IDENTIFYING NO.
NOMENCLATURE OR DESCRIPTION
MATERIAL SPECIFICATION
QTY REQD
PARTS LIST
UNLESS OTHERWISE SPECIFIED DIMENSIONS ARE IN INCHES TOLERANCES ARE:
FRACTIONS DECIMALS ANGLES
+ .XX+ .XX + 1
.XXX+.XXX
CAD GENERATED DRAWING. DO NOT MANUALLY UPDATE
APPROVALS
DATE
DRAWN
CHECKED
RESP ENG
MFG ENG
QUAL ENG
MATERIAL --
FINISH --
DO NOT SCALE DRAWING
M4 Thru All Tapped Hole x 12
Simon Chau
NEXT ASSY
USED ON
APPLICATION
SIZE A
DWG. NO.
REV.
SCALE 1:2
CAD FILE:
SHEET
OF

## Design Model 4: Platform Design

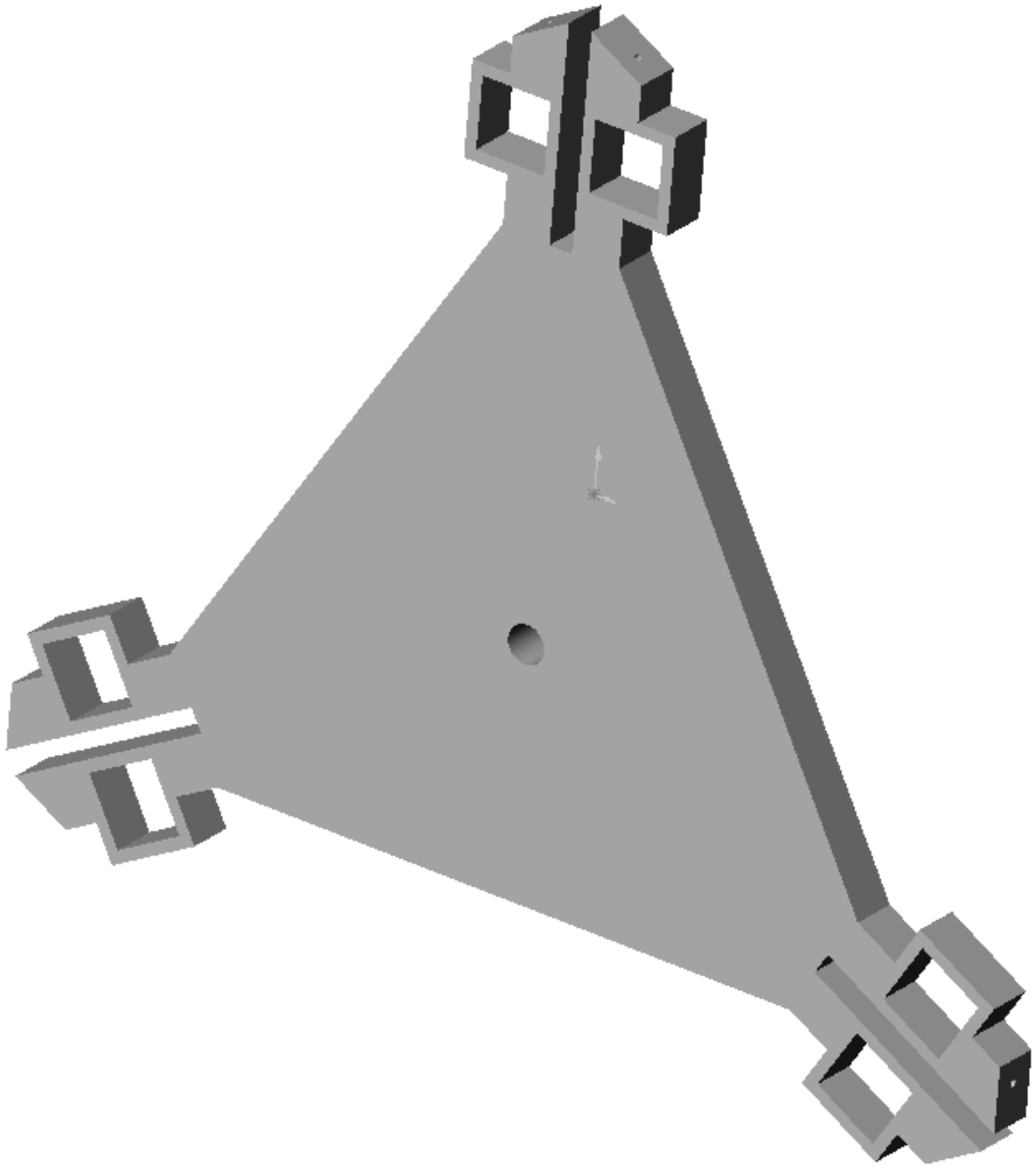

**Design Model 4: Overall Model**

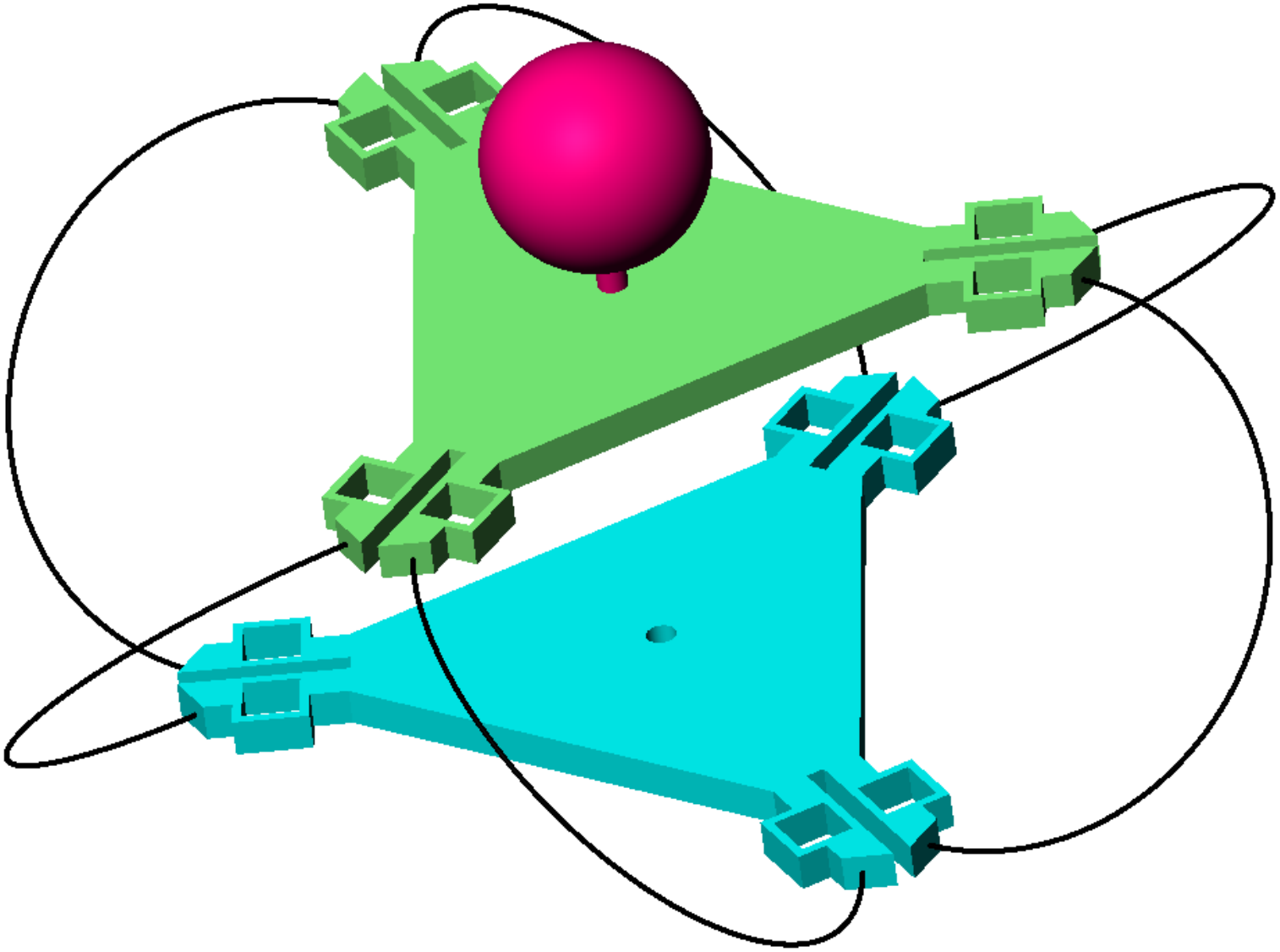

**Design Model 4: Dimension of the platform**

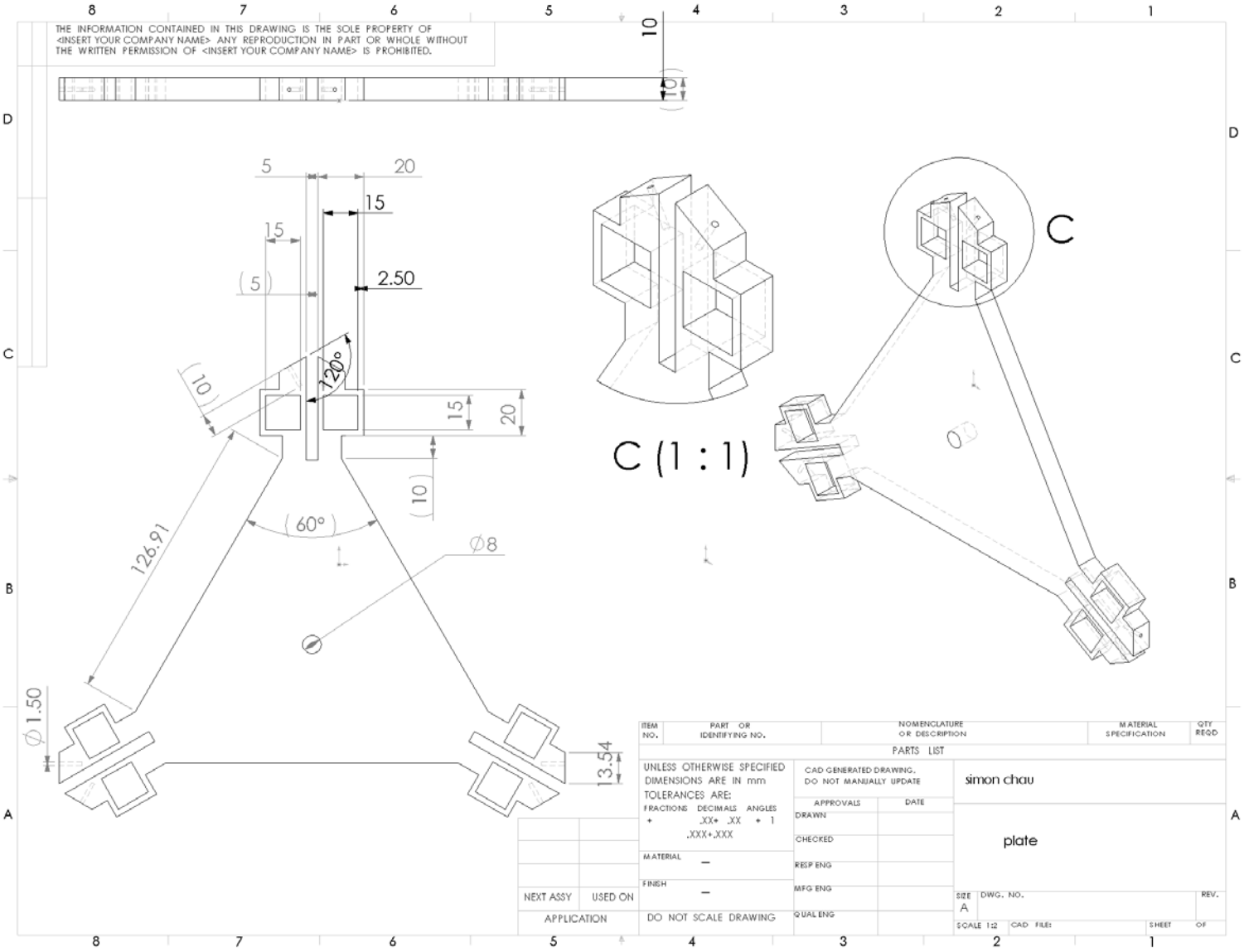
THE INFORMATION CONTAINED IN THIS DRAWING IS THE SOLE PROPERTY OF <INSERT YOUR COMPANY NAME> ANY REPRODUCTION IN PART OR WHOLE WITHOUT THE WRITTEN PERMISSION OF <INSERT YOUR COMPANY NAME> IS PROHIBITED.
10
10
5
20
15
15
(5)
2.50
120°
(10)
15
20
(10)
(60°)
126.91
Ø8
Ø1.50
13.54
C
C (1 : 1)
ITEM NO.
PART OR IDENTIFYING NO.
NOMENCLATURE OR DESCRIPTION
MATERIAL SPECIFICATION
QTY REQD
PARTS LIST
UNLESS OTHERWISE SPECIFIED
DIMENSIONS ARE IN mm
TOLERANCES ARE:
FRACTIONS DECIMALS ANGLES
± .XX± .XX ± 1
.XXX±.XXX
MATERIAL —
FINISH —
NEXT ASSY
USED ON
APPLICATION
DO NOT SCALE DRAWING
CAD GENERATED DRAWING.
DO NOT MANUALLY UPDATE
APPROVALS
DATE
DRAWN
CHECKED
RESP ENG
MFG ENG
QUAL ENG
simon chau
plate
SIZE A
DWG. NO.
REV.
SCALE 1:2
CAD FILE:
SHEET
OF

## A.2 SolidWorks Drawings of Prototype

**Prototype Platform Design**

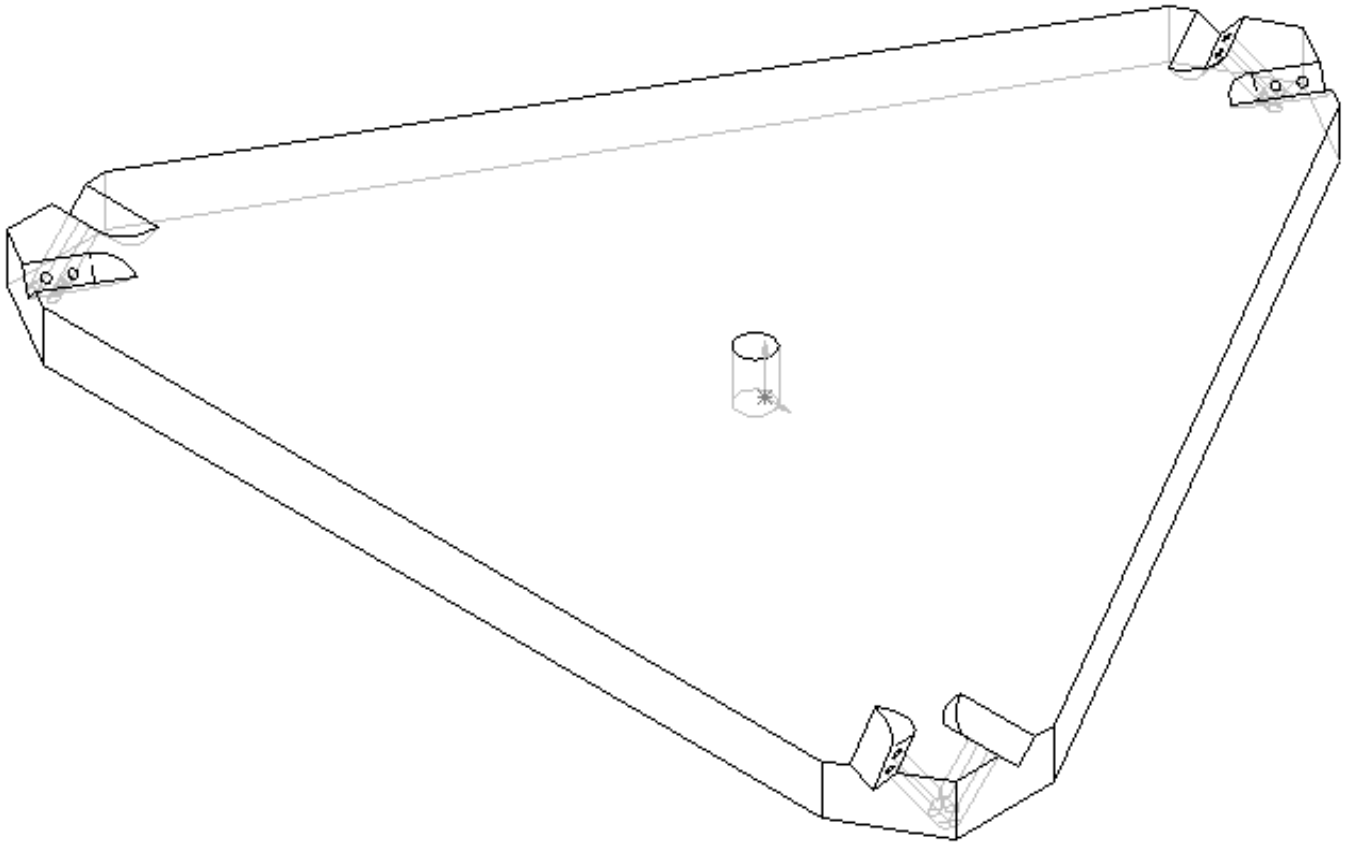

**Overall Prototype Model**

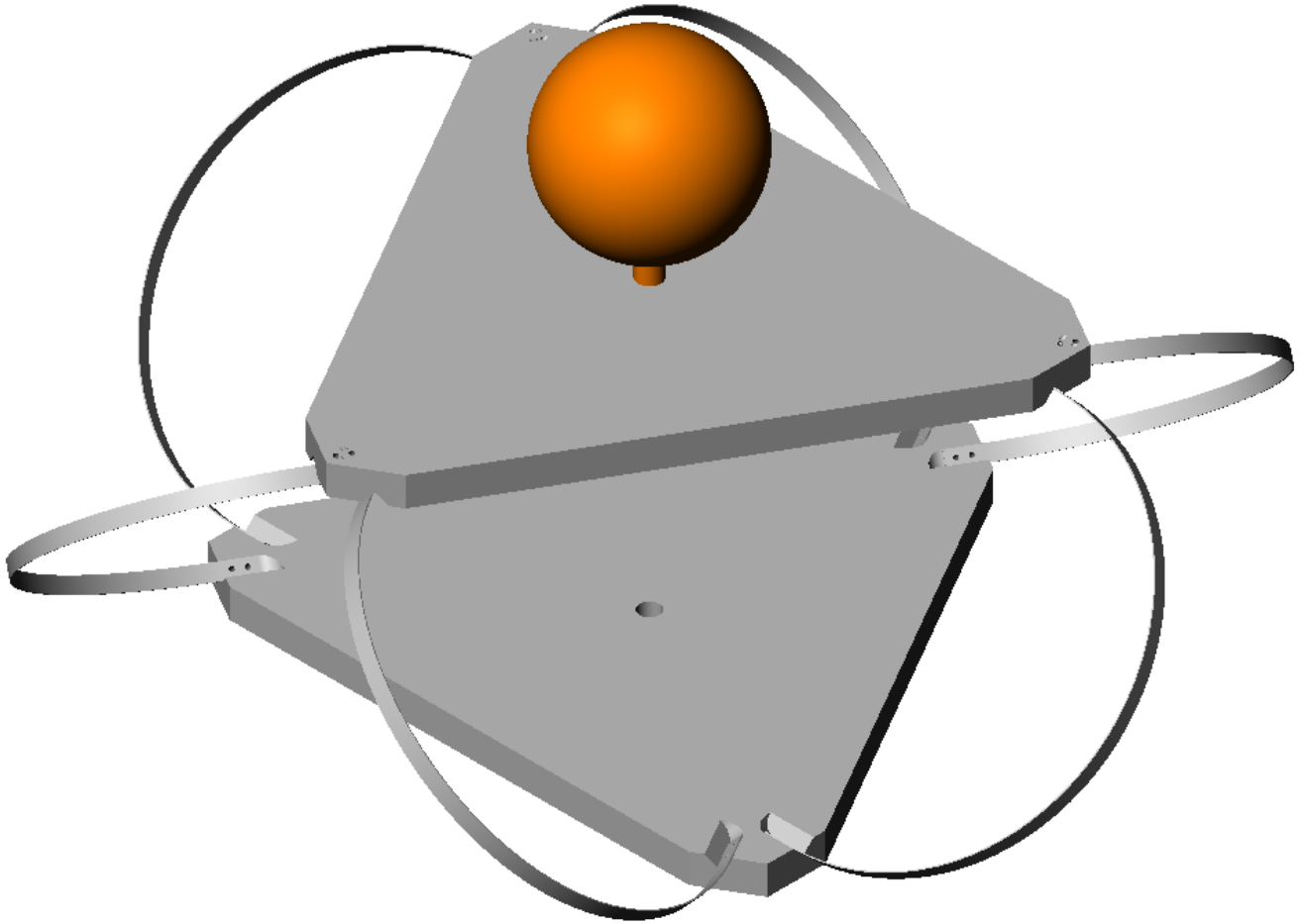

**Dimention of Prototype Platform I**

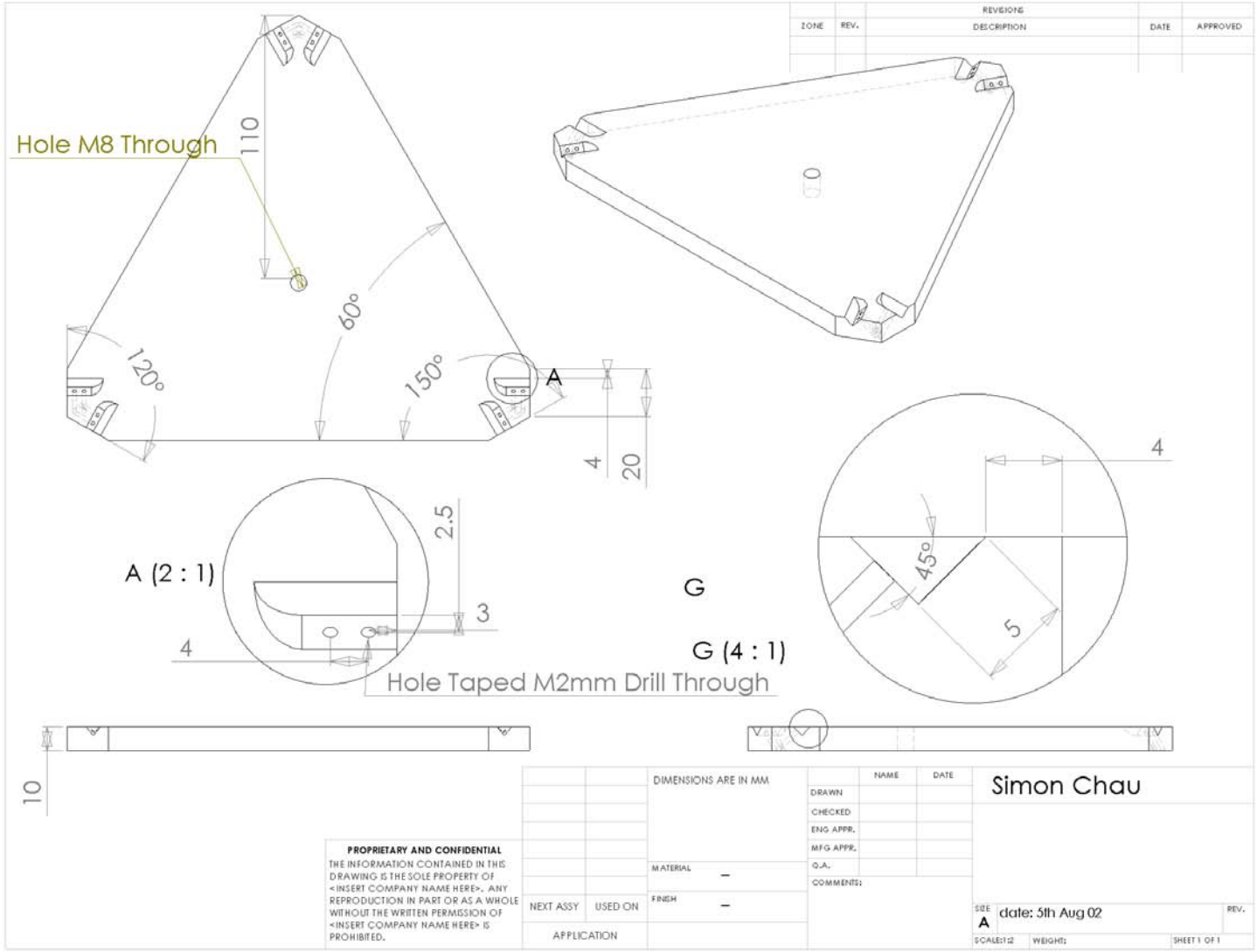

## Dimension of the Prototype Platform II

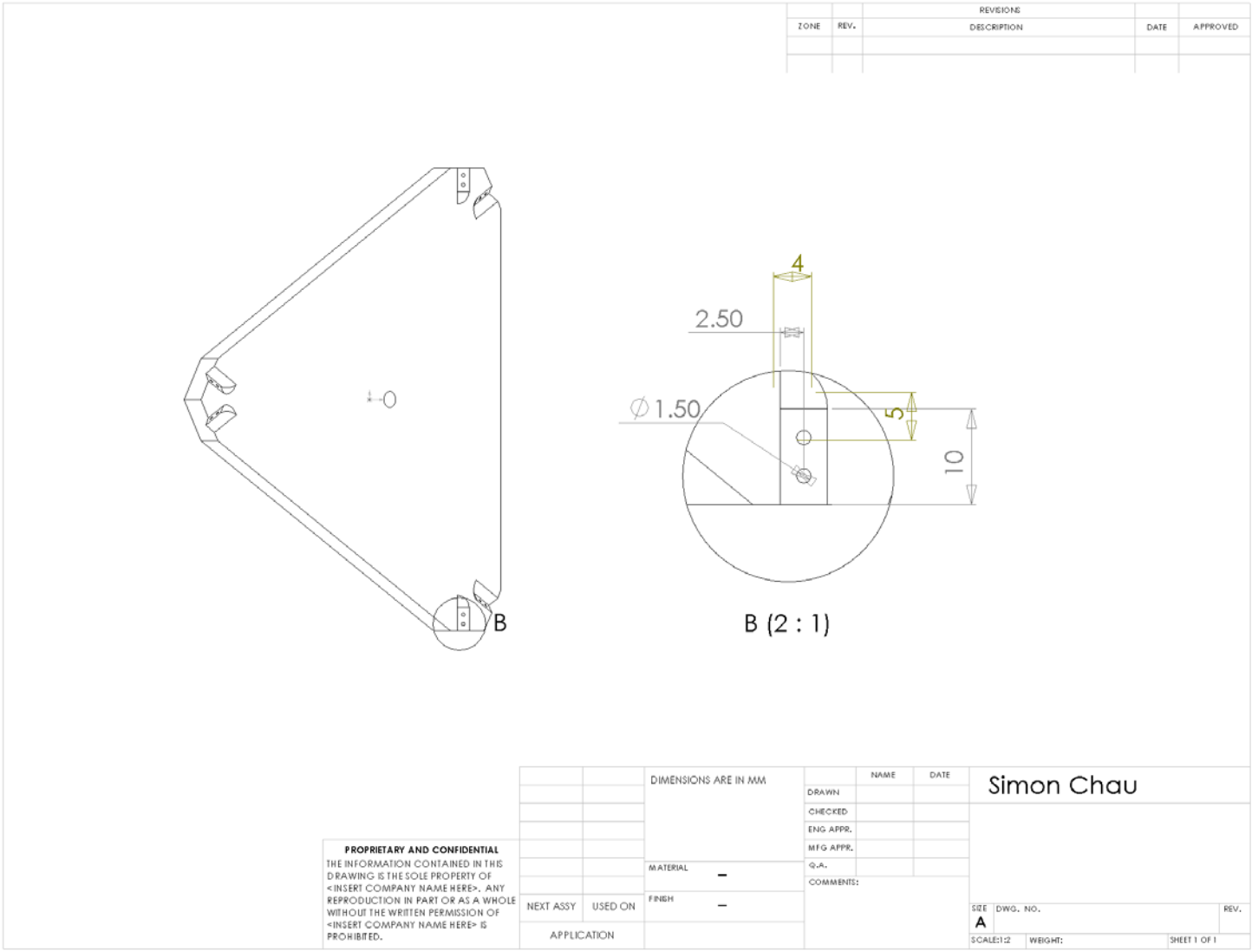

## Overall Prototype Display

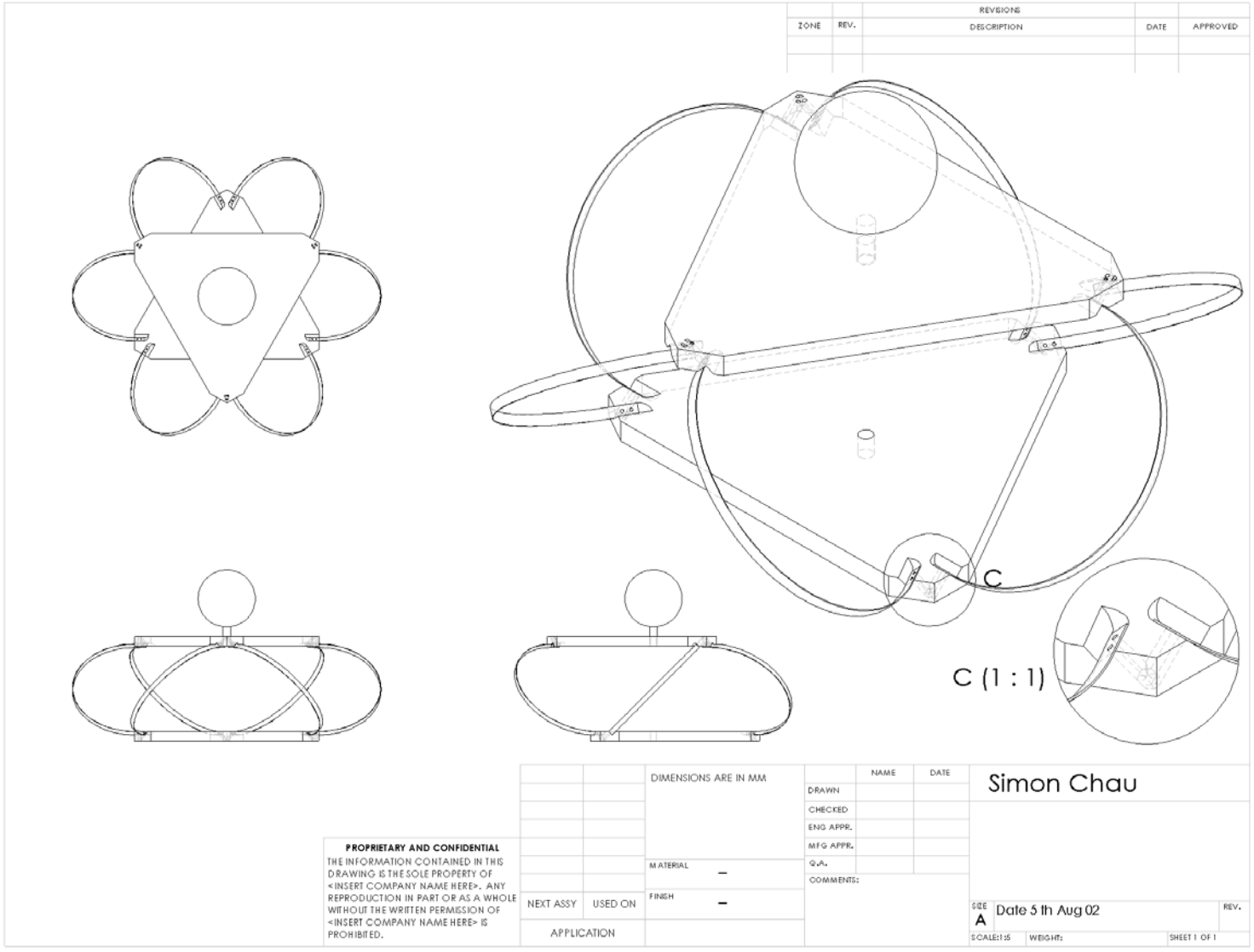
REVISIONS
ZONE
REV.
DESCRIPTION
DATE
APPROVED
C
C (1 : 1)
DIMENSIONS ARE IN MM
NAME
DATE
DRAWN
CHECKED
ENG APPR.
MFG APPR.
Q.A.
COMMENTS:
Simon Chau
PROPRIETARY AND CONFIDENTIAL
THE INFORMATION CONTAINED IN THIS DRAWING IS THE SOLE PROPERTY OF <INSERT COMPANY NAME HERE>. ANY REPRODUCTION IN PART OR AS A WHOLE WITHOUT THE WRITTEN PERMISSION OF <INSERT COMPANY NAME HERE> IS PROHIBITED.
MATERIAL
FINISH
NEXT ASSY
USED ON
APPLICATION
SIZE
A
Date 5 th Aug 02
REV.
SCALE:1:5
WEIGHT:
SHEET 1 OF 1

# APPENDIX B

# ANSYS ANALYSIS

B.1 Pseudo-Code for Single Beam

B.2 Pseudo-Code for Joystick Model

B.3 ANSYS Generated Drawings for Joystick Model

## B.1 Pseudo-Code for Single Beam

```
finish
/clear
pi=3.141592654
rad=40e-3
dia=1e-3
xload=10

yload=10
/prep7
csys,1
k
k,,-rad,0
k,,rad,90
l,2,3
csys,0
lesize,all,,1
!*
mp,ex,1,200e9
mp,nuxy,1,0.3
!*
ET,1,BEAM4
KEYOPT,1,2,0
KEYOPT,1,6,0
KEYOPT,1,7,0
KEYOPT,1,9,0
KEYOPT,1,10,0
R,1,pi*dia**2/4,pi*dia**4/64,pi*dia**4/64,dia,di
a,0,
RMORE,0,pi*dia**4/32,0,0,0,0,
!*
!ET,1,BEAM188
!*
!*
!R,1,  ,4.908738521875e-014,4.908738521875e-0
14,0.001,
!*
!SECTYPE,      1, BEAM, CSOLID, , 0
!SECOFFSET, CENT
!SECDATA,0.5e-3,0,0,0,0,0,0,0,0,0
!*
fk,3,fx,xload
fk,3,fy,yload
dk,2,all
!*
lmesh,all
!*
/solu
!nlgeom,on
!time,200
!deltim,10
!CNVTOL,M, ,0.001,2, ,
solve
/post1
/decale,,1
pldisp,2
```

## B.2 Pseudo-Code for Joystick Model

```
finish
/clear
!*
stripthk=0.4e-3
stripwdth=8e-3

height=80e-3    ! m
tridia=120e-3 ! m
outdia=110e-3 ! m
plthick=10e-3 ! m
pi=acos(-1)

!*
/prep7
k,,0,0,0
k,,-sqrt(3)*tridia/8,tridia/8,0
k,,0,outdia/2,0
k,,(kx(2)*sqrt(3)+ky(3)-ky(2))*sqrt(3)/2,(3*ky(3)
+sqrt(3)*kx(2)-ky(2))/2
k,,(kx(3)+kx(4))/2,(ky(3)+ky(4))/2,(kz(3)+kz(4))/
2
!*
a,1,3,5,4,2
arsym,x,all,,,,0,0
csys,1
agen,3,all,,,,120,,,0
agen,2,all,,,,,-height,,0
agen,,7,12,,,180,,,,1
csys,0
!*
myarc,5,58,-1/2,sqrt(3)/2
myarc,8,43,1/2,sqrt(3)/2
myarc,23,48,1,0
myarc,28,33,1/2,-sqrt(3)/2
myarc,13,38,-1/2,-sqrt(3)/2
myarc,18,53,-1,0
!*
nummrg,kp,all
!*
ET,1,BEAM4
KEYOPT,1,2,0
KEYOPT,1,6,0
KEYOPT,1,7,0
KEYOPT,1,9,0
KEYOPT,1,10,0
R,1,stripwidth*stripthk,stripwdth*stripthk**3/12,
stripthk*stripwdth**3/12,stripwdth,stripthk,0,
RMORE,0,stripwdth*stripthk**3/12+stripthk*str
ipwdth**3/12,0,0,0,0,
!*
ET,2,SHELL43
KEYOPT,2,3,0
KEYOPT,2,4,0
KEYOPT,2,5,0
KEYOPT,2,6,0
R,2,plthick,plthick,plthick,plthick,0,
RMORE, ,0,
!*
mp,ex,1,210e9
mp,nuxy,1,0.3
mp,ex,2,72e9
mp,nuxy,2,0.3
!*
!!!!!! mesh areas
asel,,,,1,6
type,2
real,2
mat,2
lsla,s
lesize,all,10e-3
amesh,all
asel,all
lsel,all
lsla,u
lesize,all,,,10
type,1
real,1
mat,1
lmesh,all
!*
allsel
eplot
```

```
!*
/view, 1 ,,,1
/ang, 1
lplot
!*
dk,58,all
dk,43,all
dk,48,all
dk,33,all
dk,38,all
dk,53,all
!*
fk,kp(0,0,0),fx,10
!*
nummrg,all
!*
/solu
solve
!*
/post1
pldisp,2
!* EOF
```

# B.3 ANSYS Generated Drawings for Joystick Model

## Overall ANSYS Generated Model

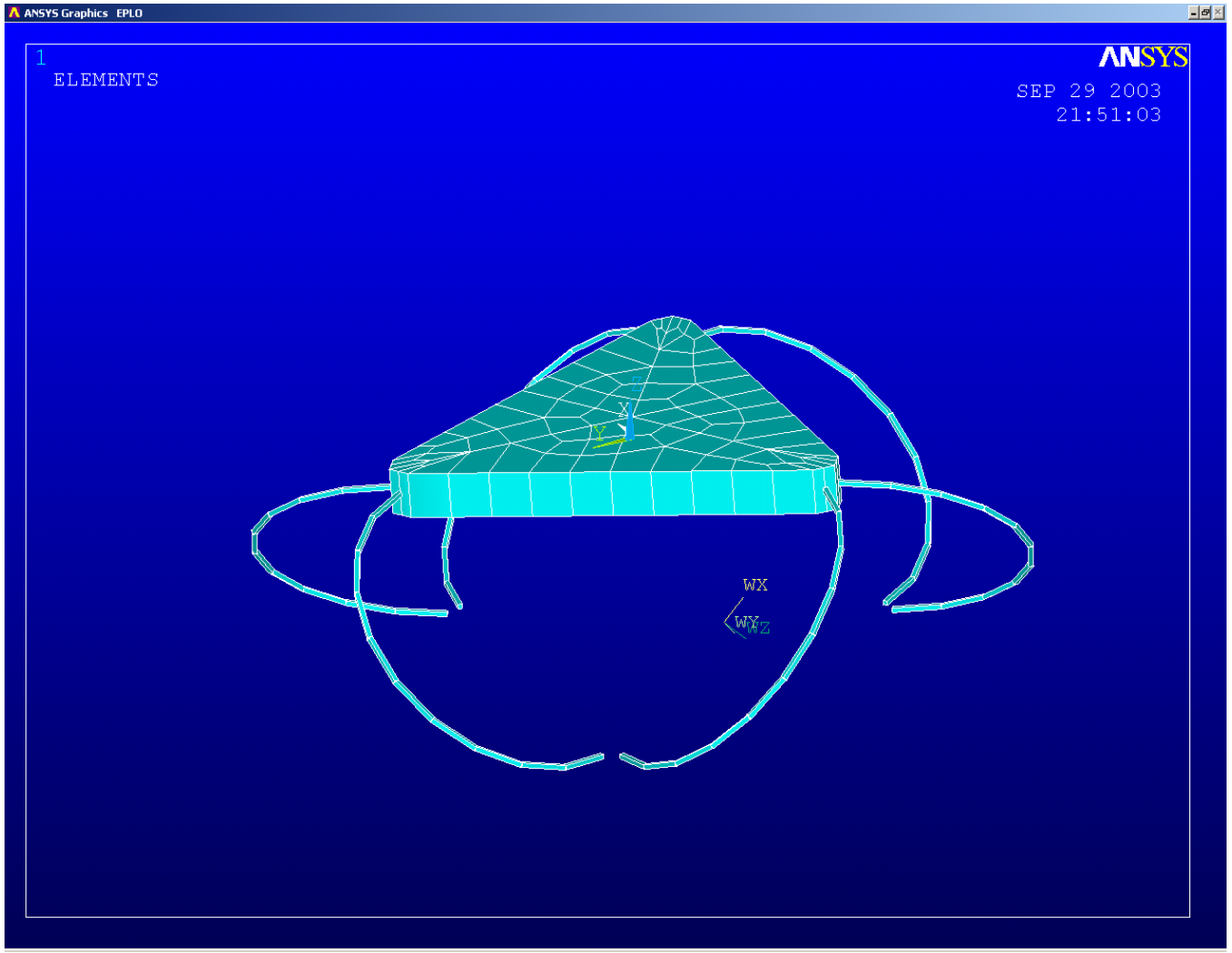

## ANSYS Generated Lined Model

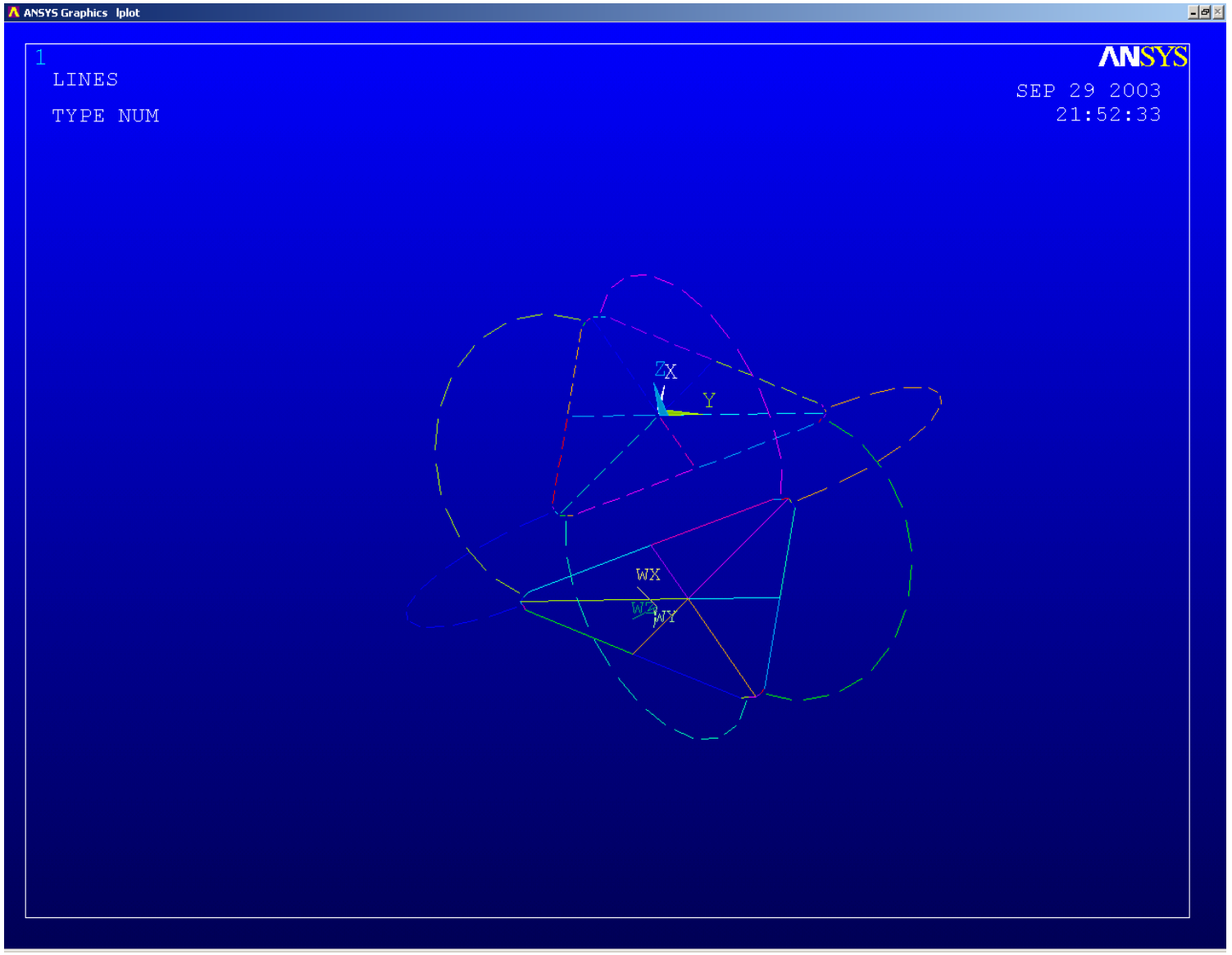

# APPENDIX C

# PATRAN ANALYSIS

C.1 PATRAN Parameters

# C.1 PATRAN Parameters

**Metal Properties as required by PATRAN**

| | modulus | Possoin ratio | density |
|---|---|---|---|
| Steel | 2.01e11Pa | 0.3 | 7.8t/m$^3$ |
| Aluminium | 7.0e10Pa | 0.3 | 2.78t/m$^3$ |

**Table C.1 Metal properties**

**Geometrical Parameter**

Diameter of section of steel wire: 1mm

Diameter of section of the joystick: 7.8mm

Thickness of plate: 10mm

**Force Applied at the Top of the Joystick**

(mm)

| | | $F_x = 5N$ | $F_y = 5N$ | $F_z = -5N$ | $F_x = 10N$ | $F_y = 10N$ | $F_z = -10N$ |
|---|---|---|---|---|---|---|---|
| A | X | 1.38e1 | -1.82e-5 | -4.16e-6 | 2.77e1 | 5.53e-5 | -8.33e-6 |
| | Y | -1.73e-1 | 1.45e1 | -1.93e-5 | -7.11e-1 | 3.07e1 | -3.86e-5 |
| | Z | -2.23e-1 | 8.33 | -3.57 | -9.08e-1 | 1.75e1 | -7.15 |
| B | X | 1.34e1 | 2.44e-5 | -4.59e-6 | 2.61e1 | 6.21e-6 | -9.20e-6 |
| | Y | -1.55e-1 | 1.37e1 | -1.99e-5 | -5.76e-1 | 2.74e1 | -3.98e-5 |
| | Z | -6.77 | -4.10 | -3.57 | -1.33e-1 | -8.47 | -7.15 |
| C | X | 1.42e1 | -6.90e-6 | -3.88e-6 | 2.95e1 | -5.56e-5 | -7.77e-6 |
| | Y | -1.93e-1 | 1.37e1 | -2.00e-5 | -8.71e-1 | 2.74e1 | -3.99e-5 |
| | Z | 7.12 | -4.10 | -3.57 | 1.48e1 | -8.47 | -7.15 |

**Table C.2 Force applied at the top of the joystick**

## Moment Applied at the top of the Joystick

(mm)

| | | $M_x = 0.5Nm$ | $M_y = 0.5Nm$ | $M_z = 0.5Nm$ | $M_x = 1Nm$ | $M_y = 1Nm$ | $M_z = 1Nm$ |
|---|---|---|---|---|---|---|---|
| A | X | -3.20e-5 | 3.29 | 5.41 | -1.38e-5 | 6.57 | 1.08e1 |
| | Y | -2.98 | -8.28e-2 | 2.11e-1 | -5.42 | -3.35e-1 | 8.53e-1 |
| | Z | -5.59 | -9.58e-2 | 4.17e-2 | -1.09e1 | -3.86e-1 | 1.68e-1 |
| B | X | 1.09e-5 | 3.09 | -2.89 | -3.18e-6 | 5.85 | -6.16 |
| | Y | -3.32 | -7.70e-2 | 4.58 | -6.75 | -3.37e-1 | 8.96 |
| | Z | 2.83 | -4.88 | 4.17e-2 | 5.61 | -9.65 | 1.68e-1 |
| C | X | 1.85e-5 | 3.50 | -2.52 | 1.10e-5 | 7.52 | -4.68 |
| | Y | -3.32 | -8.88e-2 | -4.79 | 6.75 | -3.39e-1 | -9.82 |
| | Z | 2.83 | 5.05 | 4.17e-2 | 5.61 | 1.03e1 | 1.68e-1 |

**Table C.3 Moment applied at the top of the joystick**

## Force Applied at the bottom of the Joystick

(mm)

| | | $F_x = 5N$ | $F_y = 5N$ | $F_z = -5N$ | $F_x = 10N$ | $F_y = 10N$ | $F_z = 10N$ |
|---|---|---|---|---|---|---|---|
| A | X | 1.05e1 | 3.66e-6 | -3.18e-6 | 2.10e1 | 7.63e-6 | -6.39e-6 |
| | Y | -1.62e-2 | 1.05e1 | -1.93e-5 | -6.50e-2 | 2.12e1 | -3.86e-5 |
| | Z | -2.51e-2 | 2.31 | -3.57 | -1.01e-1 | 4.67 | -7.15 |
| B | X | 1.05e1 | 6.99e-6 | -5.08e-6 | 2.09e1 | 1.36e-5 | -1.02e-5 |
| | Y | -1.63e-2 | 1.05e1 | -1.90e-5 | -6.52e-2 | 2.10e1 | -3.81e-5 |
| | Z | -1.96 | 1.15 | -3.57 | -3.88 | -2.32 | -7.15 |
| C | X | 1.05e1 | -1.61e-5 | -4.37e-6 | 2.11e1 | -3.19e-5 | -8.74e-6 |
| | Y | -1.62e-2 | 1.05e1 | -2.08e-5 | -6.50e-2 | 2.10e1 | -4.16e-5 |
| | Z | 1.99 | 1.15 | -3.57 | 4.01 | -2.32 | -7.15 |

**Table C.4 Force applied at the bottom of the joystick**

**Moment Applied at the bottom of the Joystick**

(mm)

| | | $M_x = 0.5Nm$ | $M_y = 0.5Nm$ | $M_z = 0.5Nm$ | $M_x = 1Nm$ | $M_y = 1Nm$ | $M_z = 1Nm$ |
|---|---|---|---|---|---|---|---|
| A | X | -7.57e-6 | 3.28 | 5.41 | -1.39e-5 | 6.57 | 1.08e1 |
| | Y | -2.98 | -8.27e-2 | 2.11e-1 | -5.42 | -3.35 | 8.53e-1 |
| | Z | -5.59 | -9.56e-2 | 4.17e-2 | -1.09e1 | -3.86e-1 | 1.68e-1 |
| B | X | -1.83e-6 | 3.09 | -2.89 | -3.31e-6 | 5.85 | -6.16 |
| | Y | -3.32 | -8.27e-2 | 4.58 | -6.75 | -3.37 | 8.96 |
| | Z | 2.83 | -4.88 | 4.17e-2 | 5.61 | -9.65 | 1.68e-1 |
| C | X | 5.76e-6 | 3.50 | -2.52 | 1.08e-5 | 7.52 | -4.68 |
| | Y | -3.32 | -8.29e-2 | -4.79 | -6.75 | -3.39 | -9.82 |
| | Z | 2.83 | 5.05 | 4.17e-2 | 5.61 | 1.03e1 | 1.68e-1 |

**Table C.5 Moment applied at the bottom of the joystick**

# APPENDIX D

# MATLAB ANALYSIS

D.1 Simulink Model of DSPACE interfaces

D.2 MATLAB Codes for Best-Fit Graph Approximations

# D1 Simulink Model of DSPACE Interfaces

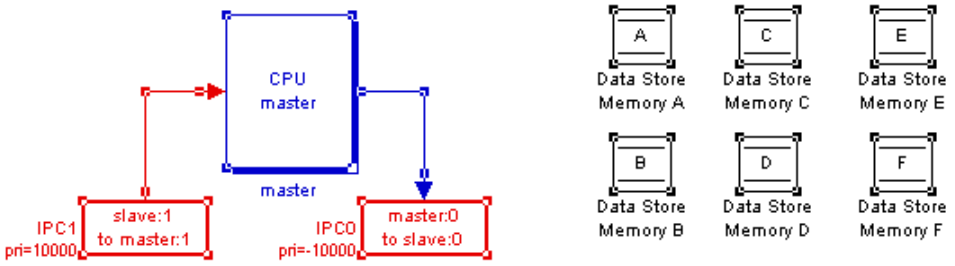


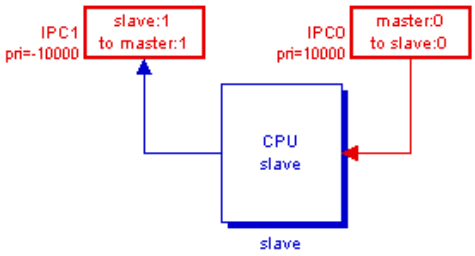


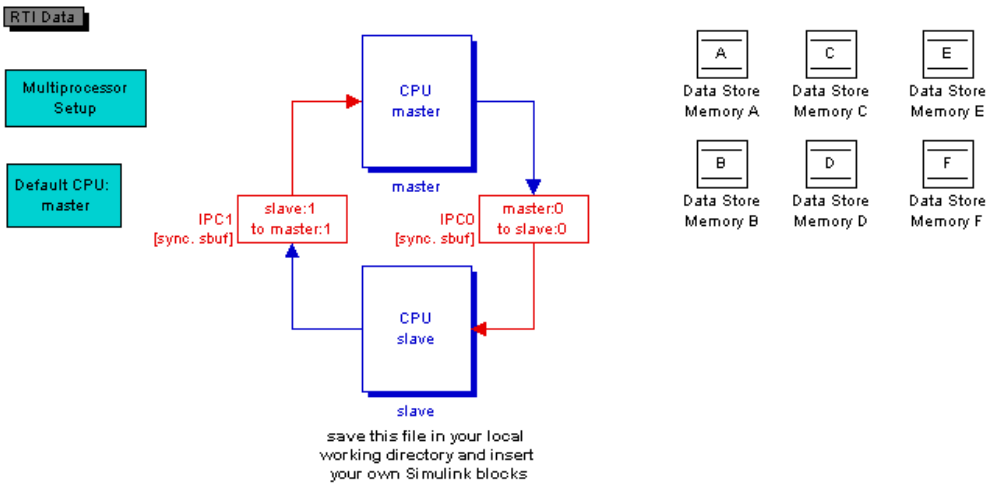

## D2 MATLAB Codes for Best-Fit Graph Approximations

```
close all; clear all;

xdata = 0:5:30;
Vxlinear1 = [-0.842 -0.782 -0.667 -0.573 -0.471 -0.346 -0.219];
Vxlinear2 = [-1.61 -1.613 -1.549 -1.526 -1.487 -1.438 -1.374];
Vxlinear3 = [-0.449 -0.439 -0.376 -0.343 -0.297 -0.231 -0.158];
Vxlinear4 = [-0.351 -0.383 -0.348 -0.349 -0.332 -0.303 -0.254];
Vxlinear5 = [-0.426 -0.354 -0.217 -0.117 -0.007 -0.118 -0.256];
Vxlinear6 = [-0.461 -0.491 -0.444 -0.446 -0.43 -0.396 -0.349];

p1 = polyfit(xdata,Vxlinear1,2);
p2 = polyfit(xdata,Vxlinear2,2);
p3 = polyfit(xdata,Vxlinear3,2);
p4 = polyfit(xdata,Vxlinear4,2);
p5 = polyfit(xdata,Vxlinear5,2);
p6 = polyfit(xdata,Vxlinear6,2);


x = 0:1:30;
model1 = p1(1)*x.^2 + p1(2)*x + p1(3);
model2 = p2(1)*x.^2 + p2(2)*x + p2(3);
model3 = p3(1)*x.^2 + p3(2)*x + p3(3);
model4 = p4(1)*x.^2 + p4(2)*x + p4(3);
model5 = p5(1)*x.^2 + p5(2)*x + p5(3);
model6 = p6(1)*x.^2 + p6(2)*x + p6(3);


plot(x,model1,x,model2,x,model3,x,model4,x,model5,x,model6)
hold on
plot(xdata,Vxlinear1,'o',xdata,Vxlinear2,'o',xdata,Vxlinear3,'o',xdat
a,Vxlinear4,'o',xdata,Vxlinear5,'o',xdata,Vxlinear6,'o')
legend('V1','V2','V3','V4','V5','V6',-1);
xlabel('Displacement');
ylabel('Voltage');
title('Voltages VS X-axis Linear Displacement');
```

# REFERENCES


1. Heney P J, “Joysticks are a Popular Control option”, Hydraulics & Pneumatics, Cleveland, Oct 2002.
2. Wang, Shih-Ming, Ehmann, Kornel F, “Error Model and Accuracy Analysis of a Six-DOF Stewart Platform”, Journal of Manufacturing Science and Engineering, H.W. Wilson – AST.
3. Niemela, E., Virvalo, T, “ Fuzzy Logic Assisted Manual Control of Joystick Operated Hydraulic Crane”, Fuzzy Systems, 1994, page 642-647 vol. 1, 26-29 Jun 1994.
4. Cooper, Rory A, Jones, Daniel K, Fitzgerald, Shirley, “Analysis of Position and Isometric Joysticks for Powered Wheelchair Driving”, IEEE Transactions on biomedical Engineering, Jul 2000, H.W. Wilson – AST
5. Jan B F Van Erp, Arjen B Oving, “Control Performance with Three Translational DOF”, Human Factors, Santa Monica, Spring 2002.
6. Bencsik, A.L., Garai, V., “A Mechatronic System with Force Feeling to increase the Activity of Manipulator Control”, Industrial Electronics, Control and Instrumentation, 1994.
7. Kazerooni, H, Snyder, Tanya J, “Case Study on Haptic Devices: Human-induced Instability in Powered Hand Controllers”, Journal of Guidance, Control and Dynamics, Jan/Feb 1995, H.W. Wilson – AST.
8. Collins, Curtis L, Long, Gregory L, “ The Singularity Analysis of an in-Parallel hand Controller for Force-Reflected Teleoperation”. IEEE Transactions on Robotics and Automation, Oct 1995, H.W. Wilson – AST.

9. Zhai, S., & Milgram, P, (1993), "Human Performance Evaluation of Isometric and Eleastic Rate Controllers in a 6 DOF Tracking Task", In Proceedings of SPIE – The International Society for Optical Engineering (Vol. 2057, pp. 130-141), Bellingham, WA: International Society for Optical Engineering.
10. Coyle, E.D., "Electronic Wheelchair Controller Desined for Operation by Hand-Operated Joystick, Ultrasonic Non-Contact Head Control and Utterance fomr a Small Word-Command Vocabulary", pages 3/1-3/4 17 Mar 1995, New Developments in Electric Vechicles for Disabled Persons, IEE Colloquium.
11. Wang, X, G. Seet, M.Lau, E.Low, K.Tan, "Exploiting Force Feedback in Pilot Training and Control of an Underwater Robotics Vehicle: An Implementation in LABVIEW", pages 2037-2042 vol.3 11 Sep 2000 – 14 Sep 2000 in OCEANS 2000 MTS/IEEE Conference and Exhibition.
12. Takahashi Y, Rabins M, Auslander D, "Control and Dynamic Systems", Addison-Wesley Pub Co, 1970
13. Taylor P. M., "Robotic Control", MacMillan, London 1990
14. McCloy D., Harris D., "Robotics: An Introduction", Milton Keynes, Philadelphia, Open University Press, 1986
15. Jean-Claude, "Robotics and Flexible Manufacturing Systems: Selected and Revised Papers from the IMACS 13th World Congress, Dublin, Ireland July 1991", Amsterdam, New York Elsevier 1992.
16. Ben-Zion Sandler, "Robotics: Designing the Mechanisms for Automated Machinery", San Diego, Academic Press 1999.
17. Pankaj K, Lydia E. Mathew T., "Robotics: The Algorithmic Perspective: the Third Worshop on the Algorithmic Foundations of Robotics", Wllesley, Mass A K Peters, 1998.
18. Geoffrey P Rathbun, "A Stewart Plaform Six Axis Milling Machine Development", a Thesis Submitted in Fulfilment of the Requirements for the Degree of Master of Engineering in the University of Canterbury.

19. Wayne H, William G, John W, “Mechanical Behaviour”, New York, John Wiley, 1965.
20. Ferdinand P. Russel E, John T Dewolf, “Mechanics of Materials”, New York McGraw-Hill 2002.
21. E.J Hearn, “Mechanics of Materials: An Introduction of the Mechanics of Elastic and Plastic Deformation of Solids and Structural Materials”, Oxford, Boston, Butterworth-Heinemann, 1997.
22. Yeh C, “Large Deflection Dynamic Analysis of Thin Shells using the Finite Element Method”, Berkeley, Calif. Structural Engineering Laboratory, University of California 1970.
23. A.E. Green, J.E. Adkins, “Large Elastic Deformations and Non-Linear Continuum Mechanics”, Berkeley, Calif. Strucutral Engineering Laboratory, university of California 1970.